Nanomaterial Based Photoelectrochemical Sensor for Multiplex Detections and the Further Study of Photocurrent Enhancement

Dissertation

zur Erlangung des Doktorgrades

an der Fakultät für Mathematik, Informatik und Naturwissenschaften

Fachbereich Physik

der Universität Hamburg

vorgelegt von

Shuang ZHAO

Hamburg

2020

The presented work in this dissertation was finished based on the supervision of Prof. Dr. Wolfgang Parak of Universität Hamburg (UHH), the Center for Hybrid Nanostructures (CHyN).

First Evaluator: Prof. Dr. Wolfgang Parak

Second Evaluator: Prof. Dr. Zhao Yue

Examination commission members:

Prof. Dr. Gabriel Bester

Prof. Dr. Fred Lisdat

Prof. Dr. Wolfgang Johann Parak

Prof. Dr. Michael Alexander Rübhausen

Prof. Dr. Zhao Yue

Disputation date: 22.07.2020

Gutachter/innen der Dissertation:	**Prof. Dr. Wolfgang Parak**
Zusammensetzung der Prüfungskommission:	**Prof. Dr. Gabriel Bester**
	Prof. Dr. Michael Rübhausen
	Prof. Dr. Fred Lisdat
	Prof. Dr. Zhao Yue
Vorsitzende/r der Prüfungskomission:	**Prof. Dr. Wolfgang Parak**
Datum der Disputation:	
Vorsitzender Fach-Promotionsausschusses PHYSIK:	**Prof. Dr. Günter H. W. Sigl**
Leiter des Fachbereichs PHYSIK:	**Prof. Dr. Wolfgang Hansen**
Dekan der Fakultät MIN:	**Prof. Dr. Heinrich Graener**

Contents

List of abbreviations 2
Zusammenfassung 3
Abstract 5

1. Preface 7

2. Sensing System 10

2.1 Optical sensing system 10
2.2 Potentiometric sensing system 11
2.3 Amperometric sensing system 12
2.3.1 Electrochemical sensing system 12
2.3.2 PEC sensing system 16

3. Multiplexed PEC Sensor 20

3.1 LAPS system 20
3.2 Light spot size 22
3.3 QD-electrode 23
3.3.1 Quantum dots 23
3.3.2 The immobilization of QDs on electrode 25
3.4 Multiplex detection using enzyme arrays 26
3.5 Photocurrent imaging 30

4. Nanozyme-based Enhanced PEC Sensor 32

4.1 Nanozyme 32
4.2 Hybrid nanomaterial 35
4.3 Layer-by-Layer (LbL) 37
4.4 H_2O_2 detection 40

Conclusions 42

Perspectives 44

References 45

List of publications 55
Bibliography 56
Acknowledgements 57
Appendix ..... A

Declaration on oath ..... B

List of abbreviations

PEC	Photoelectrochemical
QDs	Quantum dots
SAM	Self-assembly-monolayer
GOx	Glucose oxidase
SOx	Sarcosine oxidase
PBS	Phosphate buffer solution
LSPR	Localized surface plasmon resonance
LbL	Layer-by-layer
NPs	Nanoparticles
LAPS	Light-addressable potentiometric sensor
MIS	Metal–insulator–semiconductor
EIS	Electrolyte–insulator–semiconductor
CDs	Carbon dots
AuNCs	Gold nanoclusters
HPs	Halide perovskites
AuE	Gold electrode
SERS	Surface-enhanced Raman scattering
SPR	Surface plasmon resonance
ISFET	Ion-sensitive field-effect transistor
MOSFET	Metal-oxide-semiconductor FET
CV	Cyclic voltammetry
RE	Reference electrode
CE	Counter electrode
WE	Working electrode
LEDs	Light-emitting diodes
StDT	trans-4,4′-stilbenedithiol
E_F	Fermi level
ROS	Reactive oxygen species
HPNP	2-hydroxypropyl p-nitro-phenyl phosphate
HRP	Horseradish peroxidase
QCM	Quartz crystal microbalance

Zusammenfassung

In der Forschung nach Sensoren hat das Multiplex-Übertragungssystem immer mehr Aufmerksamkeit auf sich gezogen, da es mehr Informationen des zu überprüfen Objekts gleichzeitig erfassen kann, wodurch die Überprüfungsseffizienz erheblich verbessert wird. In dieser Arbeit verwirklichte eine auf einer selbstgebauten (homebuilt) photoelektrochemischen (PEC) basierenden Sensorelektrode unter der Lichtadressierungsoperation gleichzeitige Überprüfung von zwei Enzymsubstraten. Mit Hilfe einer isolierenden selbstorganisierten Schicht (trans-4,4'-Stilbenedithiol) werden CdSe/ZnS-Kern/Schale-Quantenpunkte (QDs) auf der Goldelektrodenoberfläche selbstorganisiert, um eine Sensorelektrode (QD-Elektrode) aufzubauen. Nur wenn Licht an die Elektrode angelegt wird, wird ein Fotostrom (photocurrent) erzeugt, wenn kein Licht vorhanden ist, wird kein Fotostromsignal erfasst. Glucoseoxidase (glucose oxidase) oder Sarsosin-Osidase (sarsosine osidase) ist an der QD-Elektrode selbstorganisiert, was den Überprüfung von Glucose bzw. Sarcosin ermöglicht. Auf dieser Basis werden Glucoseoxidase und Sarcosinoxidase gleichzeitig auf derselben Elektrode selbstorganisiert und bilden unterschiedliche unabhängige Sensorarrays kleiner Größe, wodurch der gleichzeitige Überprüfung von zwei Analyten mit einer Elektrode erreicht wird . Der Überprüfungsvorgang der parallele Überprüfung der beiden Analyten, wird durch den sich auf der Elektrodenoberfläche bewegenden Laserspot (Durchmesser 0,3 mm) gesteuert und der Nachweis erfolgt in drei Lösungen (Mischlösung aus Glucose, Sarcosin, Glucose und Sarcosin) kann die Enzymreaktion nur dort nachgewiesen werden, wo der Lichtfleck scheint.Wenn am Ende zwei Arten von Testobjekten gleichzeitig existieren, können sie die gegenseitige Interferenz überwinden und gleichzeitig von einem Sensorchip erfasst werden. Zusätzlich verwendeten wir die Photocurrent-Imaging-Technologie, um die Größe eines einzelnen Enzymarrays in x- und y-Achsenrichtung zu charakterisieren und die Größe ist 1,9 mm * 1,3 mm. Darüber hinaus wurde durch kontinuierliche Überwachung des Photostroms die Verteilung der Enzymaktivität auf einem einzelnen Enzymarray erfolgreich charakterisiert. Andereerseits versuchen diese Arbeit die Photoelektrochemie (Nanoenzym) durch Forschung nach Nanoenzymen (Nanoenzym), ob die Nanoenzyme im System (PEC) natürliche Enzyme und Quantenpunkte (QD) ersetzen können, um die Mängel natürlicher Enzyme wie die einfache Deaktivierung und den hohen Preis zu beheben und die durch diese

Mängel verursachte Instabilität des Photostroms zu vermeiden. CeO_2-Nanozyme haben nicht nur katalytische Eigenschaften für H_2O_2, sondern auch photoelektrische Eigenschaften als Halbleitermaterialien. Daher können CeO_2-Nanopartikel etwas Wasserstoffperoxidreduktase (H_2O_2-Reduktionsenzym) ersetzen und können sich auf der Elektrode assemblieren, um einen Photostrom zu erzeugen. Auf dieser Basis haben wir in diesem Artikel die Forschung nach heterogener (hybrider) Au / CeO_2-Schale/Kern-Nanomaterialien eingeführt, um die Photostrom-Verstärkungstechnologie weiter zu untersuchen. Im Vergleich zum Photostrom gewöhnlicher CeO_2-Nanomaterialien ist der Photostrom heterogener Au/CeO_2-Nanomaterialien in PBS und H_2O_2 erhöht, was zeigt, dass die heterogenen Nanomaterialien bessere katalytische und photoelektrische Eigenschaften aufweisen.

Die Photostromergebnisse unter verschiedenen Wellenlängen von monochromatischem Licht (Wellenlängenabhängigkeit) beweisen, dass der Au-Kern eine wichtige Rolle bei der Verbesserung des Photostroms heterogener Nanomaterialien spielt. Durch die Einführung einer Mischung aus Goldnanopartikeln (AuNP) und CeO_2 NP und den Vergleich ihres Photostroms mit dem Photostromverstärkungseffekt heterogener Nanomaterialien (Au/CeO_2) spielt die Goldhalbkontaktschnittstelle (Halbleiter-Metall) eine Rolle im Photostrom Der Verbesserungseffekt wurde ebenfalls verifiziert. Schließlich wird die Schicht-für-Schicht-Technologie (LBL) eingesetzt, um die katalytischen und photoelektrischen Eigenschaften von CeO_2-Nanomaterialien und Au / CeO_2-Nanomaterialien weiter zu verbessern. Dies liegt daran, dass LBL die Bedeckung des Nanomaterials auf der Elektrodenoberfläche verbessern kann, so dass schließlich eine gute H_2O_2-Nachweisgrenze (3 uM) erreicht wird und der lineare Nachweisbereich 2-1000 uM beträgt.

Abstract

In the effort to improve sensors, the development of multiplex sensing systems is an important trend because this type of system significantly improves the sensors' efficiency by obtaining more information at one time. In this cumulative dissertation, light-directed multiplex detections of different substrates were realized based on a homebuilt photoelectrochemical (PEC) electrode. To fabricate the electrode, CdSe/ZnS core/shell quantum dots (QDs) were immobilised on a gold (Au) electrode using an insulating self-assembly-monolayer (SAM) of trans-4,4'-stilbenedithiol, resulting in a light-triggered photocurrent when light is applied and no photocurrent when the light is turned off. Afterwards, enzymes of glucose oxidase (GOx) or sarcosine oxidase (SOx) were immobilised on the surface of the QD-electrode to detect glucose and sarcosine, respectively. Based on those results, the GOx and SOx enzymes were immobilised on a single chip together as discrete and small-sized sensing arrays to selectively detect glucose and sarcosine at the same time. The parallel detections were triggered and controlled by moving a localised laser pointer (0.3 mm) over the sensing arrays in different analytes (glucose, sarcosine, the mixture of glucose and sarcosine). Eventually, two substrates can be detected with single chip simultaneously, overcoming the interference from each other. Moreover, a photocurrent imaging technique was used to characterise the spatial size of a single enzyme array in both the x- and y-direction as 1.9 mm × 1.3 mm. It was also possible to visualise the enzymatic activity distribution of the single enzyme array using continuous photocurrent measurement.

Furthermore, to overcome the disadvantages of a natural enzyme, such as easy inactivation and high cost, also to improve the photocurrent stability brought by the disadvantages, another study was conducted for this dissertation, attempting to study if a nanozyme can replace the natural enzyme and QDs. CeO_2 nanozyme nanoparticles (NPs) have both mimicking catalytic activity towards H_2O_2 reduction and photoelectrical properties as semiconductor, so CeO_2 can replace the H_2O_2 reduction enzymes and single-layer CeO_2 NPs can be immobilised to generate the basic photocurrent on the PEC electrode. Based on that, technique of photocurrent enhancement was studied by introducing hybrid Au/CeO_2 core/shell NPs in this dissertation. The photocurrent of Au/CeO_2 was significantly enhanced in both phosphate buffer solution (PBS) and H_2O_2, indicating that the hybrid NPs have better

catalytic and photoelectrical properties than the pure CeO_2 NPs. Wavelength dependent measurements were used to verify that the Au core plays an important role in the photocurrent enhancement of hybrid NPs. By introducing a mixture of CeO_2 NPs and Au NPs and comparing with hybrid Au/CeO_2 NPs, the effect of semiconductor-metal interface on the photocurrent enhancement was also verified. Furthermore, a layer-by-layer (LbL) technique was applied to both the CeO_2 NPs and the hybrid Au/CeO_2 NPs to further enhance the catalytic and photoelectrical properties by creating more NP coverage, resulting in good H_2O_2 detection limit of 3 μM with a linear detection range of 2–1000 μM.

1. Preface

Sensor arrays, located in a geometric pattern, can obtain more sensing parameters when a group of sensors are integrated to a single chip. However, each array needs individual wires to collect the localised signals, which is wiring complexity, expensive, hard to maintain and technically challenging.[1, 2] To solve this problem, research groups around the world began to study sensing devices in which the signal can be collected at active places controlled by moving the localised illumination, thereby successfully avoiding the use of multiple wires. One type of device, a light-addressable potentiometric sensor (LAPS) can monitor the photo response (photocurrent or photovoltage) when light is applied to the semiconductor surface inducing charge carriers generating and transferring. LAPS has typical structures either a metal–insulator–semiconductor (MIS) or a electrolyte–insulator–semiconductor (EIS) structure.[3, 4] In detail, when a light beam is scanned across the discrete sections of the semiconductor surface, it is possible to obtain the photo signal from the different active regions that are illuminated.[5] LAPS devices show great potential for sensing applications for pH[6], H_2[7], ions[8], enzyme substrates[9], lipid membranes[10] and serotonin[11], as well as cell monitoring [12, 13].

However, spatial resolution is a key parameter in LAPS systems, and it still needs to be improved. Spatial resolution mainly depends on the minimum bulk length of the charge carrier diffusion inside the semiconductor wafer.[5] In other words, it is limited by how far the charge carriers can laterally move, and the photo signal can only be detected in the active range where the charge carriers are available.[1, 14, 15] Thus, in the present study, the spatial resolution was improved by replacing the semiconductor wafer with discrete semiconductor nanoparticles (NPs), which can be seen as independent individuals with no electrical connection.[1]

Today, the construction of light-switchable electrodes using NPs, such as quantum dots (QDs),[1] carbon dots (CDs),[16] gold nanoclusters (AuNCs),[17] dyes[18, 19] and halide perovskites (HPs), is a hot topic[20]. In this work, discrete QDs were immobilised on the Au electrode (AuE) as the semiconductor component of the LAPS system with the help of a self-assembly monolayer (SAM). These electrodes also have flexible optical absorption properties and multiple functionalities to meet the needs

of the light source and the analytes, which makes the electrodes can be used in a lot of applications.

In the study discussed in this paper, the AuE/QDs semiconductor electrode was measured using a homebuilt photoelectrochemical (PEC) set-up the obtain the electrical photocurrent output. As a famous photovoltaic conversion platform, PEC devices have been used for many applications, including solar cells[21], water splitting[22] and biological sensors[23]. Derived from electrochemistry, a PEC system has s lower detection limit, a larger detection range and higher sensitivity than other devices, is also has a better signal-to-noise ratio because no photocurrent can be generated in the dark due to the insulated SAM. A PEC device is usually based on a photoactive electrode (QDs electrode) that generates electron carriers, and the photocurrent can be collected with the help of the potential. In detail, the electron-hole pairs generated in the QDs under illumination result in the transfer of free electrons among the electrode, the QD, the electrolyte and the analyte. The final photocurrent is based on the competition of four electron transfer processes: (i) from the QD conduction band (CB) to the electron acceptor in the electrolyte, (ii) from the electron donor in the electrolyte to the QD valance band (VB), (iii) from the electrode to the VB of QD, and (iv) from the CB of QD to the electrode. Eventually, after the competition, the cathodic photocurrent can be collected using stepwise electron transfer from the AuE to the QD and then to the electron acceptor in the electrolyte; then, the anodic photocurrent travels in the opposite direction from the electron donor to the QD and then to the electrode. The photocurrent is also affected by the inevitable electron-hole recombination with fluorescence emission and potential polarity applied on the AuE. The cathodic and anodic potentials favour the electron transfer from and to electrode, respectively.

Based on the NP-electrode mentioned above, previous studies have also investigated building a functional sensing electrode using antibodies,[24] DNA,[25, 26] lectin,[27] molecular-imprinted polymers,[28, 29] and enzyme substrates[30, 31]. The sensing mechanism of these related PEC-electrodes can be summarised as follows: (i) direct detection with electron transfer from the PEC-electrode to the redox analytes (for example, Stoll et al. used the PEC QD-electrode to directly detect cytochrome c),[32] (ii) indirect detection using redox mediators (for example, Riedel at el. introduced hexacyanoferrate (II)/(III) mediators to detect fructose with electron transfer from the enzyme to the PEC QD-electrode via mediators)[30] and (iii) indirect detection of

the substrates using the by-product of the enzyme reactions (for example, Tanne at al. successfully detect glucose via the by-products O_2 of glucose oxidase[33].

However, these studies were usually based on a fully covered electrode, so the detection of the electron transfer via a miniaturised biological array has not been verified.[30, 34, 35] Moreover, the parallel read-out from more than one kind of enzymes immobilised on a single electrode has not been realised in a PEC system, yet. Although multiplexed PEC detection of two DNA sequences has been shown by Zheng at al.,[36] that study used wavelength-resolved illumination so it was difficult to detect more than two analytes.

To overcome this, the study discussed in this paper used single illumination and we immobilised two small enzyme arrays of glucose oxidase (GOx) and sarcosine oxidase (SOx) on a single PEC QD-electrode. The miniaturised and active enzyme arrays were used to detect two substrates (glucose and sarcosine), simultaneously. Moreover, the size and activity distribution of the enzyme array were characterised using a photocurrent imaging technique. This set-up not only offers a method for improving the spatial resolution of the original LAPS system, it is also a very promising way to develop multiplex detection for more than two substrates at the same time overcoming the interference for each other.

However, there are still disadvantages in the enzyme-based sensor mentioned above that should not be neglected. First, the activity of a natural enzyme is easily changed based on the storage and measurement conditions, such as temperature and pH. Second, the process of immobilizing the enzyme on the QD-electrode may increase the chance of inactivating it. Finally, the photocurrent amplitude of the QD-electrode is small (around 1 nA), making it difficult to obtain a good detection limit with poor practicability. To overcome these disadvantages, in this paper, we used nanozyme (CeO_2 NPs) with both light-triggered semiconductor properties and the ability to mimic the catalytic properties of a natural enzyme. The combination can effectively simplify the enzyme immobilisation step and overcome its disadvantages of instability and cost. Furthermore, we studied the increase in the photocurrent using hybrid Au/CeO_2 core/shell NPs and the layer-by-layer (LbL) technique. We found that the photocurrent was significantly enhanced by the localised surface plasmon resonance (LSPR) of the metal core and the increase in the number of NPs immobilised on the electrode.

2. Sensing System

In this section, several of the most common sensing systems are summarised and compared, including optical sensors, potentiometric sensors and amperometric sensors. Their advantages and disadvantages are stated, and the reasons we choose the PEC sensing system in this paper is discussed.

2.1 Optical sensing system

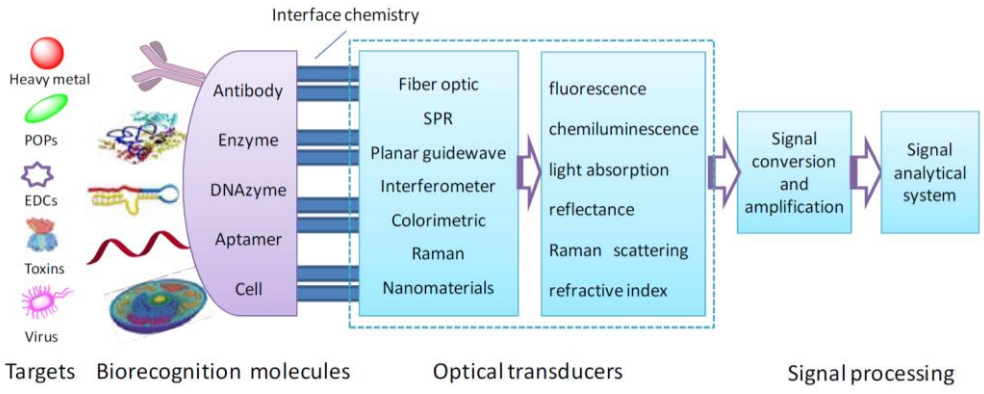

Figure 1. Diagram of an optical sensing system. Ref [37] copyright 2013 MDPI.

All of the sensing systems contains a circuit module, a signal processing module and a front-end signal transducer module. For example, Figure 1 shows the structure and working process of an optical transducer sensing system.[37] When the analytes is interact with the transfer module (biorecognition molecules), their biochemical information (analogue signal) in the solution can be transferred successfully to the electrical signal (digital signal). Different optical signal transfer modules have been reported in the past several decades, such as fluorescence spectroscopy,[38] optical-fiber,[39] surface-enhanced Raman scattering (SERS)[40] and surface plasmon resonance (SPR)[41]. These modules have been used to achieve several sensing applications, including systems for detecting pH, DNA, antibodies and ions; their advantages include their high sensitivity and rapid response. However, these systems still have some disadvantages that cannot be ignored. First, the size of their set-ups is usually large or extra-large, and they require an expensive light source and a complex optical path. Thus, they are not easy to operate and it is difficult to convert them into marketable products. Moreover, to some extent, their results are not

stable and they can be affected by unknown factors, for example, in the most often used fluorescence assay, the intensity of the spectroscopy can be decreased or shifted by continuous measurements and other external conditions.[42] In the study presented in this paper, the future task is to build a portable multiplex device or an implanted miniaturised system, so an optical system is not suitable and did not select in this paper.

2.2 Potentiometric sensing system

In addition to the optical systems, other potentiometric strategies can be used to transfer signals from analytes into electrical signals, such as the most widely used ion-sensitive field-effect transistor (ISFET) technique.

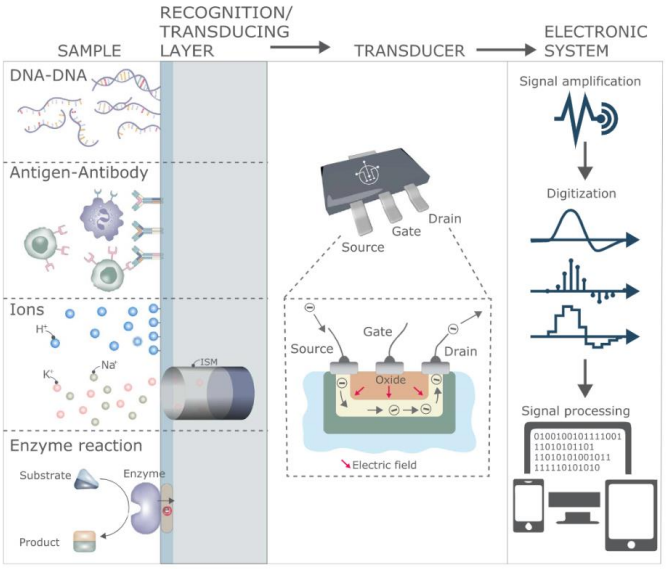

Figure 2. Diagram of an ISFET-based biological sensing system. Ref [43] copyright 2017 Elsevier.

The history of the ISFET potentiometric device can be traced back to the 1970s.[44] Based on the metal-oxide-semiconductor FET (MOSFET) technique, the metal gate of the MOSFET was replaced with a special unit composed of an ion-sensitive film, an electrolyte, and a reference electrode to fabricate a new ISFET device.[43] In the past thirty years, ISFET devices have been used to detect many targets, including DNA, antigens, ions, and enzymatic substrates (Figure 2), and their sensing mechanism can be described as follows. When different analytes interact with the ISFET sensing film, the charge distribution on the gate reaches a new balance. This changes of surface

potential of the ISFET gate. With the help of an external circuit, the change in the surface potential can be reflected by the change in the threshold voltage to be collected.

Generally, the application of an ISFET device be adjusted by the gate materials that are selected. For example, when pH is detected, different semiconductor materials, including SiO_2, Si_3N_4, Al_2O_3, can be used to fabricate the gate on which there are binding groups (Si-O and Si-NH_2) for the protons.[45, 46] By further modifying the ISFET gate, different types of molecules such as glucose and proteins, can also be detected.[47] ISFET has excellent properties; for example, it is water-proof and acid and alkali resistant, and it has a rapid response and seamless integration.[43] Moreover, ISFET is very small, so that it has the potential to be implanted into patients or used as a portable or wearable device for long-term continuously monitoring.[47, 48]

However, before its use is promoted, several problems must be overcome. In most case, ISFET device does not have a strong response to uncharged targets, especially small molecules, because only charged molecules can change the surface potential of the gate. Furthermore, the Debye screening of ISFET further limits its ability to recognise small uncharged molecules especially in high ion solutions.[47] When an ISFET device is implanted in an in vivo environment, the ion concentration cannot be diluted or adjusted. Most importantly, it is not easy to develop ISFET devices into multiplex sensors to detect multiple analytes at the same time because many wires are needed to integrate them into fabricated device, such as sensing arrays, which is very costly and technique challenging. Thus, ISFET devices are not suitable for the project conducted in our study.

2.3 Amperometric sensing system

2.3.1 Electrochemical sensing system

Besides the potentiometric method, the amperometric ones is also widely used with their own characteristics.

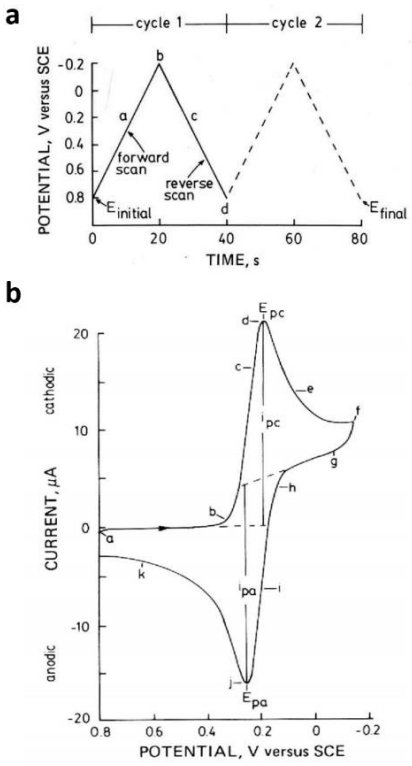

Figure 3. (a) The potential applied between electrodes in electrochemical system for the cyclic voltammetry method. (b) The representative electrochemical cyclic voltammetry curve (6 mM K3Fe(CN)6 in 1 M KCl, 50 mV/s). Ref [49] copyright 1983 American Chemical Society.

In the past 20 years, as the development of nanomaterials, the study of NPs gradually shifted from the liquid phase (such as fluorescence spectroscopy) toward immobilisation phase on an interface in the past twenty years.[23, 30, 50, 51] As a classic technique for electrode-based study, electrochemistry has been developed to effectively convert physical, chemical and biological information into electrical signals to be analysed and quantified.[52, 53] The most widely used electrochemical method is the amperometric method of cyclic voltammetry (CV) with a current curve output (Figure 3). The electrochemical experiment is measured with the help of a three-electrode system, which includes the reference electrode (RE), the counter electrode (CE) and the working electrode (WE). When the CV method is used, a potential is applied between WE and RE that changes linearly over time (Figure 3a). The change rate of the potential is defined as the scan rate (potential/time). Based on this, the related current change can be output between CE and WE with peak cathodic and anodic currents, as shown in Figure 3b. According to the Randles–Sevcik equation (Eq.1), the peak current (i_p) can be affected by several parameters, reflecting information about both the analytes in the solution and the surface condition of the

electrode. In Eq. 1, *n* is the number of electron transfers, *F* is the Faraday Constant, *A* is the electrode surface area, *D* is the diffusion coefficient, *C* is the concentration, *v* is the scan rate, *R* is the gas constant and *T* is the thermodynamic temperature. At normal room temperature, the scan rate, electrode area, concentration, and diffusion coefficient are the key electrochemistry parameters. When the scan rate increases, the current of the CV curve shifts and the peak currents increase so that normal electrochemical measurements are based on a constant scan rate value.

$$i_p = 0.4463\, nFAC\left(\frac{nFvD}{RT}\right)^{\frac{1}{2}} \quad \text{(eq.1)}$$

The basic sensing mechanism of the electrochemical system is described as follows. Generally, when an electrode is measured in the solution electrochemically, the electrode-electrolyte system can be divided into four sections: (i) the electrode, (ii) the double layer, (iii) the diffusion layer and (iv) the bulk electrolyte outside (Figure 4). The diffusion layer is very small in comparison to the bulk electrolyte outside; therefore, the electrochemical current output mainly depends on the analytes in the bulk electrolyte. The electrode acts like an electrostatic pump; it can absorb the analytes or ions with a specific charge and induce the movement of the analytes from the bulk electrolyte section to the diffusion section.[54] The analytes near the electrode will exchange electrons with the electrode, resulting in the current output amplitude. Thus, when the scan rate and electrode area are fixed, the electrochemical measurement can be used to successfully characterise the concentration of the analytes in the bulk electrolyte outside. This can be verified by the direct detection of the reactive oxygen species (ROS) in the solution, which can be successfully achieved using a bare electrochemical electrode without further modifications.[55]

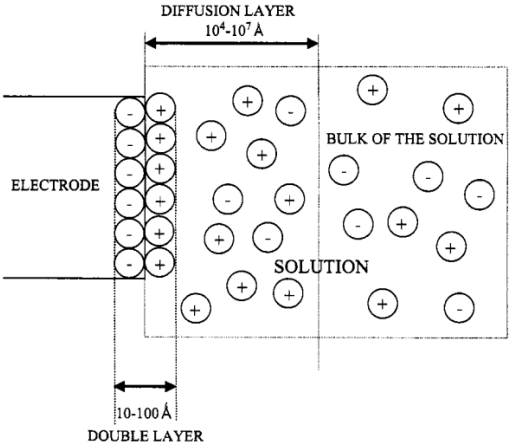

Figure 4. The different sections in a typical electrode-electrolyte system. Ref [54] copyright 2003 The Royal Society of Chemistry.

When the electrode is further modified using biological recognition elements, such as enzymes, DNA, proteins and cells,[53] the corresponding analytes can be bound to the electrode surface, inducing the change in the diffusion coefficient and electrode sensing area. Thus, as the concentration of the non-redox analytes increases, the peak current of the CV curve will be changed (Eq. 1). This can be verified by the results, which demonstrate that after absorption on the electrode surface, the current output decreases dramatically (Figure 5).

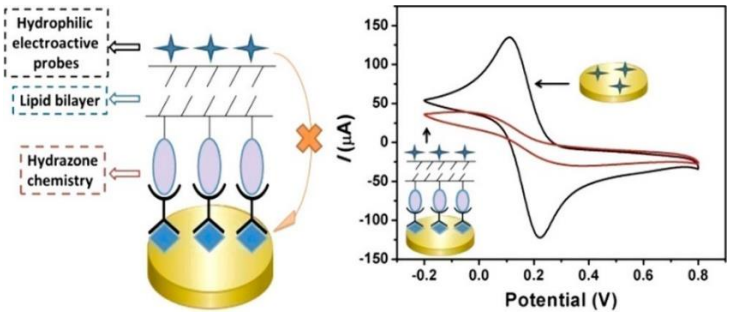

Figure 5. Schematic illustration of the biological recognition on the electrochemical surface and its effect on the CV curves. Ref [56] copyright 2017 American Chemical Society.

The study of electrochemistry occurred as early as 1964, focusing on an Si-electrolyte system.[57] After many years of development, the electrochemistry technique is mature and the theoretical study has also been well-developed by Gouy-Chapman-Stern model,[58] resulting in broader applications. However, electrochemistry can

only be used to study electrical properties; it does not describe the photoelectrical properties of nanomaterials. Moreover, biological modification is usually based very simple designs with a fully covered electrode.[53] Thus, it is difficult to develop the electrochemistry technique into a multiple detection system with a single electrode. Therefore, the original electrochemical system is also not suitable for the project conducted in our study.

2.3.2 PEC sensing system

Based on the original electrochemistry technique, a PEC system was built by applying a localised and movable illumination on the working electrode to overcome the disadvantages of electrochemistry for multiple detection.

Initially, photoelectrochemistry was introduced to utilise solar energy to produce electricity because it is time consuming and unrealistic to only rely on natural biological photosynthesis to transfer solar energy into fuels.[59] Thus, it is essential to know how to use an artificial technique to convert energy from abundant materials into electrical or fuel energy (such as H_2). Photoelectrochemistry can convert optical and chemical energy from redox species into electrical energy with an electron flow;[60] it can also generate H_2 by splitting water into hydrogen and oxygen.[61] The principle of photoelectrochemistry is based on a photoactive electrode with electron-hole pairs separated under illumination, leaving free electrons at the CB and holes at the VB. When semiconductor NPs are immobilised on the WE, free electrons are available in the NPs to exchange with the electrode or the solution. A constant potential is applied between WE and RE, and electrons will either transfer from the solution to the NPs and then to the electrode as an anodic photocurrent (Figure 6a), or they will transfer from the electrode to NPs and then to the solution as a cathodic photocurrent (Figure 6b). The two electron transfer directions occur simultaneously, and the finial polarity of the photocurrent depends on the potential that is applied and the competition between the electron transfer processes in the two directions. In addition to the parameters that influence the current in an electrochemical system, which were discussed in the previous section, in a PEC system, the photocurrent also depends on light (intensity, wavelength and light spot size).

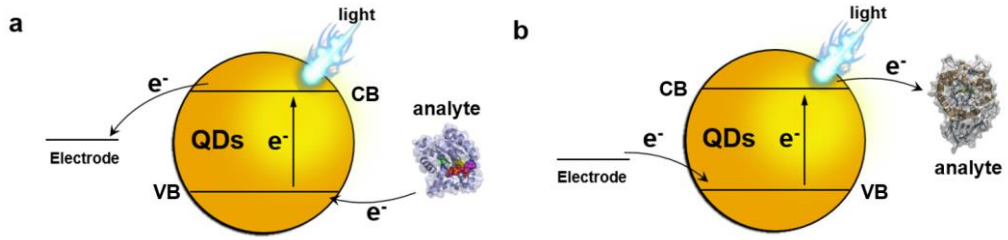

Figure 6. Diagrams of photocurrent generation from QD-based electrode at (a) anodic and (b) cathodic directions.

In comparison to the different sensing systems mentioned above, the amperometric PEC sensing system has several advantages.

First, unlike an optical sensing system, a PEC system is easily built with a simple set-up so that a traditional complex light path is not needed. Derived from electrochemical system, a potentiostat is used in a PEC system and a light source is further applied on the electrode. The simple set-up is shown in Figure 7.

In the PEC system, a three-electrode set-up is necessary. When the measurements are taken with two electrodes, the photocurrent can also be obtained between the CE and the WE. However, in this case, because the photocurrent flows through the two electrodes and the solution, an uncontrollable potential drop occurs in the solution and at the two electrode-electrolyte interfaces. Because the photocurrent is influenced by the potential applied on the WE, the potential drop will make the collected photocurrent very unstable. To overcome that, a reference electrode (RE) is added to form the three-electrode system to limit the potential drop effect. Normally , the RE is composed of three parts: an internal metal electrode inside, an internal electrolyte and contact film between the internal and external electrolyte. Usually, the contact film is fabricated using ceramic materials or porous glass. The reason why reference electrode can maintain the potential at a constant value is that there is reversible redox reaction on the internal metal electrode surface. For Ag/AgCl reference electrode, the metal electrode is Ag and its surface is covered with AgCl. The electrolyte contains Cl^- and the reversible redox reaction of Ag/AgCl reference electrode is $AgCl+e^-=Ag+Cl^-$.

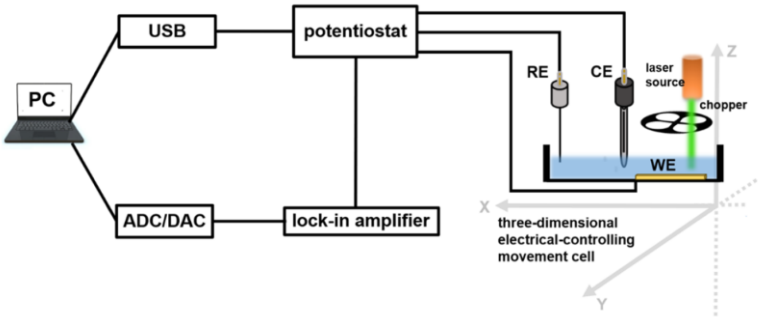

Figure 7. The illustration of homebuilt photoelectrochemical set-up based on PC, potentiostat, lock-in amplifier. The electrodes used are Ag/AgCl (3M NaCl) reference electrode, Pt counter electrode, and Au electrode (AuE) immobilized with QDs as working electrode. Ref [51] copyright 2019 American Chemical Society.

Second, with the help of a lock-in amplifier, the PEC sensor can detect a stable photocurrent without a strong shift (Figure 8a,b). The PEC photocurrent can be detected against a large electrochemical background. The lock-in amplifier, invented by Robert H. Dicke (Princeton University), is a tool that can be used to effectively extract the amplitude and phase information of the signal from the strong background noise.[17] Using the homodyne detector method and the low-pass filter technique on the frequency domain, the signal within the specified frequency band of the reference frequency can be detected successfully. Thus, transferred back to the time domain, the lock-in amplifier can detect signals with very small noise.

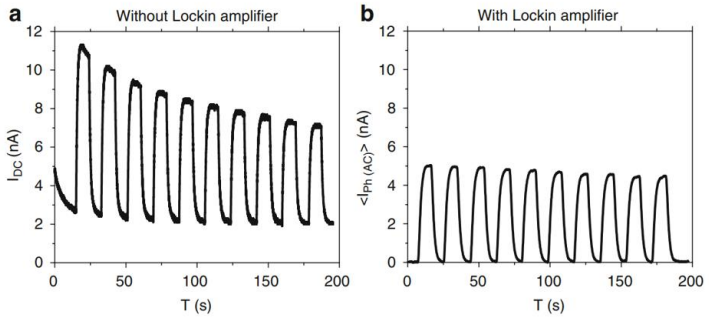

Figure 8. The photocurrent behaviour of a QD-electrode (a) without and (b) with the lock-in amplifier. Ref [1] copyright 2009 Springer-Verlag.

Third, unlike ISFET sensing arrays, fewer wires are needed to build the PEC electrode for multiple detections. The simple PEC electrode designed in this study is shown in Figure 9. With only one conductive wire output, the multiplex signal from different

sensing arrays on the AuE can be output simultaneously and successfully. Finally, when the PEC electrode is fabricated using different sensing arrays on a single electrode, different analytes can be detected simultaneously with the help of an addressable light. This is discussed in more detail in the next section.

Based on these advantages, the PEC system is used in the project to build the multiplex sensor (section 3). It can also be used for the PEC sensor enhancement study (Chapter 4).

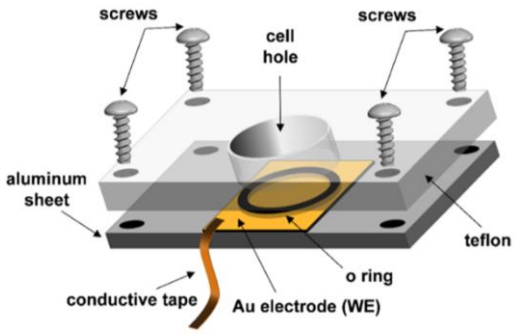

Figure 9. Illustration of the PEC teflon cell with a gold working electrode (WE) inside. The WE is connected to outside by a simple conductive type on one edge of the Au chip. The WE is sealed for waterproof properties with a rubber o ring and four screws.

3. Multiplexed PEC Sensor

In this paper, a sensing system was built using QD-electrode and small-sized illumination spot to improve the spatial resolution of the original LSPS system. Based on this, further photocurrent imaging was realized to characterise the size of enzyme array and also to visualise the enzymatic activity distribution on the enzyme array.

3.1 LAPS system

When the sensing system is used in a practical application, especially in an in vivo environment such as cells, tissues and blood, the analytes usually co-exist with many other substances. Thus, how to develop a sensing device that can detect several analytes at the same time is undoubtedly a hot topic. This capability would improve the detection efficiency of the sensing device, enabling it to obtain more information at one time. For this purpose, the LAPS method was introduced by research groups.[46] Charge carriers are only generated at the illuminated area on a semiconductor electrode where a localised output can be detected. Thus, the corresponding output can only reflect the information in the illuminated area. When scanning the light beam on the whole surface, the photo signal from different areas on the electrode can be obtained. When the electrode surface is divided and modified with different functionalities, the LAPS system can be used for multiple detections with a single electrode. Initially, as shown in Figure 10, the LAPS system was designed using planar silicon-based wafers (such as silicon nitride), which are well-known for their ability to recognise protons and detect pH because of their hydroxyl and amino groups on the surface.[62] With an illumination area within 1 mm^2, localised sensing information from different chemistries can be detected and simultaneous measurement of 23 sites can be achieved with a single chip.[46] Moreover, McConnell et al. successfully used a silicon-based LAPS system to monitor cell activity stimulated by different substances.[62] It has also been reported that the LAPS system can be used to monitor extracellular potentials.[13] Thus, the LAPS system is very practical and it has multiple potential applications and it is still used today.[63, 64]

However, in addition to its advantages, the LAPS system has some disadvantages that should be addressed. Except for its accuracy, selectivity and sensitivity, two aspects

of the LAPS system still need to be improved: (i) the measurement rate and (ii) spatial resolution.[65]

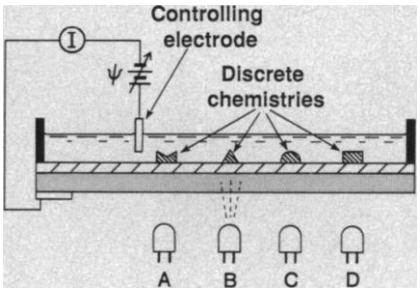

Figure 10. Illustration of a LAPS system based on a silicon wafer (grey section). Light-emitting diodes (LEDs) are placed at different position (A, B, C, D) to illuminate different chemistries. With the help of a reference electrode, the photocurrent change at different positions can be detected. Ref [46] copyright 2009 Springer-Verlag.

Many studies have been conducted to improve the measurement rate of the LAPS system. The photocurrent scanning method is a domain technique that has been used to improve the measurement rate for high speed detection.[66, 67] Zhang et al. further studied the measurement rate by analysing the digital photocurrent signal scanned on the frequency domain using a modulated laser pointer.[68] Another way to improve the measurement rate is using parallel read-out sensing arrays to obtain the signals from different arrays at the same time; this approach is employed in typical ISFET devices, which have been used to detect enzymatic substrates,[69] pH,[70] urea,[71] glucose,[72] heparin[73] and some proteins[74]. However, as described in the previous section, it is difficult to produce the hardware of the ISFET sensing arrays because multiple wires are needed. In our project, an QD-electrode with different sensing arrays was used to enhance the parallel detection to improve the multi-detection measurement rate.

Spatial resolution is another aspect of the LAPS system that also needs to be improved. There many parameters that can enhance the spatial resolution of a semiconductor-based LAPS device, such as the light spot size, carrier diffusion length, interface charge and light beam scattering.[4, 5, 75-78] In the project presented this chapter, the light spot size was significantly decreased to improve the resolution (Section 3.2). The QD-electrodes were used to decrease the carrier diffusion length to further increase the resolution (Section 3.3).

3.2 Light spot size

The light source is an important aspect for improving the spatial resolution.[64, 78] As the size of the light spot applied on the PEC electrode decreased, it was possible to obtain more information when scanning the light spot over the electrode.

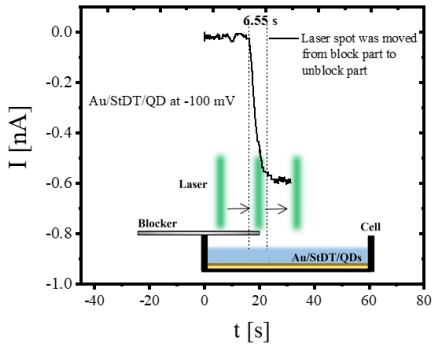

Figure 11. Illustration of the method used to calculate the laser spot size (inset) and the related photocurrent curve. Ref [51] copyright 2019 American Chemical Society.

The light source used in this project was a 532 nm laser; the size of the light spot was adjusted to be as small as possible for high resolution measurement. The laser spot size was characterised using a scanning method with continuous photocurrent measurement (Figure 11). In detail, the laser was moved over the electrode surface, which was covered with a sharp-edged blocker made by a black acrylic plate (inset of Figure 11). When the laser spot was applied to the blocked side of the electrode, no photocurrent was detected. When the laser spot was moved from the blocked side to the unblocked side, the photocurrent took Δt to reach its maximum. The zero photocurrent refers to the laser spot fully on the blocked side, and the maximum photocurrent refers to the laser sport fully on the unblocked side. Then, if the moving speed is constant and defined as v_{laser}, the laser spot diameter d_{laser} can be calculated as $d_{laser}=\Delta t^* v_{laser}$. Finally, the spot diameter is 0.3 mm, resulting in an illuminated electrode surface area of 0.07 mm^2. In comparison with the 1 mm^2 surface area results previously reported for the LAPS system,[46] undoubtedly, in this project, the light spot size was significantly improved. Thus, it was able to achieve better resolution.

3.3 QD-electrode

According to the literature, for Si-based material, the diffusion length of the charge carriers in the wafer is around 1 mm. Much effort has been made to decrease the diffusion length in the LAPS system by limiting the movement of charge carriers in a small area.[46] At first, the semiconductor electrode surface can be masked with an insulating layer so that only the localised part has contact with the electrolyte. Second, the lifetime of the minority carriers were decreased by doping additional materials in the silicon. Third, the continuous silicon-based wafer could be modified to become discrete silicon islands, so the distance between each island will stop the diffusion of the charge carriers.

In this project, inspired by the third method, the quantum dots (QDs) that are immobilised on the electrode act as very small-sized discrete islands. Moreover, there is no electrical connection between the QD "islands", so the charge carriers' diffusion between the QDs is limited. Thus, a very short diffusion length and higher spatial resolution are achieved.

3.3.1 Quantum dots

These years, an increasing number of materials have been fabricated to nanoscale showing distinct properties from the related bulk materials.[79] Typically, the nanocrystals are defined as 1-100 nm range including noble metal nanocrystal and semiconductor nanocrystal.[80] According to the quantum confinement effect, when size decreases to a certain level, the electrical energy states become discrete as shown in Figure 12.[80, 81] Based on this, semiconductor NPs show unique properties of optical,[80] electronic,[82] magnetic,[83] thermal[84] and superconductive aspects[85]. After years' development, more and more novel NPs were invented and the NPs' size, shape, composition and surface modification has been more and more controllable.[86, 87]

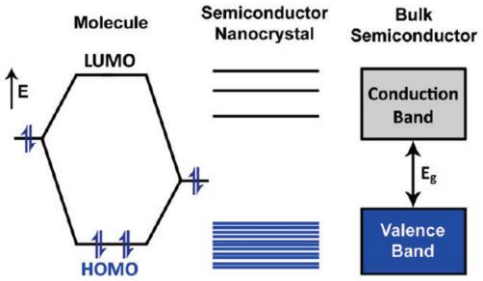

Figure 12. Diagram of the energy stare changes among bulk semiconductor, semiconductor nanoparticle, and molecule. Ref [80] copyright 2009 American Chemical Society.

Colloidal CdSe quantum dots (QDs) are stable colloidal nanomaterial that has been well studied showing well-controllable size and fluorescence range.[79, 88, 89] In the very beginning, the synthesis of QDs are mainly focused on the CdE (E=S, Se, Te), using rapid injection method to obtain homogenous crystallite with size-dependent optical properties.[90] As early as 1995, Prof. Paul Alivisatos from University of California Berkeley has introduced small-sized semiconductor material and his group is still working on the physicochemical properties and controlled synthesis of QDs today.[87, 91] After years development, the concept of QDs has been extended from the original type to novel ones including perovskite QDs, carbon QDs and other inorganic QDs without toxic heavy metals.[20, 92] More QDs related engineering has been developed with sophisticated techniques to transfer hydrophobic QDs to aqueous phase to be compatible with biological system.[79] Many applications are developed as well that QDs can be used for light-emitting diodes,[93] artificial photosynthesis[94], nanomedicines[95] and fluorescence markers to trace ions[96], tumor cells[97], and intracellular gene[98].

QDs also have great potential to design diverse PEC electrodes on which QDs act as signal chain to transfer reaction signals for biological detection.[50, 81] Furthermore, when QDs are used to decorate sensing electrode, there is larger surface area-to-volume with more contact area to analytes resulting in larger photoelectric signal. In addition, QDs immobilized on the electrode act as separate islands to limit charge carriers in a restricted area, which can improve the electrode literal resolution comparing with original LAPS device.[1] Thus, QDs immobilized PEC electrode is still worth to further studied and used in the project here.

In this paper, CdSe/ZnS core/shell QDs are used to build QD-electrode to improve the resolution of LAPS system, and to further build multiplex sensing chip for

simultaneous detection of different substrates. A ZnS shell is coated on CdSe QDs surface because the inorganic ZnS shell can effectively improve stabilization and electron utilization of CdSe core by trapping charge carriers at the interface.[80] The ZnS amounts used was carefully calculated by CdSe core size and ZnS shell thickness. From the literature, for single monolayer ZnS shell the thickness is around 0.31 nm and around 1 or 2 monolayers the quantum yield of QDs shows the maximum level.[79] Eventually, the CdSe/ZnS core/shell QDs are synthesized with 1.2 monolayers ZnS and the synthesized QDs are shown in Figure 13, diameter d_{cs}=4.6±1 nm and absorption peak at 533 nm.[51] The size and absorption peak is specially designed according to the 532 nm laser source we have, which can effectively reduce the instrument cost.

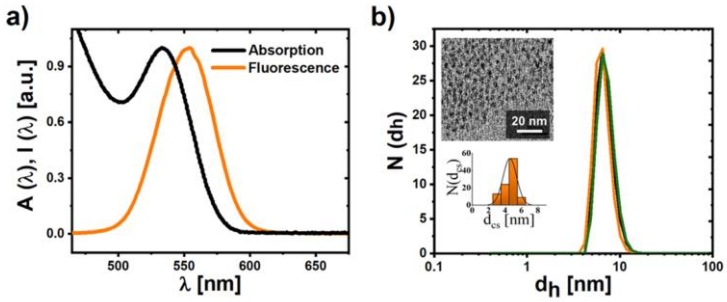

Figure 13. (a) The spectra of absorption A(λ) and fluorescence I(λ) in toluene and (b) the DLS results with three independent measurements from the CdSe/ZnS core/shell QDs. The inset in (b) refers to the TEM result of the QDs. Ref [51] copyright 2019 American Chemical Society.

3.3.2 The immobilization of QDs on electrode

As shown in Figure 14a, the CdSe/ZnS QDs are firmly immobilised on a planar electrode based on the SAM of trans-4,4'-stilbenedithiol (StDT). Khalid et al. discussed the variations in photocurrents when different SAMs molecules are used.[99] They verified that StDT results in a larger and more stable photocurrent than benzenedithiol and biphenyldithiol. With thiol groups, the sulfur atom of StDT can strongly bind to the metal and the QDs (Figure 14a). In this scenario, the StDT layer plays two roles. First,StDT is insulating, so when the light is off there is no electron exchange between the QDs and the electrode, thereby significantly improving the signal-to-volume ratio of the sensing system. As seen in Figure 14b, the time dependence from photocurrent at -100 mV from the Au/StDT/electrode indicates

that a stable photocurrent with small noise can be detected over a reasonable amount of time. Second, the StDT layer can be used to build the structure with an electrical disconnection between the QDs, limiting the electron diffusion and improving the resolution of LAPS system. Thus, applications capable of multiplex detections and photocurrent imaging for enzyme array can be achieved, as described in the next section.

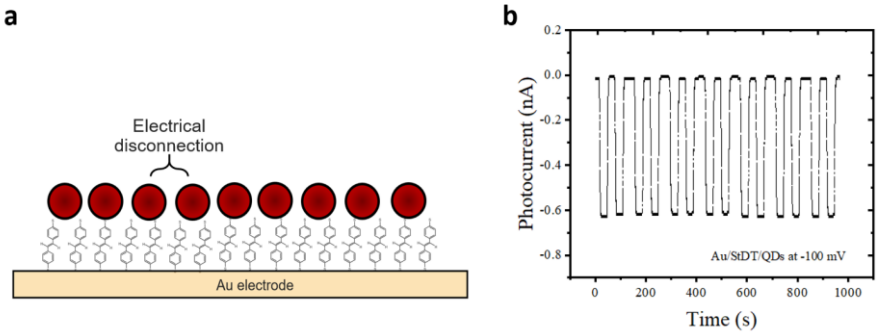

Figure 14. (a) Illustration of quantum dots (QDs) immobilised on a gold electrode (AuE) by trans-4,4'-stilbenedithiol (StDT). (b) Photocurrent from the Au/StDT/QDs electrode in a reasonable time at a constant potential of -100 mV vs. Ag/AgCl under 532 nm light in 0.01 M PBS (pH=7.4). Ref [48] copyright 2019 American Chemical Society.

3.4 Multiplex detection using enzyme arrays

With developments in the sensing field, different types of sensors have been built, including a bioaffinity sensor and a biocatalytic sensor. Affinity sensing devices usually rely on strong binding between biological molecules, such as antigen-antibody, lectin-sugar, membrane receptor-membrane protein and DNA aptamers.[24, 47, 53] The affinity ensures that the sensing device has high sensitivity and good selectivity, so it can be used in the many fields of food safety, pollution control and medical treatments.[53]

Although many types of binding assays are available, an enzymatic assay is still widely used to build a biocatalytic sensor. This is because of not only its high specificity and oldest history,[100] but also the simple fabrication of fully covered enzyme-electrode by pipetting.[51] Enzymes are catalytic proteins (few RNA) that accelerate the reactions of cell metabolism and energy generation under very mild conditions. Substances that can react with enzymes are defined as substrates. The reaction rate

(*v*) between the enzyme and the substrate (*S*) can be described using the Michaelis-Menten equation (Eq. 2), where K_M is the Michaelis-Menten constant and *Vmax* is the maximum rate of the enzymatic reaction.

$$v = \frac{v_{max}[S]}{K_M + [S]} \qquad \text{(eq.2)}$$

Different enzymes can be used, including oxidase (e.g. GOx and SOx), peroxidase (e.g. horseradish peroxidase [HRP]) and dehydrogenase (glucose dehydrogenase).[30, 101-103] In the reactions of oxidase, oxygen is consumed, which allows for building the enzyme-oxygen-electrode. Development of the enzyme-oxygen-electrode can be traced back to 1956, when Clark detected the glucose concentration via the oxygen content.[100, 104] Since then, the enzyme-electrode has drawn much research attention, and it has been developed rapidly. Today, the enzyme electrode has been applied in many fields; it is especially used in biosensors due to its high sensitivity, high specificity, rapid response, good selectivity and easy immobilisation.[30, 31, 34, 105]

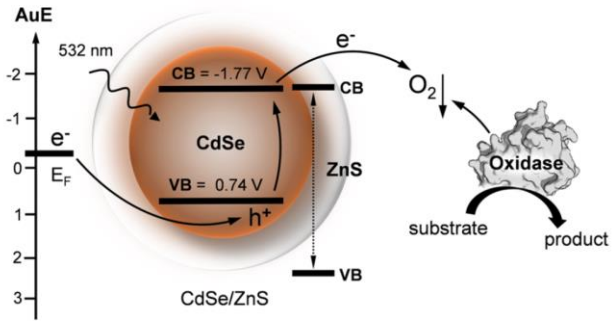

Figure 15. The sensing mechanism of using Au/QDs/enzyme electrode to detect substrate. Ref [51] copyright 2019 American Chemical Society.

In the project discussed in this paper, CdSe/ZnS QDs were immobilised on an AuE by StDT, and the enzyme (SOx or GOx) was easily immobilised on the QDs surface by cross-linking using a pipette. The sensing mechanism of the enzyme-oxygen-electrode (Au/QDs/enzyme) in the PEC system is shown in Figure 15. In detail, under illumination, the electron-hole pairs separated in the QDs. The electrons were transferred from the Fermi level (E_F) of the AuE to the holes in the VB of the QD by tunnelling through the insulated StDT layer. At the same time, oxygen grabbed the

electrons from the CB on QDs to contribute to the photocurrent that was generated. Meanwhile, the enzymatic reactions consumed oxygen, resulting in decreased oxygen concentration in the solution. Thus, as the enzymatic reaction progresses, less and less oxygen can be used in the solution. Consequently, a photocurrent decrease was detected, indicating that the substrate concentration changed.

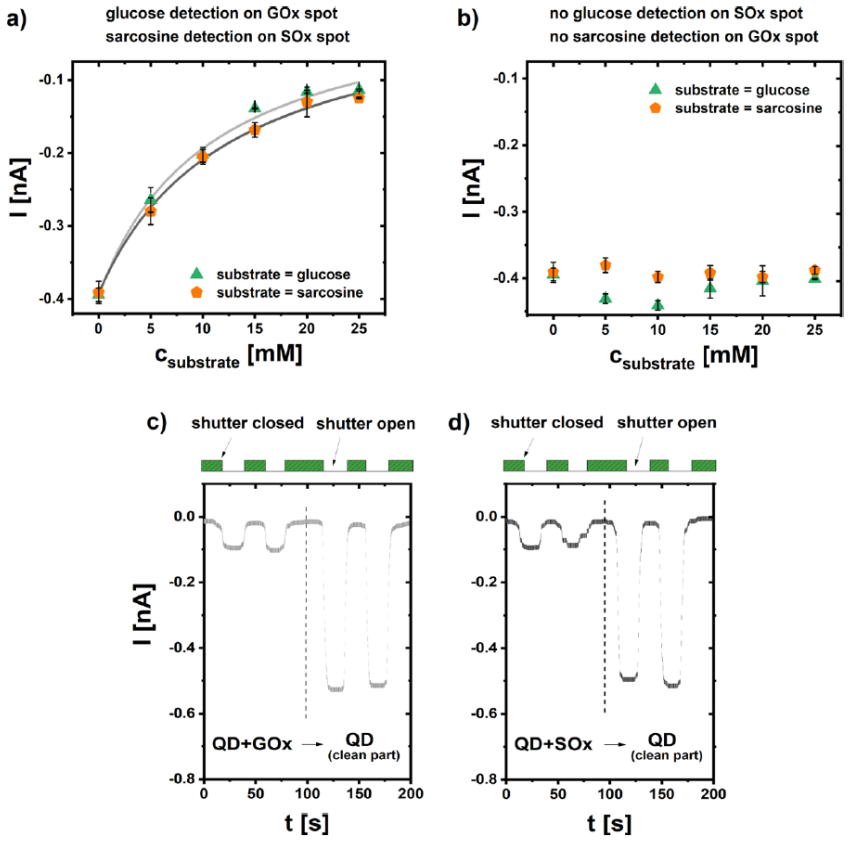

Figure 16. The photocurrent response from the enzyme-electrode with single enzyme array immobilized that (a) using glucose oxidase (GOx) and sarcosine oxidase (SOx) to detect glucose and sarcosine, respectively. (b) Control experiments using GOx electrode to detect sarcosine and using SOx electrode to detect glucose. Laser was moved from the section without enzyme to the section with enzyme of (c) GOx and (d) SOx. The experiments are finished under a 532 nm laser with Ag/AgCl reference electrode at -100 mV vs. Ag/AgCl in air-saturated 0.01 M PBS (pH=7.4). Ref [51] copyright 2019 American Chemical Society.

When a single enzyme array was immobilised on the Au/QDs electrode surface, the related photocurrent decreases when light was applied on the enzyme (Figure 16). Glucose can only be detected in the GOx section and sarcosine can be only detected in the SOx section. Thus, when localised light was applied on the enzyme-electrode

surface, the successful immobilisation (presence) of the enzyme and the related enzyme activity were monitored by the decrease in the photocurrent.

To improve the sensing efficiency of devices, it is necessary to develop multiplex sensors. Based on the excellent results from the Au/QDs/enzyme electrode with a single enzyme array, more enzyme arrays were used to fabricate a multiplex sensor. As shown in Figure 17, GOx and SOx were immobilised together, realising three sections on the electrode: the GOx section, the SOx section and the QDs reference section. When the localised light moved to the enzyme section, only the corresponding substrate was detected. The reference section was used to ensure that the QD-electrode always worked well, and did not contribute to a decrease in the photocurrent, to ensure that the photocurrent decrease was only based on the enzymatic reactions.

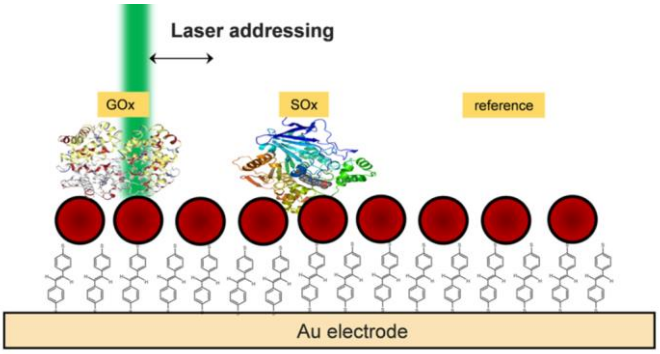

Figure 17. The light-addressable measurement using a localised light applied on the Au/QDs/enzyme electrode scanned among different sections (GOx section, SOx section, QDs reference section). Ref [51] copyright 2019 American Chemical Society.

The multiplex and parallel sensing results are shown in Figure 18. When the localised light spot was moved in parallel from the reference section to the GOx section and then to SOx section, different photocurrent responses were obtained in different analytes. When measured in glucose, the photocurrent decrease can only be seen when the light is moved to the GOx section. When measured in sarcosine, the photocurrent decrease can only be observed when the light is moved to the SOx section. When measured in the mixture of glucose and sarcosine, the photocurrent decrease can be found in both the GOx and SOx sections. Most importantly, the concentration dependences of the substrate detections for each section conform well with the results of the single enzyme array (Figure 16). Thus, the enzyme arrays chip shows excellent selectivity. For all three types of solutions, the photocurrent

remained stable in the reference section, indicating that the photocurrent change was from the enzymatic reactions.

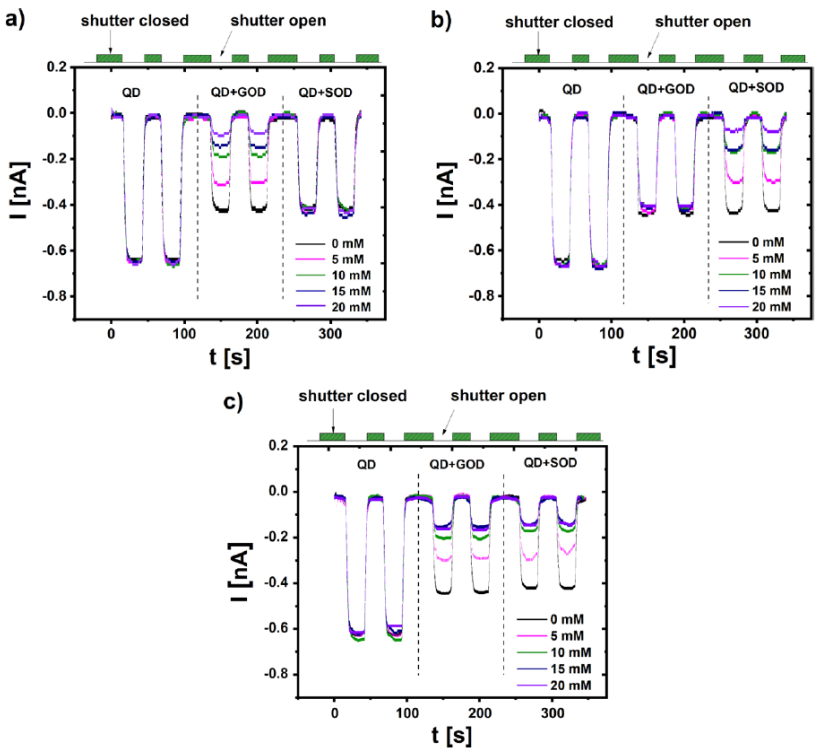

Figure 18. The parallel detections in three type solutions of (a) glucose, (b) sarcosine, (c) the mixture of glucose and sarcosine with laser moved from reference section to GOx section and then to SOx section. 532 nm laser was used as light source and measurements are finished at -100 mV vs. Ag/AgCl reference electrode in PBS (pH=7.4). Ref [51] copyright 2019 American Chemical Society.

3.5 Photocurrent imaging

Recently, photocurrent imaging has been used to study the local transport of the charged carriers of semiconductor nanowires, including generation, recombination and diffusion.[106, 107] In the project discussed in this paper, based on the photocurrent imaging, it was possible to determine the light spot size (section 3.2) and the enzyme (size and activity) distribution of the enzyme arrays. The results are shown in the photocurrent curves with a constant speed (v_{laser}) when the laser spot scans over the enzyme arrays on the electrode surface back and forth, in both the x- and y- direction (Figure 19a,b). As seen, the photocurrent only decreases when the laser light spot is applied on the enzyme part. The decrease in the photocurrent is larger when the laser light spot is on the edge of the enzyme array in comparison to

when it is on the centre of the enzyme array, indicating higher enzyme concentration (higher activity) on the edge This is supported by the corresponding microscopic image of the enzyme array seen in Figure 19c. Thus, the enzyme activity distribution can be seen from the photocurrent curves (Figure 19a and 19b). Finally, when the photocurrent decreasing time is *t*, the enzyme array size used in the multiplex chip is calculated by v_{laser}*t as 1.9 mm × 1.3 mm, which is consistent with the value obtained from microscopy (Figure 19d).

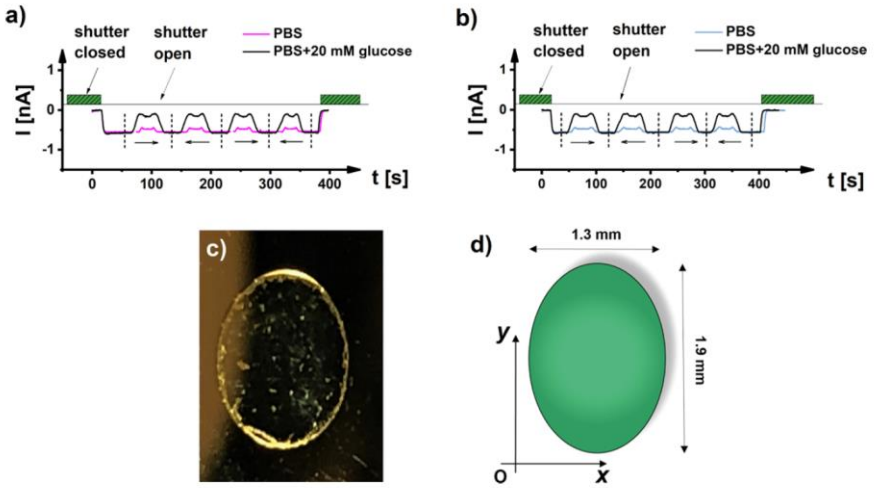

Figure 19. The parallel detections in (a) glucose, (b) sarcosine, (c) the mixture of glucose and sarcosine with laser moved from reference section to GOx section and then to SOx section. 532 nm laser was used as light source. Measurements are finished at -100 mV vs. Ag/AgCl reference electrode in 0.01 M PBS (pH=7.4) Ref [51] copyright 2019 American Chemical Society.

4. Nanozyme-based Enhanced PEC Sensor

There are two problems should not be ignored in the multiplex sensing system discussed in the last section. First, natural enzymes are widely known for their easy inactivation; they are also very expensive, hard to store and very sensitive to the environment. And when enzyme is immobilized on the electrode, the fall of enzyme from the electrode could induce unstable photocurrent. Second, the CdSe/ZnS QDs contain toxic heavy metallic ions, so that the applications of QDs in vivo should be avoided. To solve those problems, an idea is that nontoxic NPs can act the roles of both enzyme with catalytic properties and semiconductor to generate photocurrent. Thus, another project based on nanozyme NPs in aqueous solution was conducted and discussed in this section.

4.1 Nanozyme

As an emerging artificial novel nanomaterial, nanozymes have intrinsic enzyme-like catalytic activities; to a great extent, they can also can overcome the disadvantages of the natural enzyme previously mentioned.[108] Thus, as shown in Figure 20, many nanozyme applications have been developed in the field of biosensors,[109] disease therapy,[110] ultraviolet (UV) protection and anti-bacterial,[111] dealing with pollutants (heavy ions).[112] In addition to its use for detecting substances in vitro, nanozymes can be used to detect substances in vivo, such the tracing glucose in the brain of a live mouse.[113] This is attributed to the excellent stability, non-toxicity, biocompatibility and effective ROS regulation properties of NPs.

The nanozyme concept can be traced back to 2004 when Manea at al. used functionalised Au nanoclusters as a substitute of hydrolase for the cleavage of 2-hydroxypropyl p-nitro-phenyl phosphate (HPNP).[114] Since then, an increasing number of nanozymes have been discovered with different categories (Table 1). Some of the nanozymes can only mimic single enzyme, such as the Fe_3O_4 magnetic NPs that mimick peroxidase acting as an electron acceptor from substrates.[115] The nanozyme concept can be traced back to 2004 when Manea at al. used functionalised Au nanoclusters as a substitute of hydrolase for the cleavage of 2-hydroxypropyl p-nitro-phenyl phosphate (HPNP).[114] Since then, an increasing number of nanozymes have been discovered with different categories (Table 1). Some of the nanozymes can

only mimic single enzyme, such as the mimicking of peroxidase by Fe_3O_4 magnetic NPs, which can act as an electron acceptor from substrates.[115] Other nanozymes, such as naked Au NPs, show oxidase-like activity, and they can catalyse the transition of glucose to gluconic acid.[116] Still other nanozymes can mimic more than one enzyme at the same time, such as cuprous oxide (Cu_2O) NP and ceria (CeO_2) NP. Cu_2O NPs have catalytic properties that are similar to those of HRP and GOx. CeO_2 NPs can mimic the enzymes of both oxidase and catalase with intrinsic cyclic redox properties, due to the reversible change between Ce^{3+} and Ce^{4+} on the surface.[108] Thus, nanozyme NPs acting as a substitute for natural enzymes were used in the project discussed in this section.

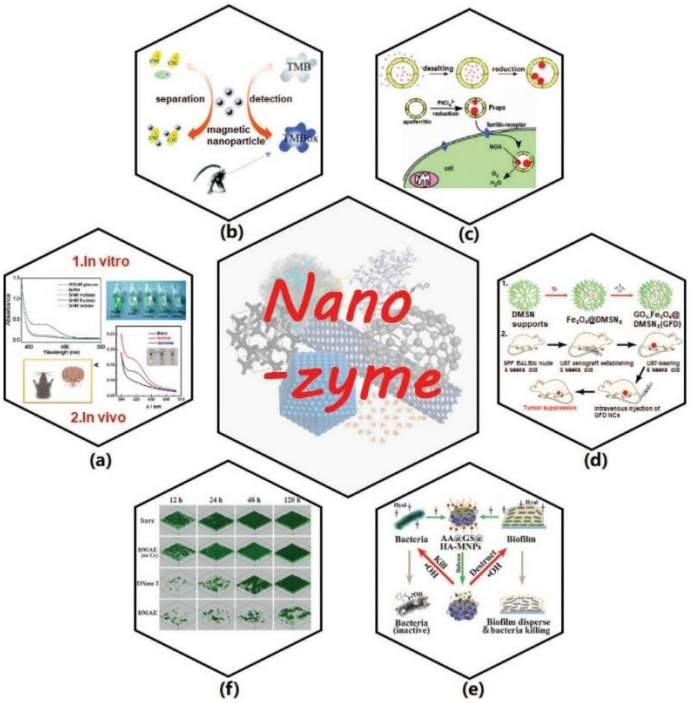

Figure 20. The diverse applications of nanozyme which can be used for sensor in vivo, tumor control, oxidation resistance and anti-bacteria. Ref [117] copyright 2019 Wiley-VCH.

In the project discussed in this section, the CeO_2 nanozyme was synthesized and immobilised on the AuE to replace the QDs/enzyme unit in the previous doctoral project. The CeO_2 nanozyme not only mimics the enzyme properties of peroxidase,[118] catalase[119] and superoxide dismutase,[120] it also has the properties of an *n* type semiconductor UV absorber with excellent optical electrical properties. It has been verified that CeO_2-based material has great potential for use

in PEC applications with photocurrent generation.[121,122] The mechanism of photocurrent generation from pure CeO_2 NPs is shown in Figure 21. Thus, the introduction of the nanozyme in the PEC system can overcome the disadvantages of natural enzymes and QDs, reduce the self-assembly step of the enzyme on the Au/QDs electrode and improve the instability caused by the enzyme falling off of the Au/QDs electrode surface.

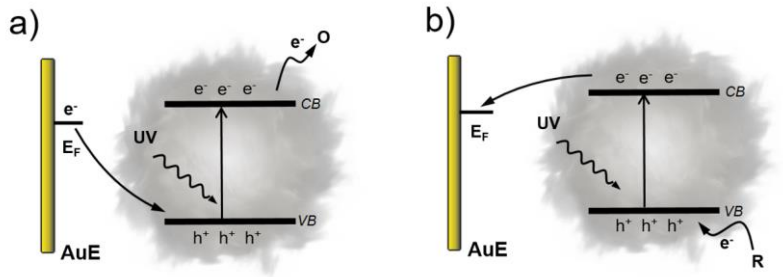

Figure 21. The photocurrent from pure CeO_2 NPs at (a) cathodic direction and (b) anodic direction. O and R refer to electron accepters and electron donors in the solution, respectively.

Nanozymes	Activity/Mechanism	Application
Au	POD	Early cancer diagnosis, combat biofouling
Au-NH_2	CAT	O_2 nanogenerator for US and MR dual modality imaging
Au/Pt	POD	Signal-amplified colorimetric immunoassay
Au/MOF	POD	Detect biomolecules
Au@MIL-101@GOx	POD	Measure glucose and lactate
V_2O_5-PDA-Au	POD, GOx	Detect biomolecules
Pt	SOD, CAT	Neuro protection
		Biomarker assays
		Reduce ROS
Fe_3O_4	POD, CAT	Decrease cytotoxicity, delay aging and ameliorate neuro degeneration, biofilm elimination, dental therapy, protein detection
Fe_3O_4@linoleic acid	Fenton-like	Single oxygen generation for cancer therapy
Fe_3O_4/rGO	POD	Kill bacteria and wound repair
Fe_3O_4/GOx/C(Si,GO,ZIF-8,polymers)	POD	Glucose detection
CeO_2	SOD, CAT	Cell protection in radiation Anti-inflammation, neuro protection, anticancer treatment, wound healing, reduced tumor growth,
CeO_2-folic acid	POD	O_2 nanogenerator for US and MR dual modality imaging, combat biofouling
Mn_3O_4	SOD, CAT, GPx	Cytoprotection in Parkinson's disease
Co_3O_4	POD, SOD, CAT	Immunohistochemistry detection
V_2O_5	GPx, POD	Cell protection, combat biofouling
MoS_2	POD	Antibacterial, wound healing
C_{60} fullerene derivatives	SOD	Protection against xenobiotic-induced oxidative stress, neuro protection, improving the oxidative stability of polymers at elevated temperatures
Graphene quantum dots	POD	Wound disinfection
Prussian blue ($KFe^{3+}[Fe^{2+}(CN)_6]$)	POD, CAT, SOD	Protection against oxidative stress

Table 1. Different types of nanozymes studied recent years and their related applications. Ref [117] copyright 2019 Wiley-VCH.

4.2 Hybrid nanomaterial

To improve the spatial resolution of the multiplex sensor described above, a very small illumination spot was applied, which induces a photocurrent amplitude from the enzyme-based multiplex chip that is very small (< 1 nA). Thus, the photocurrent must be improved to obtain a better detection limit, especially when the photocurrent keeps decreasing as the substrate concentration increases (see Figure 17 and Figure 18).

Due to the rapid development of nanotechnology, scientists have begun to engineer novel materials by combining ones with different properties to obtain enhanced or new features.[123] In this section, hybrid nanomaterials are introduced to compare with the basic semiconductor CeO_2 NPs to build a PEC electrode to enhance the photocurrent. An Au core is synthesised inside the semiconductor CeO_2 NPs to obtain hybrid Au/CeO_2 core/shell NPs (Figure 22). The new hybrid NPs have the photoelectrical properties inherited from the CeO_2 part and the LSPR properties inherited from the Au core part. Most importantly, the hybrid NPs provide extra enhancement based on the construction of the semiconductor-metal interface.[124] Moreover, in terms of light conversion, the original pure CeO_2 NPs can only absorb the irradiation in the UV range,[111] but the hybrid NPs can utilize UV light and visible light, thereby effectively enhancing the resulting photocurrent.

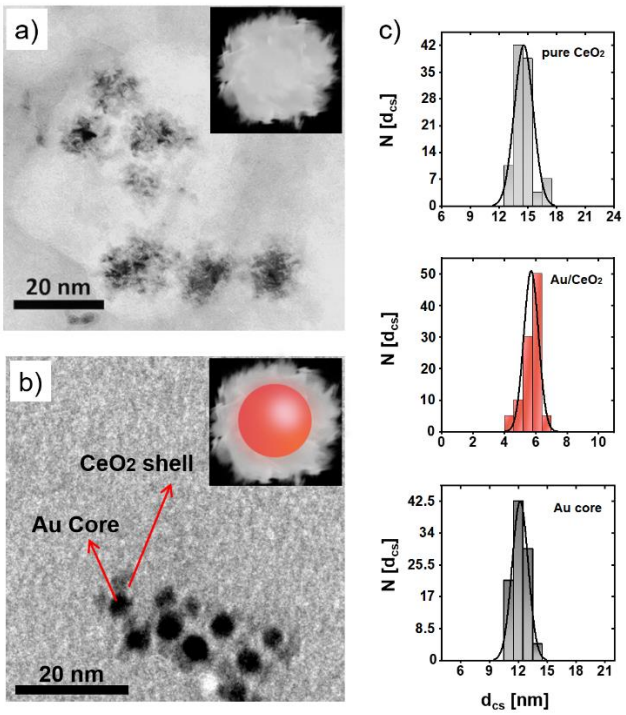

Figure 22. Transmission electron microscopy (TEM) images of the pure CeO_2 NPs and hybrid Au/CeO_2 core/shell NPs. (c) The "hydrodynamic" distribution of NP size N[d_{cs}] from the diameter of NPs.

To verify the photocurrent enhancement by the hybrid NPs, single layer of CeO_2 NPs and Au/CeO_2 NPs are immobilised on the AuE for the PEC measurement. Because both NPs are stabilised by citrate, they show negative surface potentials. Cysteamine aqueous solution was used to modify the Au surface to obtain a positive surface charge so that the NPs can be immobilised on the electrode by electrostatic interactions. In comparison to the SAM technique using covalent bonds as linker between NPs and electrode, it has been verified that the SAM using electrostatic interactions has a larger photocurrent.[16] The photocurrent results under white light are shown in Figure 23. As seen, the photocurrent more effectively improved in the hybrid NPs than the pure CeO_2 NPs at each potential, indicating the successful deposition of NPs on the electrode and the benefit from the hybrid NPs in the photocurrent generation. Moreover, the NP numbers were evaluated via Quartz crystal microbalance (QCM); the results show that the NP number (per cm^2) is comparable between the CeO_2 NPs and the hybrid NPs ($n_{CeO2}=(7.3\pm0.1)\times10^9$ and $n_{Au/CeO2}=(5.9\pm0.1)\times10^9$). Thus, the number of NPs on the electrode is not responsible for the photocurrent enhancement from the hybrid NPs.

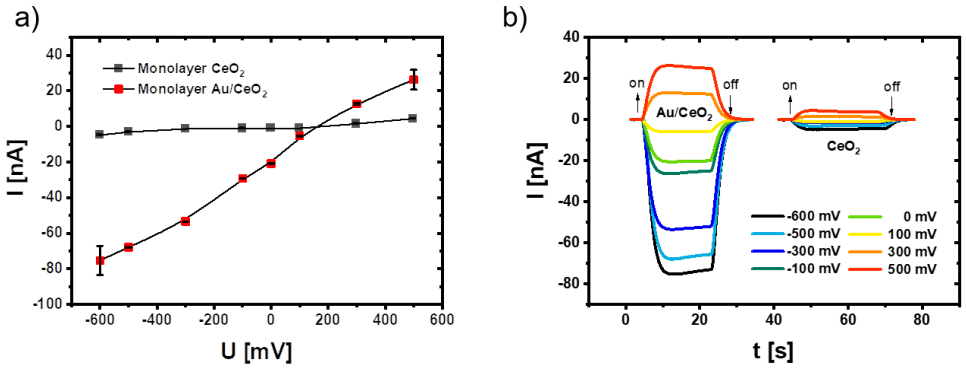

Figure 23. (a) The potential dependence from photocurrent from single layer CeO_2 NPs and hybrid Au/CeO_2 NPs immobilized on the electrode. (b) The photocurrent curves from single layer CeO_2 and hybrid Au/CeO_2 NPs. All the results are measured under white light in 0.01 M PBS (pH=7.4).

4.3 Layer-by-Layer (LbL)

Introduced three decades ago,[50] layer-by-layer (LbL) has been widely used as coating technique in diverse fields. When applied to a metal surface, an LbL coating can provide anti-corrosion or anti-graffiti properties.[125, 126] For metal implants, the LbL coating can help create an antibacterial surface.[127, 128] Moreover, LbL can be applied as a purification technology for fabricating liquid or gas permeation membranes.[129] In biological applications, LbL can be used for cell surface engineering by mild coating, and for drug delivery as vehicles for micro- and nanoencapsulation.[130-132]

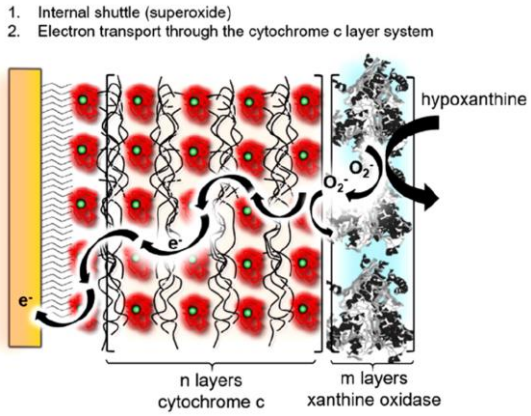

Figure 24. LbL can be used for the nanomaterial immobilization on sensing electrode. Ref [50] copyright 2019 American Chemical Society.

Surface LbL can also be used in PEC sensing applications.[1, 133-135] As described above, the generated photocurrent is generally based on the number of free electrons activated from the light-sensitive materials and exchanged with the working electrode. The LbL coating can increase the number of electrons by effective increasing the coverage of the NPs that are immobilised. My previous studies have verified that the PEC electrode with LbL-coated NPs can both increase the signal amplitude and the signal-to-noise ratio of the system. Moreover, an LbL coating has a porous structure, which can be penetrated to let analytes (such as oxygen and substrates) contact the NPs in each of the layers.[33, 99, 101] When NPs are immobilised in an LbL structure, an electron chain is feasible due to the electron transfer from the outermost layer to the electrode through different layers (Figure 24).

In this paper, together with the hybrid NPs technique, LbL technique is used to further enhance the photocurrent by increasing the number of NPs and building a three-dimensional structure that are immobilised on the electrode (Figure 25a). From Figure 25b, it can be seen that the multilayer NPs have an obvious photocurrent in comparison to the single layer NPs (Figure 23) for both the CeO_2 NPs and the Au/CeO_2 NPs. As the number of layers increases, the related photocurrent increases linearly for both the anodic and cathodic values. Moreover, the photocurrent enhancement is greater in the hybrid NPs than in the pure CeO_2 NPs. The mechanism of the photocurrent enhancement from the hybrid NPs was studied using wavelength dependence measurements (Figure 26). Different wavelengths of monochromatic light were used to generate the photocurrent. As seen, at visible light, only the hybrid NPs show photocurrent activity; no photocurrent activity is seen in the pure CeO_2, indicating that LSPR at visible light is responsible for the photocurrent activity from the hybrid NPs. These results firmly verify that the hybrid NP has better photoelectrical properties, and that the LbL method can enhance the photocurrent.

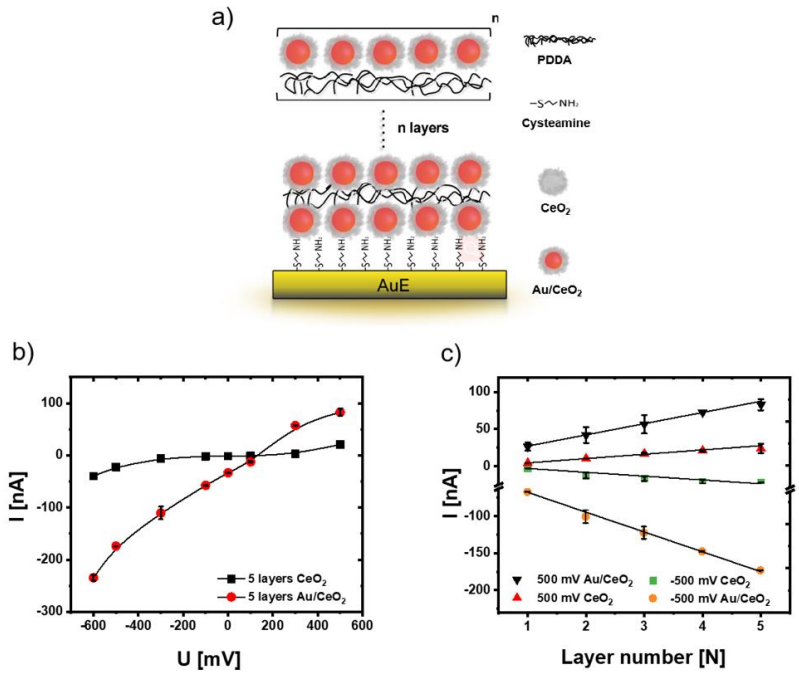

Figure 25. (a) The diagram of multilayer structure immobilized on the PEC working electrode. (b) Potential dependence from 5 layers CeO_2 NPs and 5 layers Au/CeO_2 NPs. (c) Layer number dependence from 5 layers CeO_2 NPs and 5 layers Au/CeO_2 NPs at +500 mV and -500 mV vs. Ag/AgCl. The whole measurements are finished under white light in 0.01 M PBS (pH=7.4).

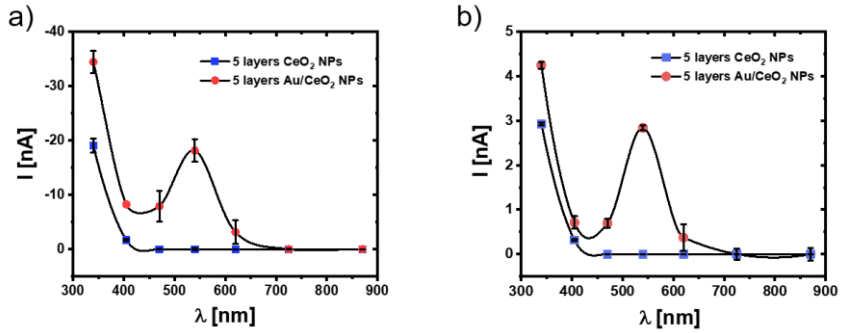

Figure 26. Wavelength dependence from photocurrent based on 5 layers CeO_2 NPs and 5 layers Au/CeO_2. at (a) +500 mV and (b) -500 mV vs. Ag/AgCl. Different filters are inserted between white light and the PEC cell to obtain monochromatic lights.

Moreover, the effect from the semiconductor-metal interface was studied using a mixture of the Au NPs and pure CeO_2 NPs (Figure 27). The diameter of the Au NPs was found to be similar to the Au core of the hybrid NPs. The NP mixture was used to

study the distance. It was found that the hybrid NPs had close contact with the semiconductor-metal interface. In the mixture containing the Au NPs and the pure CeO_2 NPs, distance between the CeO_2 NPs and the Au NPs was relatively longer than the hybrid Au/CeO_2 NPs. Eventually, the photocurrent difference in the PBS can be conducted as: $I_{(CeO2)} < I_{(mixture\ of\ AuNPs\ and\ pure\ CeO2\ NPs)} < I_{(hybrid\ Au/CeO2)}$. This result indicates that the closed contact of the semiconductor-metal interface plays an important role in the photocurrent enhancement from hybrid Au/CeO_2 NPs.

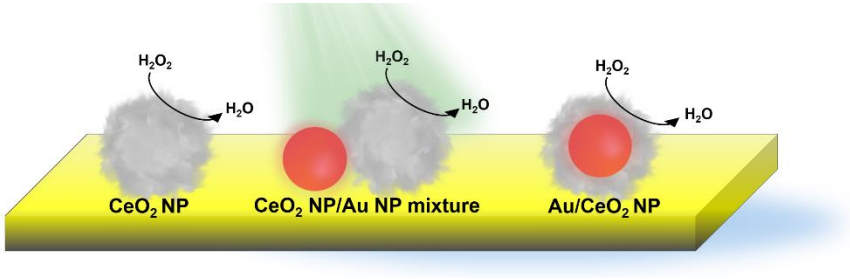

Figure 27. Three types of NPs are immobilised on the electrode for photocurrent measurements, CeO_2 NPs, a mixture of AuNPs and pure CeO_2 NPs, and hybrid Au/CeO_2 NPs.

4.4 H_20_2 detection

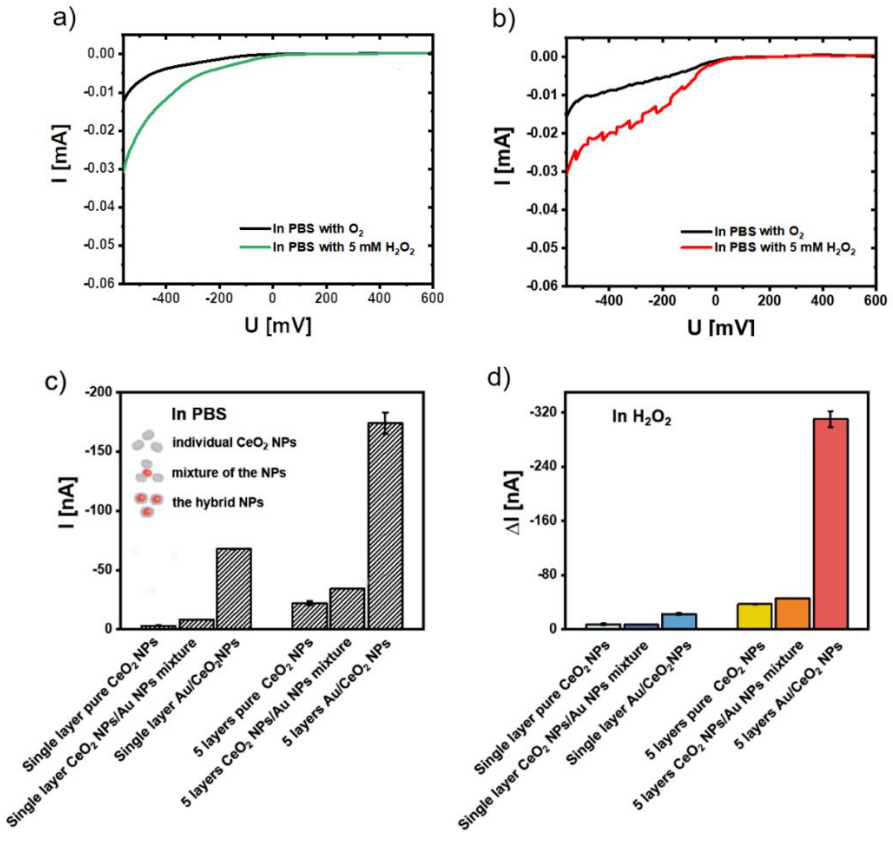

Figure 28. Chopped light voltammetry of (a) 5 layer CeO_2 NPs and (b) 5 layers Au/CeO_2 NPs in PBS and 5 mM H_2O_2. Comparison of photocurrent from single and multilayer CeO_2 NPs, mixture of AuNPs and pure CeO_2 NPs (N(CeO_2)/(N(CeO_2)+N(Au)) = 40% mixing ratio)), and hybrid Au/CeO_2 NPs (c) in PBS and (d) 1 mM H_2O_2. The whole results are obtained with white light in 0.01 PBS (pH=7.4). PEC results are obtained at -500 mV vs. Ag/AgCl.

Because CeO_2 NPs can mimic the properties of a natural enzyme, the catalytic properties of the CeO_2-elecrode were studied here using H_2O_2 detection. H_2O_2 is an important analyte for monitoring cellular activities, and because H_2O_2 is a by-product of many enzymatic reactions, studying H_2O_2 detection is meaningful.[136, 137] The catalytic property on H_2O_2 was initially studied using chopped light voltammetry. The obvious current enhancement after the addition of 1 mM H_2O_2 to five layers of the CeO_2 NPs indicates that the CeO_2 surface has excellent catalytic activity (Figure 28a). Furthermore, photocurrent enhancement due to the H_2O_2 response was seen in the hybrid Au/CeO_2 NPs in comparison to the CeO_2 NPs, indicating that the hybrid NPs had better photoelectrical properties (Figure 28a,b). From Figure 28c,d it can be seen that the photocurrent difference based on PBS and H_2O_2 detection was: $I_{(CeO2)} < I_{(\text{mixture of Au NPs and pure CeO2 NPs})} < I_{(\text{hybrid Au/CeO2})}$. Eventually, the good detection limit of H_2O_2 from 5 layers Au/CeO2 NPs 3 µM with a linear detection range of 2–1000 µM. These results firmly verify that the CeO_2 NPs has good catalytic properties based on H_2O_2 detection, and the hybrid NP provided a better PEC benefit than the pure CeO_2 NP.

Conclusions

The study's findings can be summarised as follows:

1. CdSe/ZnS QDs with a 533 nm absorption peak were successfully designed and synthesised based on the laser wavelength of 532nm. The QD-electrode was successfully fabricated to fix the QDs on the AuE. In comparison to the LAPS system, the charge diffusion in the QD-electrode was limited, enabling the PEC system to achieve higher spatial resolution. And the laser spot size is adjusted as small as possible for better resolution.

2. Very small-sized enzyme spots (GOx or SOx) were immobilised on the QD-electrode surface as arrays; this verifies that substrates can be detected successfully using a small enzyme array immobilized simply by pipetting. The successful detection of substrates also verifies that the enzymatic reaction can be monitor via oxygen dependence.

3. By immobilising two different enzyme arrays on a single chip, simultaneous multiplex detections of two substrates is feasible. The good selectivity, good practicability and high accuracy of the multiplex sensing chip was verified when there was an interference of a second enzyme substrate.

4. The multiplex detection verified that the enzymatic reactions are only active on the area that is illuminated. This supports the possibility of developing sensing chips with more than two enzyme arrays.

5. The photocurrent imaging technique characterised the enzyme array size as 1.9 mm × 1.3 mm. The photocurrent curves verify and visualise the enzyme activity distribution. Thus, it was also verified that the low-cost PEC system can fully satisfy the requirements for complex detections.

6. The CeO_2 nanozyme based PEC sensor was successfully built by immobilising CeO_2 NPs on the AuE. The catalytic properties and photoelectrical properties of the CeO_2 nanozyme were verified. The good catalytic properties of CeO_2 toward H_2O_2 makes it possible to use the CeO_2 nanozyme to replace the natural H_2O_2 enzyme. And also the CeO_2 nanozyme can generate photocurrent so that the utilization of the QDs can be avoided in PEC system.

7. Control experiments using a mixture of CeO_2 and AuNPs verifies that the close contact of semiconductor-metal interface plays an important on the enhancement.

8. The wavelength dependence results verify that photocurrent generation under visible light is feasible, and the Au core can enhance the photocurrent by LSPR. Consequently, a UV light source can be avoided in many applications to reduce biological damage.

9. The LbL method can be used to enhance the photoelectrical and catalytic properties of NPs by building three-dimensional structures introducing higher NPs coverage on the electrode. The hybrid NPs were found to have better catalytic and photoelectrical properties than the pure CeO_2 NPs.

Perspectives

In this paper, a multiplex sensing system was built to detect two enzymatic substrates simultaneously. They can be detected with single PEC chip by overcoming the interference from each other. In the future, a single sensing chip with more than two enzymic arrays will be developed to detect more substrates simultaneously. Several efforts to improve the photocurrent in both stability and amplitude will be introduced, to make sure the system can be applied not only in the lab but also in practical use. Eventually, the multiplex sensor should be integrated and fabricated as wearable size for commercial production.

In the meanwhile, more semiconductor nanomaterials will be tried to be synthesized in nanoscale for better photocurrent performance. Besides the basic photoelectrical properties for photocurrent generation, these nanomaterials should also have other interesting properties (such as thermal, magnetic and catalytic ones) for the development of diverse sensing applications. Different material, shape or size of metal core will be studied to support the semiconductor part to obtain better photocurrent enhancement. When the photocurrent is stable enough, further practical used could be considered.

On the other hand, the normal photocurrent was usually detected from bulk immobilisation of nanoparticles on the electrode, and it will be affected by the immobilisation technique and aggregation of nanoparticle on the electrode. Thus, the normal photocurrent from many nanoparticles on the electrode cannot uncover the real photoelectrical properties of this type nanoparticle. Based on that, the details of the enhancement mechanism from hybrid nanoparticles could be studied via the photocurrent from single nanoparticle via microscopy technique in the future.

References

1. Yue, Z., Khalid, W., Zanella, M., Abbasi, A.Z., Pfreundt, A., Rivera Gil, P., Schubert, K., Lisdat, F., and Parak, W. J., *Evaluation of Quantum Dots Applied as Switchable Layer in a Light-Controlled Electrochemical Sensor.* Analytical and Bioanalytical Chemistry, 2010. **396**: p. 1095-1103.
2. George, M., Parak, W. J., and Gaub, H. E., *Highly Integrated Surface Potential Sensors.* Sensors and Actuators B, 2000. **69**: p. 266-275.
3. Sartore, M., Adami, M., Nicolini, C., Bousse, L., Mostarshed, S., and Hafeman, D., *Minority Carrier Diffusion Length Effects on Light-addressable Potentiometric Sensor (LAPS) Devices.* Sensors and Actuators A, 1992. **32**: p. 431-436.
4. Parak, W. J., Hofmann, U. G., Gaub, H. E., and Owicki, J. C., *Lateral Resolution of Light Addressable Potentiometric Sensors: An Experimental and Theoretical Investigation.* Sensors and Actuators A: Physical, 1997. **63**: p. 47-57.
5. George, M., Parak, W. J., Gerhardt, I., Moritz, W., Kaesen, F., Geiger, H., Eisele, I., and Gaub, H.E., *Investigation of the Spatial Resolution of the Light-addressable Potentiometric Sensor (LAPS).* Sensors and Actuators A, 2000. **86**: p. 187-196.
6. Adami, M., Sartore, M., Baldini, E., Rossi, A., and Nicolini, C., *New Measuring Principle for LAPS Devices.* Sensors and Actuators B, 1992. **9**: p. 25-31.
7. Pecora, A., Fortunato, G., Carluccio, R., and Sacco, S., *Hydrogenated amorphous silicon based Light-Addressable Potentiometric Sensor (LAPS) for Hydrogen Detection.* Journal of Non-Crytalline Solids, 1993. **164-166**: p. 793-796.
8. Reshetilov, A. N. and Khomutov, S. M., *Development of FET- and LAPS-based biosensors.* Advances in Biosensors, 1995. **3**: p. 53-76.
9. Lee, W. E., Thompson, H. G., Hall, J. G., and Bader, D. E., *Rapid Detection and Identification of Biological and Chemical Agents by Immunoassay, Gene Probe Assay and Enzyme Inhibition Using a Silicon-based Biosensor.* Biosensors & Bioelectronics, 2000. **14**: p. 795-804.
10. Sasaki, Y., Kanai, Y., Uchida, H., and Katsube, T., *Highly Sensitive Taste Sensor with a New Differential LAPS Method.* Sensors and Actuators B, 1995. **24-25**: p. 819-822.
11. Jun, X., Ping, W., and Wuwei, F. *A novel Application of LAPS for the determination of serotonin*. Proceedings of International Solid State Sensors and Actuators Conference. Chicago, US.
12. Stein, B., George, M., Gaub, H. E., and Parak, W. J., *Extracellular Measurements of Averaged Ionic Currents with the Light-addressable Potentiometric Sensor (LAPS).* Sensors and Actuators B: Chemical, 2004. **98**: p. 299-304.
13. Parak, W. J., George, M., Domke, J., Radmacher, M., Gaub, H. E., Behrends, J. C., and Denyer, M. C., *Can the Light-addressable Potentiometric Sensor (LAPS) Detect Extracellular Potentials of Cardiac Myocytes?* IEEE Transactions on Biomedical Engineering, 2000. **47**: p. 1106-1113.

14. Stein, B., George, M., Gaub, H. E., Behrends, J. C., and Parak, W. J., *Spatially Resolved Monitoring of Cellular Metabolic Activity with a Semiconductor-based Biosensor.* Biosensors & Bioelectronics, 2003. **18**: p. 31-41.
15. Bousse, L., Mostarshed, S., D. Hafeman, Sartore, M., Adami, M., and Nicolini, C., *Investigation of Carrier Transports through Silicon Wafers by Photocurrent Measurements.* Journal of Applied Physics, 1994. **75**: p. 4000-4008.
16. Li, Z., Zhang, J., Li, Y., Zhao, S., Zhang, P., Zhang, Y., Bi, J., Liu, G., and Yu, Z., *Carbon Dots based Photoelectrochemical Sensors for Ultrasensitive Detection of Glutathione and Its Applications in Probing of Myocardial Infarction.* Biosensors and Bioelectronics, 2018. **99**: p. 251-258.
17. Shuang, Z., Jun, Z., Zhengping, L., Peixin, Z., and Yunxiao, L., *Photoelectrochemical Determination of Hydrogen Peroxide Using a Gold Electrode Modified with Fluorescent Gold Nanoclusters and Graphene Oxide.* Microchimica Acta, 2017. **184**: p. 1-10.
18. Tel-Vered, R., Yildiz, H. B., Yan, Y. M., and Willner, I., *Plugging into Enzymes with Light: Photonic "Wiring" of Enzymes with Electrodes for Photobiofuel Cells.* Small, 2010. **6**: p. 1593-1597.
19. S., M. T., Gupta, C. C., Vered, R. T., Roy, S., and Itamar, W., *Donor/Acceptor-Modified Electrodes for Photoelectrochemical and Photobioelectrochemical Applications.* Advanced Functional Materials, 2016. **26**: p. 7148-7155.
20. Liang, J., Chen, D., Yao, X., Zhang, K., Qu, F., Qin, L., Huang, Y., and Li, J., *Recent Progress and Development in Inorganic Halide Perovskite Quantum Dots for Photoelectrochemical Applications.* Small, 2019: p. 1903398.
21. Licht, S. and Peramunage, D., *Efficient Photoelectrochemical Solar Cells from Electrolyte Modification.* Nature, 1990. **345**: p. 330-333.
22. Ye, Z., Hu, Z., Yang, L., and Xiao, X., *Stable p‐type Cu:$CdS_{1-x}Se_x$/Pt Thin‐Film Photocathodes with Fully Tunable Bandgap for Scavenger‐Free Photoelectrochemical Water Splitting.* Solar RRL, 2020. **4**: p. 1900567.
23. Riedel, M., Hölzel, S., Hille, P., Schörmann, J., Eickhoff, M., and Lisdat, F., *InGaN/GaN Nanowires as a New Platform for Photoelectrochemical Sensors–detection of NADH.* Biosensors & Bioelectronics, 2017. **94**: p. 298.
24. Zhao, W. W., Xu, J. J., and Chen, H. Y., *Photoelectrochemical Immunoassays.* Analytical Chemistry, 2017. **90**: p. 615-627.
25. Willner, I., Patolsky, F., and Wasserman, J., *Photoelectrochemistry with Controlled DNA-Cross-Linked CdS Nanoparticle Arrays.* Angewandte Chemie International Edition, 2001. **40**: p. 1861-1864.
26. Zhao, W. W., Xu, J. J., and Chen, H. Y., *Photoelectrochemical DNA Biosensors.* Chemical Reviews, 2014. **114**: p. 7421-7441.
27. Zhao, W. W., Zhang, L., Xu, J. J., and Chen, H. Y., *Cell Surface Carbohydrates Evaluation via a Photoelectrochemical Approach.* Chemical Communications, 2012. **48**: p. 9456-9458.
28. Sun, G., Wang, P., Ge, S., Ge, L., Yu, J., and Yan, M., *Photoelectrochemical Sensor for Pentachlorophenol on Microfluidic Paper-based Analytical Device based on the Molecular Imprinting Technique.* Biosensors and Bioelectronics, 2014. **56**: p. 97-103.

29. Shi, H., Zhao, G., Liu, M., and Zhu, Z., *A Novel Photoelectrochemical Sensor based on Molecularly Imprinted Polymer Modified TiO_2 Nanotubes and Its Highly Selective Detection of 2,4-dichlorophenoxyacetic Acid.* Electrochemistry Communications, 2011. **13**: p. 1404-1407.
30. Riedel, M., Sabir, N., Scheller, F. W., Parak, W. J., and Lisdat, F., *Connecting Quantum Dots with Enzymes: Mediator-based Approaches for the Light-directed Read-out of Glucose and Fructose Oxidation.* Nanoscale, 2017. **9**: p. 2814-2823.
31. Riedel, M., Parak, W. J., Schuhmann, W., and Lisdat, F., *Light as Trigger for Biocatalysis: Photonic Wiring of Flavin Adenin Dinucleotide-Dependent Glucose Dehydrogenase to Quantum Dot-Sensitized Inverse Opal TiO_2 Architectures via Redox Polymers.* ACS Catalysis, 2018. **8**: p. 5212−5220.
32. Stoll, C., Kudera, S., Parak, W. J., and Lisdat, F., *Quantum Dots on Gold:Electrodes For Photoswitchable Cytochrome c Electrochemistry.* Small, 2006. **2**: p. 741-743.
33. Tanne, J., Schafer, D., Khalid, W., Parak, W. J., and Lisdat, F., *Light-Controlled Bioelectrochemical Sensor Based on CdSe/ZnS Quantum Dots.* Analytical Chemistry, 2011. **83**: p. 7778-7785.
34. Riedel, M. and Lisdat, F., *Integration of Enzymes in Polyaniline-Sensitized 3D Inverse Opal TiO_2 Architectures for Light-Driven Biocatalysis and Light-to-Current Conversion.* ACS Applied Materials & Interfaces, 2017. **10**: p. 267-277.
35. Lisdat, F., Schäfer, D., and Kapp, A., *Quantum Dots on Electrodes—new Tools for Bioelectroanalysis.* Analytical & Bioanalytical Chemistry, 2013. **405**: p. 3739-3752.
36. Zheng, Y., Liang, W., Yuan, Y., Xiong, C., Xie, S., Wang, H., Chai, Y., and Yuan, R., *Wavelength-resolved Simultaneous Photoelectrochemical Bifunctional Sensor on Single Interface: A Newly in Vitro Approach for Multiplexed DNA Monitoring in Cancer Cells.* Biosensors & Bioelectronics, 2016. **81**: p. 423-430.
37. Long, F., Zhu, A., and Shi, H., *Recent Advances in Optical Biosensors for Environmental Monitoring and Early Warning.* Sensors, 2013. **13**: p. 13928-13948.
38. Wu, X., He, X., Wang, K., Xie, C., Zhou, B., and Qing, Z., *Ultrasmall Near-infrared Gold Nanoclusters for Tumor Fluorescence Imaging in Vivo.* Nanoscale, 2010. **2**: p. 2244-2249.
39. Webb, D. J., *Optical-Fiber Sensors: An Overview.* MRS Bulletin, 2002. **27**: p. 365-369.
40. Ruan, C. M., Luo, W. S., Wang, W., and Gu, B. H., *Surface-Enhanced Raman Spectroscopy for Uranium Detection and Analysis in Environmental Samples.* Analytica Chimica Acta, 2007. **605**: p. 80-86.
41. Homola, J., Yee, S. S., and Gauglitz, G., *Surface Plasmon Resonance Sensors: Review.* Sensors and Actuators B, 1999. **54**: p. 3-15.
42. Feng, F., Tang, Y., He, F., Yu, M., Duan, X., Wang, S., Li, Y., and Zhu, D., *Cationic Conjugated Polymer/DNA Complexes for Amplified Fluorescence Assays of Nucleases and Methyltransferases.* Advanced Materials, 2007. **19**: p. 3490-3495.
43. Kaisti, M., *Detection Principles of Biological and Chemical FET Sensors.* Biosensors and Bioelectronics, 2017. **98**: p. 437-448.
44. Bergveld, P., *Thirty Years of ISFET Technology: What Happened in the Past 30 Years and What May Happen in the Next 30 years.* Sensors and Actuators B, 2003. **88**: p. 1-20.

45. Bousse, L., DeRooij, N. F., and Bergveld, P., *Operation of Chemically Sensitive Field-Effect Sensors as a Function of the Insulator-Electrolyte Interface.* IEEE Transactions on Electron Devices, 1983. **30**: p. 1263-1270.
46. Hafeman, D. G., Parce, J. W., and McConnell, H. M., *Light-Addressable Potentiometric Sensor for Biochemical Systems.* Science, 1988. **240**: p. 1182-1185.
47. Zhao, S., Shi, C., Hu, H., Li, Z., Xiao, G., Yang, Q., Sun, P., Cheng, L., Niu, W., Bi, J., and Zhao, Y., *ISFET and Dex-AgNPs Based Portable Sensor for Reusable and Real-time Determinations of Concanavalin A and Glucose on Smartphone.* Biosensors and Bioelectronics, 2020. **151**: p. 111962.
48. Nakata, S., Arie, T., Akita, S., and Takei, K., *Wearable, Flexible, and Multifunctional Healthcare Device with an ISFET Chemical Sensor for Simultaneous Sweat pH and Skin Temperature Monitoring.* ACS Sensors, 2017. **2**: p. 443-448.
49. Kissinger, P. T. and Heineman, W. R., *Cyclic voltammetry.* Journal of Chemical Education, 1983. **60**: p. 702.
50. Zhao, S., Caruso, F., Dähne, L., Decher, G., Geest, B.G.D., Fan, J., Feliu, N., Gogotsi, Y., Hammond, P.T., Hersam, M.C., Khademhosseini, A., Kotov, N., Leporatti, S., Li, Y., Lisdat, F., Liz-Marzán, L. M., Moya, S., Mulvaney, P., Rogach, A. L., Roy, S., Shchukin, D. G., Skirtach, A. G., Stevens, M. M., Sukhorukov, G. B., Weiss, P. S., Yue, Z., Zhu, D., and Parak, W. J., *The Future of Layer-by-Layer Assembly: A Tribute to ACS Nano Associate Editor Helmuth Möhwald.* ACS Nano, 2019. **13**: p. 66151-6169.
51. Zhao, S., Völkner, J., Riedel, M., Witte, G., Yue, Z., Lisdat, F., and Parak, W. J., *Multiplexed Readout of Enzymatic Reactions by Means of Laterally Resolved Illumination of Quantum Dot Electrodes.* Applied Materials & Interfaces, 2019. **11**: p. 21830-21839.
52. Frew, J. E. and Hill, H. A. O., *Electrochemical Biosensors.* Analytical Chemistry, 1987. **59**: p. 933A-944A.
53. Ronkainen, N. J., Halsall, H. B., and Heineman, W. R., *Electrochemical Biosensors.* Chemical Society Reviews, 2010. **39**: p. 1747-1763.
54. Zanello, P., *Fundamentals of Electrode Reactions* in *Inorganic Electrochemistry: Theory, Practice and Application*. 2003, The Royal Society of Chemistry: Cambridge Cambridge, UK p. 7-48.
55. Dungchai, W., Chailapakul, O., and Henry, C. S., *Electrochemical Detection for Paper-Based Microfluidics.* Analytical Chemistry, 2009. **81**: p. 5821-5826.
56. Zhang, J., Wang, X., Chen, T., Feng, C., and Li, G., *Electrochemical Analysis of Enzyme Based on the Self-Assembly of Lipid Bilayer on an Electrode Surface Mediated by Hydrazone Chemistry.* Analytical Chemistry, 2017. **89**: p. 13245-13251.
57. Hurd, R. M. and Wrotenbery, P. T., *Electrochemistry of the silicon-electrolyte interface.* Annals New York Academy of Science, 1964. **101**: p. 876-903.
58. Oldham, K. B., *A Gouy–Chapman–Stern Model of the Double Layer at a (Metal)/(Ionic liquid) Interface.* Journal of Electroanalytical Chemistry, 2008. **613**: p. 131-138.
59. Bard, A. J., *Photoelectrochemistry.* Science 1980. **207**: p. pp. 139-144.
60. Schubert, K., Khalid, W., Yue, Z., Parak, W. J., and Lisdat, F., *Quantum-Dot-Modified Electrode in Combination with NADH-Dependent Dehydrogenase Reactions for Substrate Analysis.* Langmuir, 2010. **26**: p. 1395-1400.

61. Zappia, M.I., Bianca, G., Bellani, S., Serri, M., Najafi, L., Oropesa‐Nuñez, R., Martín‐Garc ía, B., Bouša, D., Sedmidubský, D., Pellegrini, V., Sofer, Z., Cupolillo, A., and Bonaccorso, F., *Solution‐Processed GaSe Nanoflake‐Based Films for Photoelectrochemical Water Splitting and Photoelectrochemical‐Type Photodetectors.* Advanced Functional Materials, 2020. **30**: p. 1909572.
62. McConnell, H. M., Owicki, J. C., Parce, J. W., Miller, D. L., Baxter, G. T., Wada, H. G., and Pitchford, S., *The Cytosensor Microphysiometer: Biological Applications of Silicon Technology.* Science, 1992. **257**: p. 1906 - 1912.
63. Dasa, A., Chen, T. C., Yang, C. M., and Lai, C. S., *A High-speed, Flexible-scanning Chemical Imaging System Using a Light-addressable Potentiometric Sensor Integrated with an Analog Micromirror.* Sensors and Actuators B: Chemical, 2014. **198**: p. 225-232.
64. Werner, C. F., Wagner, T., Miyamoto, K. I., Yoshinobu, T., and Schöning, M. J., *High Speed and High Resolution Chemical Imaging Based on a New Type of OLED-LAPS Set-up.* Sensors and Actuators B: Chemical, 2012. **175**: p. 118-122.
65. Ito, Y., *High-spatial Resolution LAPS.* Sensors and Actuators B, 1998. **52**: p. 107-111.
66. Uchida, H., Zhang, W. Y., and Katsube, T., *High Speed Chemical Image Sensor with Digital LAPS System.* Sensors and Actuators B, 1996. **34**: p. 446-449.
67. Yoshinobu, T., Oba, N., Tanaka, H., and Iwasaki, H., *High-speed and High-precision Chemical-imaging Sensor.* Sensors and Actuators A, 1995. **51**: p. 231-235.
68. Qintao, Z., Ping, W., Parak, W. J., George, M., and Zhang, G., *A Novel Design of Multi-light LAPS Based on Digital Compensation of Frequency Domain.* Sensors and Actuators B, 2001. **73**: p. 152-156.
69. Schoot, B. H. V. D. and Bergveld, P., *ISFET Based Enzyme Sensors.* Biosensors, 1987. **3**: p. 161-186.
70. Van Der Schoot, B. H. and Bergveld, P., *The pH-static Enzyme Sensor-An ISFET-based Enzyme Sensor, Insensitive to the Buffer Capacity of the Sample.* Analytica Chimica Acta, 1987. **199**: p. 157-160.
71. Alegret, S., Bartroli, J., Jimenez, C., Martinez-Fabregas, E., Martorell, D., and Valdes-Perezgasga, F., *ISFET-based Urea Biosensor.* Sensors and Actuators B, 1993. **15-16**: p. 453-457.
72. Saito, A., Ito, N., Kumura, J., and Kuriyama, T., *An ISFET Glucose Sensor with a Silicone Rubber Membrane for Undiluted Serum Monitoring.* Sensors and Actuators B: Chemical, 1994. **20**: p. 125-129.
73. Kerkhof, J. C. V. and Bergveld, P., *The ISFET based Heparin Sensor with a Monolayer of Protamine as Affinity Ligand.* Biosensors & Bioelectronics, 1995. **10**: p. 269-282.
74. Koch, S., Woias, P., Meixner, L. K., Drost, S., and Wolf, H., *Protein Detection with a Novel ISFET-based Zeta Potential Analyzer.* Biosensors & Bioelectronics, 1999. **14**: p. 413-421.
75. Hedborg, E., Winquist, F., Sundgren, H., and Lundström, I., *Charge Migration on Hydrophobic and Hydrophilic Silicon Dioxide.* Thin Solid Films, 1999. **340**: p. 250-256.
76. Holmberg, M. and Ingemar, L., *A New Method for the Detection of Hydrogen Spillover.* Applied Surface Science, 1996. **93**: p. 67-76.
77. Filippini, D. and Lundström, I., *Hydrogen Detection on Bare SiO_2 between Metal Gates.* Journal of Applied Physics, 2002. **91**: p. 3896.

78. Moritz, W., Yoshinobu, T., Finger, F., Krause, S., Martin-Fernandez, M., and Schöning, M. J., *High Resolution LAPS Using Amorphous Silicon as the Semiconductor Material.* Sensors and Actuators B, 2004. **103**: p. 436-441.
79. Hühn, J., Carrillo-Carrion, C., Soliman, M. G., Pfeiffer, C., Valdeperez, D., Masood, A., Chakraborty, I., Zhu, L., Gallego, M., Zhao, Y., Carril, M., Feliu, N., Escudero, A., Alkilany, A. M., Pelaz, B., Pino, P. D., and Parak, W. J., *Selected Standard Protocols for the Synthesis, Phase Transfer, and Characterization of Inorganic Colloidal Nanoparticles.* Chemistry of Materials, 2017. **29**: p. 399-461.
80. Smith, A. M. and Nie, S., *Semiconductor Nanocrystals: Structure, Properties, and Band Gap Engineering.* Accounts of Chemical Research, 2001. **43**: p. 190-200.
81. Alivisatos, A. P., *Semiconductor Clusters, Nanocrystals, and Quantum Dots.* Science, 1996. **271**: p. 933-937.
82. Li, T. and Galli, G., *Electronic Properties of MoS_2 Nanoparticles.* The Journal of Physical Chemistry C, 2007. **111**: p. 16192-16196.
83. Park, T. J., Papaefthymiou, G.C., Viescas, A.J., Moodenbaugh, A.R., and Wong, S. S., *Size-Dependent Magnetic Properties of Single-Crystalline Multiferroic $BiFeO_3$ Nanoparticles.* Nano Letters, 2007. **7**: p. 766-772.
84. Sow, C., Riedl, B., and Blanchet, P., *UV-waterborne Polyurethane-acrylate Nanocomposite Coatings Containing Alumina and Silica Nanoparticles for Wood: Mechanical, Optical, and Thermal Properties Assessment.* Journal of Coatings Technology and Research, 2011. **8**: p. 211-221.
85. Li, W. H., Yang, C. C., Tsao, F. C., Wu, S. Y., Huang, P. J., Chung, M. K., and Yao, Y. D., *Enhancement of Superconductivity by the Small Size Effect in In Nanoparticles.* Physical review B, 2005. **72**: p. 214516.
86. Wang, J., *Nanomaterial-based Electrochemical Biosensors.* Analyst, 2005. **130**: p. 421-426.
87. Alivisatos, A.P., *Semiconductor Nanocrystals: New Materials through Control of Size.* Abstracts of Papers of the American Chemical Society, 1998. **216**: p. U337-U337.
88. Frese, K. W., *A High Efficiency Single-crystal CdSe Photoelectrochemical Solar Cell and an Associated Loss Mechanism.* Applied Physics Letters, 1982. **40**: p. 275-277.
89. Kobayashi, A., Sankey, O. F., Volz, S. M., and Dow, J. D., *Semiempirical Tight-binding Band Structures of Wurtzite Semiconductors: AlN, CdS, CdSe, ZnS, and ZnO.* Physical Review B, 1983. **28**: p. 935-945.
90. Murray, C. B., Norris, D. J., and Bawendi, M. G., *Synthesis and Characterization of Nearly Monodisperse CdE (E = S, Se, Te) Semiconductor Nanocrystallites.* Journal of the American Chemical Society, 1993. **115**: p. 8706-8715.
91. Alivisatos, A. P., *Semiconductor Nanocrystals.* MRS Bulletin, 1995. **1995**: p. 23-32.
92. Li, Q., Ohulchanskyy, T. Y., Liu, R. L., Koynov, K., Wu, D. Q., Best, A., Kumar, R., Bonoiu, A., and Prasad, P. N., *Photoluminescent Carbon Dots as Biocompatible Nanoprobes for Targeting Cancer Cells in Vitro.* Journal Of Physical Chemistry C, 2010. **114**: p. 12062-12068.
93. Colvin, V. L., Schlamp, M. C., and Alivisatos, A. P., *Light-emitting Diodes Made from Cadmium Selenide Nanocrystals and a Semiconducting Polymer.* Nature, 1994. **370**: p. 354-357.

94. Li, X. B., Tung, C. H., and Wu, L. Z., *Semiconducting Quantum Dots for Artificial Photosynthesis.* Nature Reviews Chemistry, 2018. **2**: p. 160-173.
95. Wang, Y. and Chen, L., *Quantum Dots, Lighting up the Research and Development of Nanomedicine.* Nanomedicine-Nanotechnology Biology and Medicine, 2011. **7**: p. 385-402.
96. Guo, C., Wang, J., Cheng, J., and Dai, Z., *Determination of Trace Copper Ions with Ultrahigh Sensitivity and Selectivity Utilizing CdTe Quantum Dots Coupled with Enzyme Inhibition.* Biosensors and Bioelectronics, 2012. **36**: p. 69-74.
97. Popović, Z., Liu, W., Chauhan, V. P., Lee, J., Wong, C., Greytak, A. B., Insin, N., Nocera, D. G., Fukumura, D., Jain, R. K., and Bawendi, M. G., *A Nanoparticle Size Series for In Vivo Fluorescence Imaging.* Angewandte Chemie International Edition, 2010. **49**: p. 8649-8652.
98. Shao, D., Li, J., Xiao, X., Zhang, M., Pan, Y., Li, S., Wang, Z., Zhang, X., Zheng, H., Zhang, X., and Chen, L., *Real-Time Visualizing and Tracing of HSV-TK/GCV Suicide Gene Therapy by Near-Infrared Fluorescent Quantum Dots.* ACS Applied Materials & Interfaces, 2014. **6**: p. 11082-11090.
99. Khalid, W., Helou, M. E., Murböck, T., Yue, Z., Montenegro, J. M., Schubert, K., Göbel, G., Lisdat, F., Witte, G., and Parak, W. J., *Immobilization of Quantum Dots via Conjugated Self-Assembled Monolayers and Their Application as a Light-Controlled Sensor for the Detection of Hydrogen Peroxide.* ACS Nano, 2011. **5**: p. 9870-9876.
100. Zhao, W. W., Xu, J. J., and Chen, Y. H., *Photoelectrochemical Enzymatic Biosensors.* Biosensors & Bioelectronics, 2016. **92**: p. 294.
101. Sabir, N., Khan, N., Völkner, J., Widdascheck, F., Pino, P. D., Witte, G., Riedel, M., Lisdat, F., Konrad, M., and Parak, W. J., *Photo-electrochemical Bioanalysis of Guanosine Monophosphate Using Coupled Enzymatic Reactions at a CdS/ZnS Quantum Dot Electrode.* Small, 2015. **43**: p. 5844-5850.
102. Cao, X. D., Chen, C., Yu, H. J., and Wang, P., *Horseradish Peroxidase-encapsulated Chitosan Nanoparticles for Enzyme-prodrug Cancer Therapy.* Biotechnology Letters, 2015. **37**: p. 81-88.
103. Riedel, M., Göbel, G., Abdelmonem, A. M., Parak, W. J., and Lisdat, F., *Photoelectrochemical Sensor based on Quantum Dots and Sarcosine Oxidase.* ChemPhysChem, 2013. **14**: p. 2338-2342.
104. Jr., L. C. C. and Lyons, C., *Electrode Systems For Continuous Monitoring in Cardiovascular Surgery.* Annals of the New York Academy of Sciences, 1962. **102**: p. 29-45.
105. Riedel, M., Wersig, J., Ruff, A., Schuhmann, W., Zouni, A., and Lisdat, F., *A Z‐Scheme‐Inspired Photobioelectrochemical H_2O/O_2 Cell with a 1 V Open‐Circuit Voltage Combining Photosystem II and PbS Quantum Dots.* Angewandte Chemie, 2019. **58**: p. 801-805.
106. Allen, J. E., Perea, D. E., Hemesath, E. R., and Lauhon, L. J., *Nonuniform Nanowire Doping Profiles Revealed by Quantitative Scanning Photocurrent Microscopy.* Advanced Materials, 2009. **21**: p. 3067-3072.
107. Howell, S.L., Padalkar, S., Yoon, K., Li, Q., Koleske, D. D., and Lauhon, J. L., *Spatial Mapping of Efficiency of GaN/InGaN Nanowire Array Solar Cells Using Scanning Photocurrent Microscopy.* Nano Letters., 2013. **13**: p. 5123-5128.

108. Jiang, D., Ni, D., Rosenkrans, Z. T., Huang, P., Yan, X., and Cai, W., *Nanozyme: New Horizons for Responsive Biomedical Applications.* Chemical Society Reviews, 2019. **48**: p. 3683-3704.
109. Bracamonte, M. V., Melchionna, M., Giuliani, A., Lucía Nasi, C., Tavagnacco, C., Prato, M., and Fornasiero, P., *H_2O_2 Sensing Enhancement by Mutual Integration of Single Walled Carbon Nanohorns with Metal Oxide Catalysts: The CeO_2 case.* Sensors and Actuators B: Chemical, 2017. **239**: p. 923-932.
110. Xu, C., Lin, Y., Wang, J., Wu, L., Wei, W., Ren, J., and Qu, X., *Nanoceria‐Triggered Synergetic Drug Release Based on CeO_2-Capped Mesoporous Silica Host-Guest Interactions and Switchable Enzymatic Activity and Cellular Effects of CeO_2.* Advanced healthcare materials, 2013. **2**: p. 1591-1599.
111. Lu, Z., Mao, C., Meng, M., Liu, S., Tian, Y., Yu, L., Sun, B., and Li, C. M., *Fabrication of CeO_2 Nanoparticle-modified Silk for UV Protection and Antibacterial Applications.* Journal of Colloid and Interface Science, 2014. **435**: p. 8-14.
112. Xie, Y. L., Zhao, S. Q., Ye, H. L., Yuan, J., Song, P., and Hu, S. Q., *Graphene/CeO_2 Hybrid Materials for the Simultaneous Electrochemical Detection of Cadmium(II), Lead(II), Copper(II), and Mercury(II).* Journal of Electroanalytical Chemistry, 2015. **757**: p. 235-242.
113. Cheng, H., Zhang, L., He, J., Guo, W., Zhou, Z., Zhang, X., Nie, S., and Wei, H., *Integrated Nanozymes with Nanoscale Proximity for in Vivo Neurochemical Monitoring in Living Brains.* Analytical Chemistry, 2016. **88**: p. 5489-5497.
114. Manea, F., Houillon, F. B., Pasquato, L., and Scrimin, P., *Nanozymes: Gold-Nanoparticle-BasedTransphosphorylation Catalysts.* Angewandte Chemie International Edition, 2004. **43**: p. 6165-6169.
115. Gao, L., Zhuang, J., Nie, L., Zhang, J., Zhang, Y., Gu, N., Wang, T., Feng, J., Yang, D., and Perrett, S., *Intrinsic Peroxidase-like Activity of Ferromagnetic Nanoparticles.* Nature nanotechnology, 2007. **2**: p. 577.
116. Comotti, M., Pina, C.D., Matarrese, R., and Rossi, M., *The Catalytic Activity of "Naked" Gold Particles.* Angewandte Chemie, 2004. **43**: p. 5812-5815.
117. Wang, H., Wan, K., and Shi, X., *Recent Advances in Nanozyme Research.* Advanced Materials, 2018. **31**: p. 1805368.
118. Chen, J., Patil, S., Seal, S., and McGinnis, J. F., *Rare Earth Nanoparticles Prevent Retinal Degeneration Induced by Intracellular Peroxides.* Nature Nanotechnology 2006. **1**: p. 142-150.
119. Henning, D. F., Merkl, P., Yun, C., Lovino, F., Xie, L., Mouzourakis, E., Moularas, C., Deligiannakis, Y., Henriques-Normark, B., Leifer, K., and Sotiriou, G.A., *Luminescent CeO_2: Eu^{3+} Nanocrystals for Robust in Situ H_2O_2 Real-time Detection in Bacterial Cell Culture.* Biosensors and Bioelectronics, 2019. **132**: p. 286-293.
120. Wang, Y. J., Dong, H., Lyu, G. M., Zhang, H. Y., Ke, J., Kang, L. Q., Teng, J. L., Sun, L. D., Si, R., Zhang, J., Liu, Y. J., Zhang, Y. W., Huang, Y. H., and Yan, C. H., *Engineering the Defect State and Reducibility of Ceria based Nanoparticles for Improved Anti-oxidation Performance.* Nanoscale, 2015. **7**: p. 13981-13990.
121. Li, Y., Sun, Q., Kong, M., Shi, W., Huang, J., Tang, J., and Zhao, X., *Coupling Oxygen Ion Conduction to Photocatalysis in Mesoporous Nanorod-like Ceria Significantly Improves*

Photocatalytic Efficiency. The Journal of Physical Chemistry C, 2011. **115**: p. 14050-14057.

122. Lu, X., Zheng, D., Zhang, P., Liang, C., Liu, P., and Tong, Y., *Facile Synthesis of Free-standing CeO_2 Nanorods for Photoelectrochemical Applications.* Chemical Communications, 2010. **46**: p. 7721-7723.
123. Zhou, J., Wang, P., Wang, C., Goh, Y. T., Fang, Z., Messersmith, P. B., and Duan, H., *Versatile Core–Shell Nanoparticle@Metal–Organic Framework Nanohybrids: Exploiting Mussel-Inspired Polydopamine for Tailored Structural Integration.* ACS Nano, 2015. **9**: p. 6951-6960.
124. O. Katz, G.B. and Salzman, J., *Persistent Photocurrent and Surface Trapping in GaN Schottky Ultraviolet Detectors.* Applied Physics Letters, 2004. **84**: p. 4092.
125. Andreeva, D. V., Fix, D., Möhwald, H., and Dmitry G. Shchukin, *Buffering Polyelectrolyte Multilayers for Active Corrosion Protection.* Journal of Materials Chemistry, 2008. **18**: p. 1738-1740.
126. Andreeva, D. V., Skorb, E. V., and Shchukin, D. G., *Layer-by-Layer Polyelectrolyte/Inhibitor Nanostructures for Metal Corrosion Protection.* ACS Applied Materials & Interfaces, 2010. **2**: p. 1954-1962.
127. Muzzio, N. E., Pasquale, M. A., Diamanti, E., Gregurec, D., Moro, M. M., Azzaroni, O., and Moya, S. E., *Enhanced Antiadhesive Properties of Chitosan/Hyaluronic Acid Polyelectrolyte Multilayers Driven by Thermal Annealing: Low Adherence for Mammalian Cells and Selective Decrease in Adhesion for Gram-positive Bacteria.* Materials Science & Engineering C, 2017. **80**: p. 677-687.
128. Hammond, P. T., *Building Biomedical Materials Layer-by-layer.* Materials Today, 2012. **15**: p. 196-206.
129. Miller, M. D. and Bruening, M. L., *Controlling the Nanofiltration Properties of Multilayer Polyelectrolyte Membranes through Variation of Film Composition.* Langmuir, 2004. **20**: p. 11545-11551.
130. Skorb, E. V. and Möhwald, H., *"Smart" Surface Capsules for Delivery Devices.* Advanced Materials Interfaces, 2015. **1**: p. 1400237.
131. Skirtach, A., Yashchenok, A., and Mohwald, H., *Encapsulation, Release and Applications of LbL Polyelectrolyte Multilayer Capsules.* Chemical Communications, 2011. **47**: p. 12736-12746.
132. Liu, X. Y., Gao, C. Y., Shen, J. C., and Möhwald, H., *Multilayer Microcapsules as Anti-cancer Drug Delivery Vehicle: Deposition, Sustained Release, and in Vitro Bioactivity.* Macromolecular Bioscience, 2005. **5**: p. 1209-1219.
133. Bonk, S. M. and Lisdat, F., *Layer-by-layer Assembly of Electro-active Gold Nanoparticle/Cytochrome C Multilayers.* Biosensors & Bioelectronics, 2009. **25**: p. 739-44.
134. Lisdat, F., Dronov, R., Mohwald, H., Scheller, F. W., and Kurth, D.G., *Self-assembly of Electro-active Protein Architectures on Electrodes for the Construction of Biomimetic Signal Chains.* Chemical Communications, 2009: p. 274-283.
135. Dronov, R., Kurth, D. G., Mohwald, H., Spricigo, R., Leimkuehler, S., Wollenberger, U., Rajagopalan, K. V., Scheller, F. W., and Lisdat, F., *Layer-by-layer Arrangement by Protein-*

protein Interaction of Sulfite Oxidase and Cytochrome C Catalyzing Oxidation of Sulfite. Journal of The American Chemical Society, 2008. **130**: p. 1122.

136. Zhang, J., Tu, L., Zhao, S., Liu, G., Wang, Y., Wang, Y., and Yue, Z., *Fluorescent Gold Nanoclusters based Photoelectrochemical Sensors for Detection of H_2O_2 and Glucose.* Biosensors & Bioelectronics, 2015. **67**: p. 296-302.

137. Kim, J. H., Patra, C. R., Arkalgud, J. R., Boghossian, A. A., Zhang, J., Han, J. H., Reuel, N. F., Ahn, J. H., Mukhopadhyay, D., and Strano, M. S., *Single-Molecule Detection of H_2O_2 Mediating Angiogenic Redox Signaling on Fluorescent Single-Walled Carbon Nanotube Array.* ACS Nano, 2011. **5**: p. 7848-7857.

List of publications

1、 **Shuang Zhao**, Johannes Völkner, Marc Riedel, Gregor Witte, Zhao Yue*, Fred Lisdat*, Wolfgang J. Parak*, Multiplexed Readout of Enzymatic Reactions by Means of Laterally Resolved Illumination of Quantum Dot Electrodes, ACS Appl. Mater. Interfaces 2019, 11, 24, 21830-21839, DOI: 10.1021/acsami.9b03990.

2、 **Shuang Zhao**, Frank Caruso, Lars Dähne, Gero Decher, Bruno G. De Geest, Jinchen Fan, Neus Feliu, Yury Gogotsi, Paula T. Hammond, Mark C. Hersam, Ali Khademhosseini, Nicholas Kotov, Stefano Leporatti, Yan Li, Fred LisdatLuis M. Liz-Marzán, Sergio Moya, Paul Mulvaney, Andrey L. Rogach, Sathi Roy, Dmitry G. Shchukin, Andre G. Skirtach, Molly M. Stevens, Gleb B. Sukhorukov, Paul S. Weiss, Zhao Yue, Dingcheng Zhu, Wolfgang J. Parak*, The Future of Layer-by-Layer Assembly: A Tribute to ACS Nano Associate Editor Helmuth Möhwald, ACS nano, 2019, 13, 6, 6151-6169, DOI: 10.1021/acsnano.9b03326.

3、 **Shuang Zhao**, Marc Riedel, Javier Patarroyo, Neus Bastus, Victor Puntes, Peter Nordlander, Zhao Yue*, Fred Lisdat*, Wolfgang J. Parak*, Introducing Visible-light Sensitivity into CeO_2 Nanozymes for Enhanced Photoelectrocatalysis and Application in Hydrogen Peroxide Sensing, Advanced Functional Materials, 2020, In revision

Bibliography

Personal Information	
Name: Shuang	Family name: Zhao
Birthplace: Hebei, China	Nationality: Chinese

Education	
2016.09-2020.06	Hamburg University, AG Biophotonics (Prof. Wolfgang Parak) Doctor of Natural Sciences
2014.09-2016.06	Nankai University Master in Microelectronics
2009.09-2013.06	Yanshan University Bachelor in Electronic Information and Engineering

Acknowledgements

Here I would like to express my great thanks when my PhD study is about to be finished. It was not easy to study along abroad in another country. But with the help and company from all my colleagues, I always feel safety and confidence because there is always people who will give me a hand. Sincerely hope I also could have the power to help them in the future and undoubtedly I will fight for this in my future career.

First of all, I want to thank my supervisor Wolfgang Parak. Because of him, I could have the chance to study in Germany with the interesting and promising projects, which gives me a better and deeper understanding into the nano science. It was always he, who first came to help me anytime, who replied to my questions the first time, who gave me wisdom and patience to do my projects, and who give his full support to my projects. Besides, I also would like to thanks Prof. Fred Lisadt and Dr. Marc Riedel from collaboration group. They gave me many help to improve the experiments, to writing the thesis and to improve the outline. Their insightful comments on every draft, which provide me with many enlightening ideas, have inspired me to a great extent. I also would like to thank my co-supervisor Prof. Zhao Yue. His careful thinking and encouraging and humorous characteristics always motivate me and give me energy and hope to finish my hard project. I also would like to thank our technician Marten Rittner who provided me with beneficial help in the daily works. He is an interesting guy who always infects me with enthusiasm. And also I would like to thank my parents. Even they are far away from me, I still can feel their company and encouragement. Many thanks to them for supporting me to do whatever I want to do. Finally, I would like to thank all of my friends coming to my life in this period of time. Their love is always the source of my strength during the period of my worries and frustrations.

Appendix

ACS APPLIED MATERIALS & INTERFACES

Research Article

Cite This: ACS Appl. Mater. Interfaces 2019, 11, 21830−21839

www.acsami.org

Multiplexed Readout of Enzymatic Reactions by Means of Laterally Resolved Illumination of Quantum Dot Electrodes

Shuang Zhao,[†] Johannes Völkner,[‡] Marc Riedel,[∥] Gregor Witte,[‡] Zhao Yue,*[,§] Fred Lisdat,*[,∥] and Wolfgang J. Parak*[,†]

[†]Fachbereich Physik, CHyN, Universität Hamburg, 22761 Hamburg, Germany

[‡]Fachbereich Physik, Philipps-Universität Marburg, Renthof 5, 35032 Marburg, Germany

[§]Department of Microelectronics, Nankai University, 300350 Tianjin, China

[∥]Biosystems Technology, Institute of Life Sciences and Biomedical Technologies, Technical University of Applied Sciences Wildau, Hochschulring 1, 15745 Wildau, Germany

Supporting Information

ABSTRACT: Triggering electrochemical reactions with light provides a powerful tool for the control of complex reaction schemes on photoactive electrodes. Here, we report on the light-directed, multiplexed detection of enzymatic substrates using a nonstructured gold electrode modified with CdSe/ZnS quantum dots (QDs) and two enzymes, glucose oxidase (GOx) and sarcosine oxidase (SOx). While QDs introduce visible-light sensitivity into the electrode architecture, GOx and SOx allow for a selective conversion of glucose and sarcosine, respectively. For the QD immobilization to the gold electrode, a linker-assisted approach using *trans*-4,4′-stilbenedithiol has been used, resulting in the generation of a photocurrent. Subsequently, GOx and SOx have been immobilized in spatially separated spots onto the QD electrode. For the local readout of the QD electrode, a new measurement setup has been developed by moving a laser pointer across the surface to defined positions on the chip surface. The amplitudes of the photocurrents upon illumination of the GOx or SOx spot depend in a concentration-dependent manner on the presence of glucose and sarcosine, respectively. This measurement also allows for a selective detection in the presence of other substances. The setup demonstrates the feasibility of multiplexed measurements of enzymatic reactions using a focused light pointer, resulting in an illumination area with a diameter of 0.3 mm for analyzing spots of different enzymes. Moving the laser pointer in the *x*- and *y*-direction and simultaneously detecting the local photocurrent also allow a spatial imaging of enzyme immobilization. Here, not only the spot dimensions but also the activity of the enzyme can be verified.

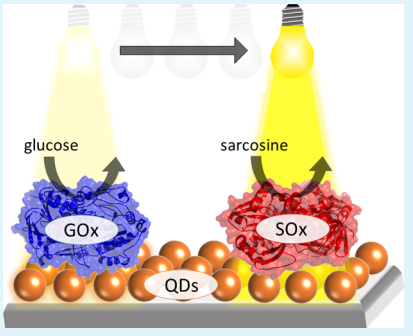

KEYWORDS: *photoelectrochemistry, glucose oxidase, sarcosine oxidase, quantum dots, multiplexed detection, imaging*

1. INTRODUCTION

The integration of biological recognition elements in light-switchable electrode arrangements has gained growing interest during the last decade for the construction of photoelectrochemical (PEC) sensors[1−3] as well as for solar-to-chemical[4,5] and solar-to-current converting systems.[6,7] Particularly, PEC sensing systems represent a promising alternative to electrochemical approaches because of high sensitivity and light-controllable readout.[3] Also, the construction of solar-powered, self-driven sensors for point-of-care analysis has become feasible.[8] All PEC approaches rely on the linkage of a light-sensitive entity to an electrode to trigger electron-transfer reactions under illumination and the concomitant generation of a photocurrent. In detail, electrons in the photoactive material are transferred from the highest occupied molecular orbital into the lowest unoccupied molecular orbital, resulting in the generation of electron−hole pairs. While radiative recombination processes cause unwanted emission of light, the application of an appropriate electrode potential favors the electron transfer between the light-sensitive entity and the electrode. If electrons are transferred from the electrode toward the light-sensitive entity to an acceptor molecule, a cathodic photocurrent is formed. In the reverse direction, an anodic signal is established if electrons flow from a donor molecule to the light-sensitive entity and finally to the electrode. A huge number of different photoactive nanomaterials have been applied for the construction of PEC sensors such as quantum dots (QDs),[9,10] gold nanoclusters,[11] nanowires,[12,13] and dyes,[14,15] giving access to various photocatalytic features and excitation wavelengths.

Besides affinity-based PEC sensorial systems based on DNA,[16] antibodies,[17] and molecular-imprinted polymers,[18] particularly biocatalytic approaches have moved into the focus of PEC sensors for the detection of enzymatic substrates or the

Received: March 8, 2019
Accepted: May 22, 2019
Published: May 22, 2019

DOI: 10.1021/acsami.9b03990
ACS Appl. Mater. Interfaces 2019, 11, 21830−21839

evaluation of enzyme activity.[19] Many biological molecules can be photoelectrochemically detected with the help of selective, enzyme-catalyzed reactions.[1,9,20−22] Here, mainly three PEC transduction principles were established, which are based on (1) the detection of enzymatic cosubstrates or products such as O_2,[10,23] H_2O_2,[11,12] acetylthiocholine,[9] and nicotinamide adenine dinucleotide;[15,20,21] (2) electron mediators which shuttle charge carriers between the enzyme and the light-sensitive element;[24−26] and (3) direct electron transfer.[27−30] For example, in previous studies, we have exploited the competitive situation between a light-switchable, oxygen-reducing QD electrode and oxygen-consuming oxidases for the detection of enzymatic substrates by following the depression of the cathodic photocurrent.[10,31] The principle is illustrated in Figure 1a. Despite the great progress in the

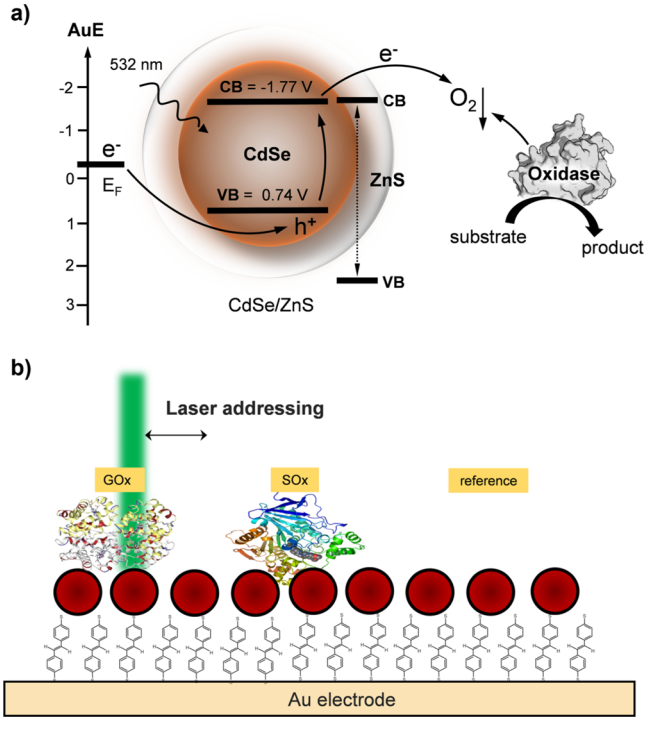

Figure 1. (a) Electrons (e^-) can be transferred from the Fermi level (E_F) of a Au electrode (AuE) through linker molecules to QDs in case electrons have been photoexcited here from the valence band to the conduction band, leading also to the creation of holes (h^+). Photoexcited electrons can reduce molecular oxygen at the QD surface, leading to a reduction of oxygen in solution ($O_2\downarrow$). The presence of oxidases at the QDs competes for oxygen consumption, thus modulating the photocurrent. The energy level is drawn with the reference to the normal hydrogen electrode scale. The conduction and valence bands have been calculated according to Jasieniak et al.[47] (b) GOx and SOx are immobilized on a QD-coated Au electrode by local spotting. By moving a laser pointer across the electrode surface, the position where the local photocurrent is measured can be selected.

construction of enzyme-based PEC sensors, these systems are currently only suitable for single analyte analysis. The parallel detection of several enzyme substrates on one light-addressable electrode by immobilization of several biocatalysts spatially separated from each other, and individual readout with a focused light beam has not been shown yet.

Usually, multiplexed electrochemical measurements are possible with electrode arrays. In this way, several electrochemical reactions can be followed in parallel. However, there are limitations in the number of recording sites because every single electrode needs to be wired to the outside.[32] This can be circumvented by using light-addressable potentiometric sensor (LAPS) electrodes,[33−35] in which illumination with light creates a virtual electrode, which defines the location where the local electrochemical reaction is recorded.[36] However, LAPS is limited to processes, which allow a stable potential formation at the sensing surface. PEC systems can here provide access to a much larger number of analytes and higher accuracy because of the principle of current detection in combination with biochemical recognition. Recently, first PEC multiplexing examples for DNA and immunosensing using light-addressable electrode arrays[37,38] and structured electrodes[39,40] have been shown. In another study, the use of two wavelength-selective materials and wavelength-resolved readout have been shown to allow for the detection of two different DNA sequences in parallel.[41] However, in this case, an upscaling to more than two analytes can be an issue. Furthermore, a more simple illumination of the sensor would be desirable for practical implementation in bioanalysis.

As a proof of principle, we demonstrate in the present work the multiplexed detection of glucose and sarcosine by a light-directed measurement of the local depletion of molecular oxygen at spots with immobilized glucose oxidase (GOx) and sarcosine oxidase (SOx), respectively. Selection of the enzyme spots is possible by moving a light pointer to the respective position on the nonstructured QD-modified gold electrode (see Figure 1b). The easy integration of two enzymatic reactions into a one-electrode setup in combination with light-addressable readout overcomes not only the needs for electrode array-based technologies but also the structuring of the electrode systems, for example, by the utilization of insulating paints. Moreover, this proof-of-concept study provides the basis for extending the multiplexed light-addressable working scheme on a QD-modified electrode to a large number of oxidases and may also be useful for PEC enzyme-linked immunosorbent assays.

2. RESULTS AND DISCUSSION

2.1. QD Synthesis and Characterization. Hydrophobic CdSe/ZnS core/shell QDs with trioctylphosphine oxide (TOPO) as a capping ligand have been synthesized by a protocol according to Hühn et al.[42] CdSe has been chosen as a QD core material because of the rather small band gap (~1.7 eV for bulk),[43] allowing the excitation with visible light and avoiding the need to apply UV light and thus preventing potential biomolecule degradation. The ZnS shell helps to prevent the photodegradation of the QDs[44,45] and improves the photophysical properties of the QDs.[46] In Figure 2a, the UV/vis absorption and fluorescence spectra of the QDs dissolved in toluene are shown. The wavelengths of the absorption and fluorescence peaks are 533 and 554 nm, respectively. During the synthesis, the size and thus the absorption have been adjusted to the 532 nm laser used for excitation. The transmission electron microscopy (TEM) results shown in Figure 2b indicate an average diameter of the inorganic CdSe/ZnS core/shell part of d_{cs} = 4.6 ± 1 nm. From the QD diameter of the CdSe core (~3.8 nm), the conduction band and valence band have been calculated to be −1.77 and 0.74 V versus Ag/AgCl, respectively.[42,47] From the dynamic light scattering (DLS) results from three independent measurements, a mean "hydrodynamic" diameter of d_h = 7 nm has been observed in toluene. Because DLS does not only

DOI: 10.1021/acsami.9b03990
ACS Appl. Mater. Interfaces 2019, 11, 21830−21839

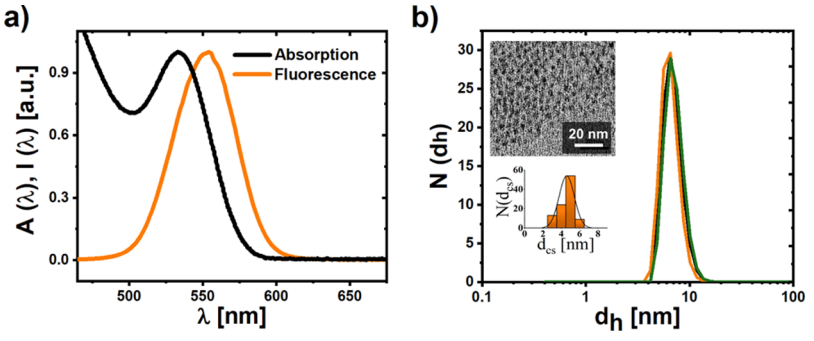

Figure 2. (a) Absorption $A(\lambda)$ and fluorescence intensity $I(\lambda)$ spectra of QDs in toluene. (b) Number distribution $N(d_h)$ of the "hydrodynamic" diameter as determined by DLS in three times independent measurements. Inset: TEM image of QDs (the scale bar corresponds to 20 nm) and a corresponding histogram of the core/shell diameter d_{cs}.

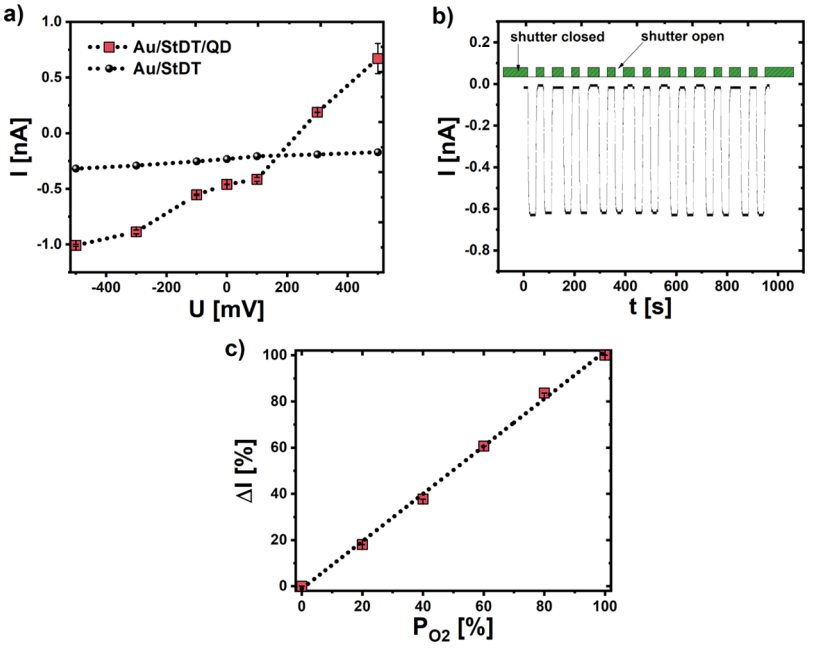

Figure 3. (a) Photocurrent amplitude I in dependence of the applied bias potential U for Au/StDT/QD and Au/StDT electrodes without QDs. The bias potential refers to the potential difference to the Ag/AgCl reference electrode. (b) Photocurrent measurement of a Au/StDT/QD electrode at a constant bias of $U = -100$ mV and giving light pulses to the electrode. During the period of 1000 s, the shutter controlling the illumination of the WE has been switched on and off several times. No current has been detected when the shutter was closed. (c) Dependence of photocurrent change $\Delta I = (I - I_{min})/(I_{max} - I_{min})$ on the degree of air-saturation p_{O_2} in PBS buffer at $U = -100$ mV vs Ag/AgCl (static light spot with ca. 0.3 mm diameter, Au/StDT/QD electrode); $I_{min} = (p_{O_2}) = 0\%$, $I_{max} = (p_{O_2}) = 100\%$. p_{O_2} is 0% for PBS purged with N_2 and 100% for air-saturated PBS.

detect the inorganic part of the QDs but also the organic capping ligand and interaction with the solvent, the overall QD diameter appears in DLS measurements larger than in TEM experiments.

2.2. Study of the Basic PEC Properties of the Au/StDT/QD Electrode Immersed in PBS. After synthesis, the QDs have been immobilized on a gold chip electrode by means of a dithiol compound (*trans*-4,4′-stilbenedithiol, StDT) as reported previously[20,21] and described in the Experimental Section. The QD binding is based on a partial ligand exchange of the nonpolar TOPO capping ligand by the immobilized dithiol, resulting in the formation of a stable QD layer on top of the gold electrode. The successful immobilization of the QDs can be confirmed by UV/vis absorption spectroscopy experiments, showing the typical absorbance features of the QDs in the Supporting Information (Figure S14). In order to verify the functionality of the prepared QD electrode, first PEC experiments have been performed by giving light pulses with a laser having a beam diameter d_{laser} of about 0.3 mm and applying different potentials U in the range between −500 and +500 mV versus Ag/AgCl. The challenge here is a sufficiently small laser spot to exploit the full potential of multiplexing on the sensing surface and also a sufficiently large one such that the signal-to-noise ratio (SNR) is suitable for an analytical application of the photocurrent measurement.

For illumination, monochromatic light with a wavelength of 532 nm has been applied, which allows for a defined excitation of the QDs (see UV/vis absorption spectrum in Figure 2a). In Figure 3a, the amplitude I of the photocurrent (i.e., the signal of the modulated photocurrent rectified by the lock-in amplifier when the shutter is opened) is plotted versus the applied bias voltage U. While the whole working electrode

DOI: 10.1021/acsami.9b03990
ACS Appl. Mater. Interfaces 2019, 11, 21830−21839

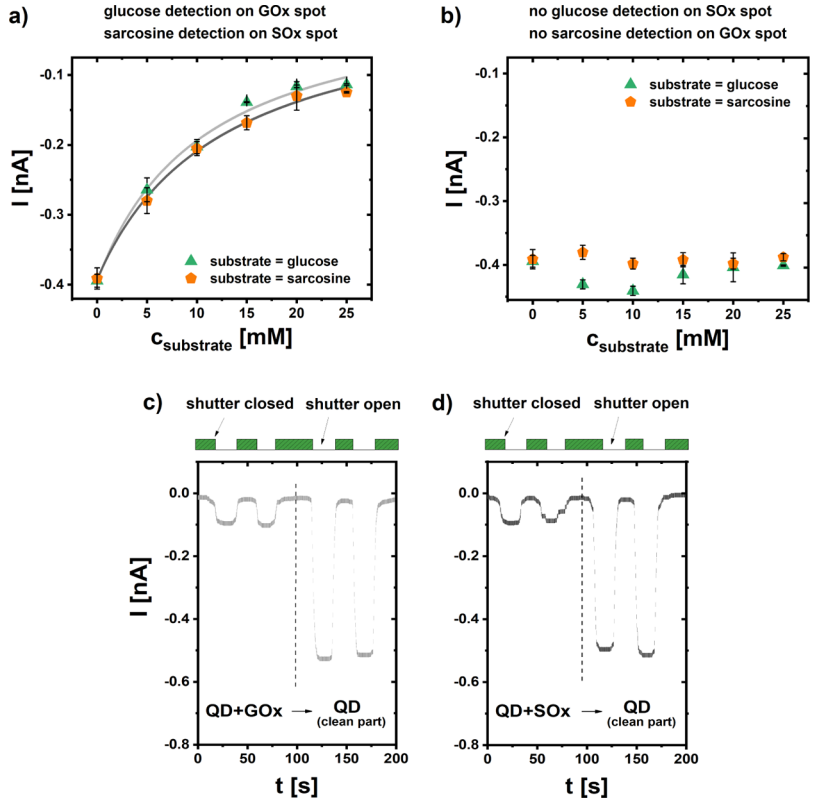

Figure 4. Photocurrent behavior of Au/StDT/QD WEs with only one enzyme immobilized as a spot on the QD electrode: (a–c) GOx, (a,b,d) SOx. (a) Concentration-dependent amplitude I of photocurrent for different glucose and sarcosine concentrations ($c_{substrate}$) for WEs with immobilized GOx and SOx, respectively. (b) Control, showing the unaffected photocurrent for different glucose and sarcosine concentrations ($c_{substrate}$) for WEs with immobilized SOx and GOx, respectively. The raw data for this figure are presented in the Supporting Information (Figures S7 and S8). (c,d): PEC experiments in which the laser was moved from the enzyme spot to an enzyme-free part of the QD electrode. During the measurements, the shutter was closed for five intervals at which no photocurrent was measured. The laser movement happened when the shutter was closed for the third time, that is, without illumination. (c) $c_{substrate}$ = 25 mM glucose, GOx spot on the chip. (d) $c_{substrate}$ = 25 mM sarcosine, SOx spot on the chip. (Laser spot diameter d_{laser} ca. 0.3 mm, static laser spot illuminating the enzyme-covered region; U = −100 mV vs Ag/AgCl, measurements performed in air-saturated PBS pH 7.4).

(WE) has been covered with QDs, the static laser spot only illuminates a spherical area with a diameter d_{laser} of about 0.3 mm. When QDs are immobilized on the gold chip, a clear bias-dependent photocurrent can be recorded (Au/StDT/QD electrode). This photocurrent is light-intensity-dependent and increases with increasing number of photons (Figure S16). Moreover, wavelength-resolved measurements in the Supporting Information (Figure S15) demonstrate that the photocurrent follows the absorbance properties of the QDs and confirm that the QDs are the main origin of the photocurrent. The current through the Au/SAM/QD electrode is thus controlled by light and follows in a defined response to the applied bias potential. The magnitude of the photocurrent signal is not large but sufficiently pronounced to allow the defined analysis of changes.

By varying the applied potential, even the direction of the photocurrent can be switched. In the following, focus will be given on the study of cathodic photocurrents at −100 mV versus Ag/AgCl. Here, oxygen acts as an electron acceptor at the excited QDs.[10] Although lower potentials up to −350 mV versus Ag/AgCl would provide higher photocurrents, measurements at −100 mV versus Ag/AgCl have been found to be less noisy, thus allowing a better SNR. Furthermore, it can be shown that the photocurrent is stable over a reasonable period of time (see Figure 3b) and that the QD electrode can be stored in phosphate-buffered saline (PBS) in the dark for at least 14 days with a constant photocurrent response (Supporting Information, Figure S17).

Additionally, the immobilization of enzymes on top of the QD surface has not influenced the photocurrent stability of the chip electrode. This is exemplified in the Supporting Information (Figure S4). The rather good stability provides a profound basis for the analysis of the oxygen concentration based on a pulsed illumination of the QD electrode and photocurrent detection.

2.3. Study of the O_2 Dependence of the Photocurrent. In a next step, it has been verified that under the negative bias of U = −100 mV versus Ag/AgCl, oxygen can be detected (Figure 3c). To study the dependence of the photocurrent on different oxygen concentrations, air-saturated buffer has been mixed with nitrogen-purged buffer, and the photocurrent response of the Au/StDT/QD electrodes has been measured. When the oxygen concentration in solution rises, the amplitude of the cathodic photocurrent increases. This verifies that the immobilized QDs can interact with dissolved oxygen and transfer electrons upon excitation. The applied bias to the Au electrode can subsequently fill up the holes in the QDs, and thus, the photocurrent follows the oxygen concentration. The electrochemical experiments are also supported by fluorescence studies of QDs in the presence of oxygen.[10,48,49] The observed oxygen sensitivity provides the

DOI: 10.1021/acsami.9b03990
ACS Appl. Mater. Interfaces 2019, 11, 21830–21839

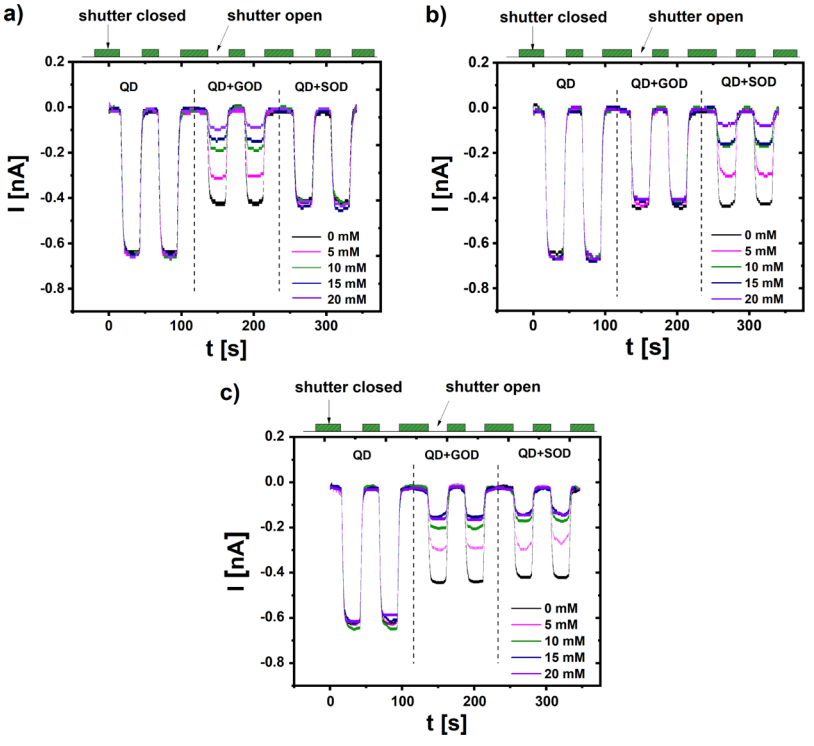

Figure 5. Photocurrent behavior of Au/StDT/QD WEs modified with two enzyme spots on the sensor electrode. Photocurrent measurements have been performed in which the laser spot illuminated first the bare part without immobilized enzyme, followed by the GOx-modified region and the SOx-coated zone (from left to right). This is done by moving the laser pointer focus along the surface of the electrode. During measurements, the laser spot has been blocked 7 times for intervals of a few tens of seconds with a shutter, at which no photocurrent was recorded. Measurements are performed with a light spot of ca. 0.3 mm diameter at a constant bias of $U = -100$ mV vs Ag/AgCl in 0.01 M PBS pH 7.4 containing (a) glucose, (b) sarcosine, and (c) glucose and sarcosine at different concentrations ($c_{substrate}$, refer to legend). Shown results correspond to the mean values of the photocurrent amplitudes I as recorded from three independent chips. The raw data are shown in the Supporting Information (Figures S9 and S10).

basis for the combination of QD-modified electrodes with enzymatic reactions in which oxygen is involved.

2.4. Characterization of Single Enzyme Reactions on Au/StDT/QD Electrodes. In a first step, only one enzyme (GOx or SOx) has been immobilized in a spot on top of the Au/SAM/QD electrode, and glutaraldehyde has been used for cross-linking. The successful binding of the enzyme to the electrode can be followed by a small decrease of the photocurrent of about 30%, when the laser is focused onto the enzyme spot. This can be attributed to the altered accessibility of O_2 to the Au/StDT/QD electrode at the spot. After addition of the substrate for both Au/StDT/QD/GOx and Au/StDT/QD/SOx electrodes, a further decrease of the cathodic photocurrent up to 75% of the initial signal can be followed with increasing analyte concentration (see Figure 4a). This proves that both enzymes retain their catalytic functionality after immobilization to the Au/StDT/QD electrode and confirms the PEC sensing principle shown in Figure 1, allowing for the detection of glucose and sarcosine. Here, a competitive situation with respect to oxygen is created between the QDs and the enzymes under illumination and in the presence of a substrate, resulting in a decrease of the cathodic photocurrent. To exclude a participation of enzymatically produced H_2O_2 on the signal generation, control experiments with up to 5 mM H_2O_2 have been performed (Figure S13). At −100 mV versus Ag/AgCl, no photocurrent change has been observed upon addition of H_2O_2, demonstrating that H_2O_2 is not involved in the light-directed electron-transfer processes under the chosen experimental conditions and also confirming the PEC sensing principle shown in Figure 1.

Furthermore, when sarcosine has been added, no photocurrent change can be observed at the GOx electrode, and when SOx has been immobilized, no photocurrent response has been obtained when glucose is added to the solution (see Figure 4b). The selectivity in response provides a solid foundation for a multiplexed detection with both enzymes immobilized on one chip.

Further control experiments verify that the change in photocurrent upon presence of the substrate is indeed connected to the enzymatic activity. This can be demonstrated by moving the light pointer to areas on the Au/StDT/QD electrode where no enzyme is immobilized. Here, no change in photocurrent response has been found upon addition of the substrate (see Figure 4c,d). Despite the noise level obtained, a clear signal discrimination between chip electrode areas with and without enzyme can be seen. Consequently, the feasibility of local photocurrent measurements with a light pointer illuminating only selected areas of the Au/StDT/QD chip can be shown.

The operational stability of the Au/StDT/QD/enzyme electrodes has been tested by performing repetitive measurements, showing a constant signal response for at least five measurements for both GOx- and SOx-modified electrodes (Figure S18a,b). Also, a sufficient storage stability up to 7 days has been obtained for the Au/StDT/QD/enzyme electrodes corresponding to a signal reduction to 93 and 92% of the signal obtained at the first day for the GOx and SOx spots,

DOI: 10.1021/acsami.9b03990
ACS Appl. Mater. Interfaces 2019, 11, 21830−21839

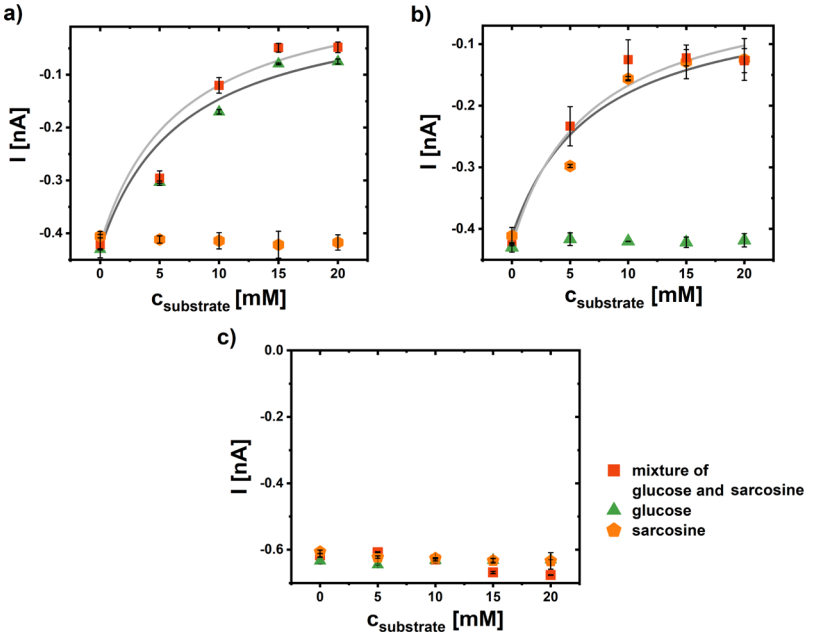

Figure 6. Dependence of the photocurrent change of Au/StDT/QD electrodes with two enzyme spots on the chip electrode upon addition of different concentrations of glucose and sarcosine (bias potential $U = -100$ mV vs Ag/AgCl, 0.01 M PBS buffer pH 7.4). The laser spot (ca. 0.3 mm diameter) has been moved to different parts of the Au/StDT/QD surface: (a) GOx-covered part, (b) SOx-covered part, and (c) part without immobilized enzyme. The error bars result from measurements with three independent WEs.

respectively (Figure S18c,d). The PEC data nicely correlate with photoluminescence enzyme assays performed on Au/StDT/QD/enzyme electrodes, showing an enzyme activity which corresponds to 90% of its initial rate after 7 days (Figures S19 and S20). This demonstrates that not only QDs but also the enzyme can be stably fixed to the electrode without altering the enzyme activity, allowing the repetitive detection of glucose and sarcosine for several days.

2.5. Multiplexed Detection of Two Analytes in Parallel on a Chip Electrode Surface Modified with Two Distinct Spots of Different Enzymes. Here, two distinct enzyme spots made out of GOx or SOx have been immobilized on the surface of Au/SAM/QD electrodes. Thus, each sensing chip comprises three parts: an unmodified part, a zone with immobilized GOx, and a zone with immobilized SOx (see Figure S1c). By moving the light spot along the surface of the WE, the different regions can be illuminated independently, leading to a laterally controlled photocurrent measurement. Measurements have been performed by successively illuminating the three parts of the electrode in the presence of glucose, in the presence of sarcosine, and in the presence of both substrates. In Figure 5, for all three situations, photocurrents at the unmodified, the GOx-, and the SOx-coated regions are shown. The results demonstrate that the amplitude of the photocurrent only decreases when the laser is on the enzyme spot and the corresponding substrate is in solution, for example, upon illumination of the GOx spot in the presence of glucose.

In fact, when the laser illuminates the GOx spot, the amplitude of the photocurrent only decreases if glucose or a mixture of glucose and sarcosine is in solution, while the addition of sarcosine without glucose results in no signal change. When the laser illuminates the SOx spot, the amplitude of the photocurrent only decreases in solution of sarcosine and a mixture of glucose and sarcosine. In contrast, if the laser illuminates areas, which are not covered by the enzyme, the photocurrent remains unchanged upon addition of enzymatic substrates. The photocurrent change found at the enzyme spots increases in a defined way with the substrate concentration in solution, which is caused not only by the enzymatic conversion but also by the signal generation at the QD surface by oxygen reduction. Thus, the PEC system demonstrates a good sensitivity and selectivity.

In order to analyze the sensing performance in more detail, the concentration dependence of the photocurrent as recorded on the three different regions is plotted in Figure 6. The dose–response curves are fitted by the model of Michaelis Menten: $\Delta I(c_{substrate}) = \Delta I_{max} \cdot c_{substrate}/(K_M + c_{substrate})$, whereby ΔI_{max} is the maximum amplitude of the photocurrent change and K_M is the apparent Michaelis Menten constant, which indicates the substrate concentration at which the photocurrent has reached half of the maximum amplitude change ($\Delta I_{max}/2$); $\Delta I(c_{substrate}) = I(c_{substrate}) - I_{max}$; $I_{max} = I(c_{substrate} = 0)$. From the measurements, the following parameters can be extracted: for the GOx-coated part with glucose in solution $K_M = 6.9 \pm 0.2$ mM and for the SOx-coated part with sarcosine in solution $K_M = 7.2 \pm 0.3$ mM. Compared with the K_M values determined for the enzymes in free solution (GOx: 26 mM,[50] SOx: 12.2 mM[51]), they are smaller but in good agreement with apparent K_M values reported for the immobilized GOx (2–31 mM)[10,52–54] and SOx (2–22 mM)[31,50,55,56] in sensor constructions.

The lower limit of detection (LOD) $3\sigma/S$ is determined by analyzing the noise level without an analyte (standard deviation in blank solutions, σ) and taking the signal change slope (S) from the linear range.[8] For glucose detection, a $LOD_{glucose} = 0.09$ mM, and for sarcosine detection, a $LOD_{sarcosine} = 0.11$ mM, can be evaluated at the respective enzyme spot. The slopes in the sensing graphs [$I = f(c_{substrate})$] for glucose and sarcosine are always similar to the ones using a mixture of glucose and sarcosine.

DOI: 10.1021/acsami.9b03990
ACS Appl. Mater. Interfaces 2019, 11, 21830–21839

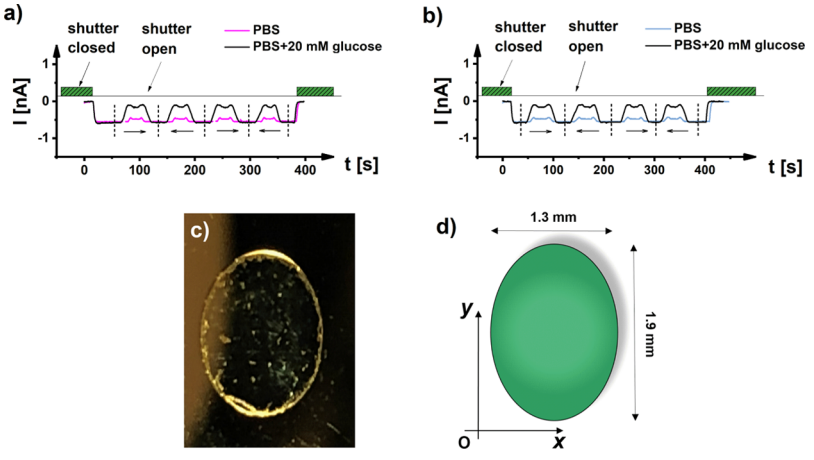

Figure 7. PEC imaging measurements at a Au/StDT/QD/GOx electrode: (a,b) the laser spot has been moved back and forth two times in (a) *x*-direction and (b) *y*-direction across the GOx spot, while the photocurrent amplitude is recorded at constant bias potential $U = -100$ mV with and without the presence of glucose in solution. The diameter of the laser spot d_{laser} is around 0.3 mm. The spot dimensions can be calculated from the scan velocity: $\Delta x = v_{laser} \cdot \Delta t$; $\Delta y = v_{laser} \cdot \Delta t$. A replication of the results is shown in the Supporting Information (Figure S11), which demonstrates reproducibility. (c) Microscopic image of the GOx spot on the surface of the Au/StDT/QD electrode. (d) Sketch of the dimensions of the GOx spot and indication of *x*- and *y*-direction.

These measurements clearly demonstrate the advantage of light-triggered sensing for multiplexing for enzymatic substrate analysis. Clearly, sufficient discrimination between the sensor output and the different spots on the nonstructured planar QD-modified gold electrode can be achieved by spatially resolved illumination and photocurrent detection. Well-defined concentration dependencies can be retained in the multiplex format.

2.6. Imaging of the Photocurrent Distribution along the WE Surface. When the laser is scanned over the electrode surface while measuring the photocurrent continuously, local photocurrent profiles can be recorded. This might be useful to analyze enzyme activity distributions on the surface or to evaluate enzyme immobilization protocols. In order to demonstrate the feasibility of this concept, we have inspected the spotlike immobilization of GOx on the QD surface by moving the light pointer across the electrode surface in the absence and presence of the enzymatic substrate.

For these kinds of measurements, a compromise between the speed of surface analysis and the noise level in continuous photocurrent detection has to be found. The laser pointer has been moved with a velocity of about $v_{laser} = 42\ \mu m\ s^{-1}$, allowing still reasonable photocurrent measurements. (For details, see the Supporting Information, Figure S3.)

For surface analysis, the laser pointer has been moved two times back and forth in the *x*- and *y*-direction over the enzyme spot in the absence of a substrate. The results in Figure 7a,b clearly show that the enzyme spot can be imaged by the photocurrent recordings, as the variation in intensity clearly mirrors the geometrical structure of the spot. The diminished photocurrent results from the cross-linked enzyme layer on top of the QDs, which limits the oxygen access slightly compared to the unmodified QD electrode area.

In Figure 7c, the corresponding microscopic image of the enzyme spot is shown for comparison. A distinct coherence of the photocurrent measurement with the dimensions of the enzyme spot can be noticed. More quantitatively, the spot size from photocurrent analysis can be estimated to be 1.8 mm × 1.2 mm in blank PBS and 1.9 mm × 1.3 mm in glucose solution, whereas the microscopic analysis gives 1.9 mm × 1.3 mm. Furthermore, the slightly inhomogeneous deposition can be visualized because higher photocurrent changes are found at the boarders of the enzyme spot.

In contrast to a microscopic image, the photocurrent measurement also allows for the test of activity of the deposited enzymes. Here, the photocurrent in the presence of glucose in solution has been evaluated by scanning over the surface. These measurements match very well with the structural analysis without the substrate but clearly show the activity by reduced oxygen availability at the QDs. Also, here the inhomogeneous deposition of the enzyme can be verified. The photocurrent change covers a larger area than the structural analysis shows because oxygen is also consumed around the GOx spot.

This first example may illustrate the potential of photocurrent measurements for imaging purpose because structural aspects and activity patterns can be detected on top of the QD surface.

3. CONCLUSIONS

In contrast to LAPS systems, which are based on potentiometry, the PEC system developed here exploits defined electron-transfer cascades incorporating the semiconductor material itself. This offers great potential for the design of well-defined signal chains starting from an analyte molecule in solution. We demonstrate here the proof of principle for a multiplexed analysis on a nonstructured sensing electrode by immobilizing two different enzymes that are spatially separated on a QD-modified electrode and using a focused light beam as the triggering element. We have been able to detect the respective enzyme substrate without observing an interference of a second enzyme substrate present in solution. This allows for a readout of two analytes on one sensing platform by exploiting the spatially resolved illumination of defined areas of the sensing electrode. GOx and SOx have been used as biological recognition elements and glucose and sarcosine as respective specific interaction partners. Both enzymatic reactions are detected by a competitive situation in front of the QD electrode with respect to oxygen. The performance of the multiplexed analysis is quite comparable to

DOI: 10.1021/acsami.9b03990
ACS Appl. Mater. Interfaces 2019, 11, 21830−21839

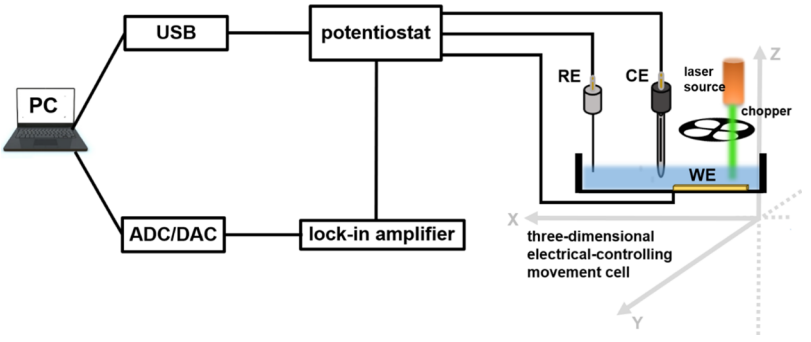

Figure 8. Schematic diagram of the homebuilt setup of the PEC measurement system. The QD-modified gold chip acts as the WE, whereas an Ag/AgCl (3 M NaCl) and a Pt-wire serve as reference and counter electrodes, respectively. The whole cell can be moved under the laser pointer. The light is modulated by a chopper, which is connected to the lock-in amplifier.

the analysis of individual enzyme−QD electrodes. This shows good practicability and high accuracy of the multiplexed system. Also, it proves that small enzyme spots can be used to achieve multichannel detection successfully, when reliable photocurrents can be generated with a small beam diameter as shown here with 0.3 mm. The study thus opens good perspectives to detect more analytes at the same time in the future by means of multiple enzyme spots immobilized on one single chip.

Furthermore, it can be demonstrated that continuous photocurrent measurements are feasible while moving the light pointer over the sensing electrode. Collected photocurrent profiles can directly indicate the structural deposits of enzymes immobilized on the surface. This has been exemplified with the imaging of an immobilized thin GOx layer. The photocurrent measurements can however detect not only structural deposits but also the activity of such features. This allows for the evaluation of the efficiency of immobilization protocols in addition to the characterization of the homogeneity of deposition procedures.

In summary, this new concept which is based on a low-cost PEC setup has good selectivity, rapid response, and high accuracy and will undoubtedly open new directions in the area of surface imaging techniques.

4. EXPERIMENTAL SECTION

4.1. QD Synthesis. CdSe/ZnS QDs were synthesized following a previously published protocol with slight modification.[42] For the synthesis of the CdSe core, 0.03 g of CdO, 0.11 g of hexylphosphonic acid, and 3.5 g of TOPO were put into a three-necked flask and degassed for 20 min at 120 °C. In nitrogen, the mixture was heated afterward to 300−320 °C to form a transparent solution. Then, this mixture was cooled down to 270 °C, and 1.2 mL of selenium stock solution (as obtained by dissolving 0.0255 g of selenium powder in 1.5 mL of TOP) was injected swiftly. The temperature was dropped by about 20 °C because of the injection, and then it was maintained at 250 °C in the core synthesis. After the injection, the color of the mixture started to change from colorless to yellow-orange, red, and finally dark red in 30−40 min. The size of the CdSe cores was checked every 5 min by UV/vis absorption measurements.[42] When the CdSe cores had grown to the desired size, a ZnS shell (ca. 1.2 monolayers) was further grown on top of them with the solution temperature maintained at 250 °C. For this, a Zn/S/TOP solution was made by adding 1.75 mL of diethylzinc solution ($ZnEt_2$ 1 M in hexane) and 0.37 mL of hexamethyldisilathiane in 10.38 mL of TOP. The Zn/S/TOP solution (1.5 mL) was added to the mixture slowly and dropwise via a funnel within 10 min. Eventually, the QD solution was cooled down to 90 °C and stirred for another 3 h at this temperature to form a stable shell. When the mixture was cooled down to room temperature (RT), it was diluted with 10 mL of toluene and was transferred to a glass vial for the further purification. Methanol (10 mL) was added to the diluted QDs to form a cloudy solution. This solution was centrifuged at 5000 rcf (relative centrifugal field, ×*g*) for 7 min. Afterward, the supernatant was removed, and the QDs at the vial bottom were collected and diluted by toluene again. This purification process was repeated at least three times until the last supernatant was colorless. The cleaned QDs were dispersed in toluene and diluted to the desired concentration for further use. UV/vis absorption and fluorescence spectra were recorded in toluene. The QD concentration was determined from their absorbance.[42] The diameter of the inorganic part of the CdSe/ZnS QDs was determined by TEM, and the "hydrodynamic" diameter in toluene was recorded by DLS.

4.2. Fabrication of the WE. The gold electrodes were cleaned by ultrasonication in acetone, ultrapure water, and ethanol for at least 7 min each. The temperature in the ultrasonic bath was adjusted to RT. Afterward, the cleaned electrodes were immersed in a 100 μM solution of StDT dissolved in dry and water-free toluene for 24 h at 350 K to immobilize StDT as a linker on the gold surface.[57] The preparation took place in the N_2 atmosphere (glovebox with ≤1 ppm H_2O, ≤1 ppm O_2). After being rinsed with toluene and dried, the StDT-modified chips were further modified with QDs. Therefore, the chips were immersed for 24 h in 16 μM QD solution at RT. Then, the resulting Au/StDT/QD chips were rinsed with toluene and dried by N_2. Before measurements and enzyme immobilization, the chips were equilibrated in PBS for at least 6 h.

4.3. Preparation of PBS with Different Oxygen Contents. First, PBS buffer was purged with pure N_2 for 4 h in order to remove dissolved O_2. After that, the O_2-free PBS was mixed with air-saturated PBS, resulting in buffer with different O_2 contents (p_{O_2}) ranging from 0 to 100% (air saturation).[10]

4.4. Enzyme Immobilization. Four microliters of 400 μM enzyme (GOx or SOx) dissolved in PBS was pipetted onto the surface of Au/StDT/QD chips. After that, 4 μL of 0.05% glutaraldehyde in PBS was pipetted into the enzyme solution on the Au/StDT/QD chips in order to cross-link the enzymes. When the mixture was dried in air at 4 °C, PBS was used to rinse the chips to remove unbound enzyme and glutaraldehyde from the surface.

4.5. Photocurrent Measurement System. A homebuilt setup was used, which has been described in a previous study.[58] A sketch of the setup is shown in Figure 8, and a photograph is given in the Supporting Information (Figure S1). A laser light source with a wavelength of 532 nm was used for the illumination of the electrode (Changchun New Industries Optoelectronics Tech. Co., Ltd. China). The illumination of the WE was controlled by a shutter and modulated with a frequency of 71 Hz by an optical chopper (Scitec Instruments). The laser was focused by an objective lens from a microscope and an adjustable pinhole to the surface of the WE. The diameter of the laser spot d_{laser} was determined to be 0.3 mm (see Figure S3), and the absolute output power P of the laser was adjusted to give an illumination power of ca. 4 mW on the WE. This value was

DOI: 10.1021/acsami.9b03990
ACS Appl. Mater. Interfaces 2019, 11, 21830−21839

measured with a PM100 series high sensitivity optical power meter from Thorlabs (Supporting Information, Figure S2). For laterally resolved measurements, the laser remained fixed, but the electrochemical cell with the WE was moved. The movement of the cell was done with a three-dimensional electrically controlled movement system (Luigs & Neumann). For the PEC measurements, a three-electrode setup consisting of a QD-modified gold electrode as the WE, a Pt wire-based counter electrode, and an Ag/AgCl (3 M NaCl) reference electrode. The photocurrent was measured with the use of a lock-in amplifier (EG&G model #5210), which was triggered with the modulation frequency of 71 Hz. Use of the lock-in amplifier improved the SNR. The resulting output was then transferred to a personal computer equipped with an analog-to-digital-converter/digital-to-analog-converter module (National Instruments). The whole signal acquisition processes, including the shutter switch, were controlled by a homebuilt software programmed in LabVIEW (National Instruments). All measurements were performed at RT.

■ ASSOCIATED CONTENT

Supporting Information

The Supporting Information is available free of charge on the ACS Publications website at DOI: 10.1021/acsami.9b03990.

Additional details of enzymatic and redox reactions, experimental setup, determination of laser spot diameter, dependence of the photocurrent on QD coverage and diameter of the laser spot, repeated experiments of single and multiplexed detections, repeated results of photocurrent imaging, and control experiments (PDF)

■ AUTHOR INFORMATION

Corresponding Authors

*E-mail: yuezhao@nankai.edu.cn (Z.Y.).
*E-mail: flisdat@th-wildau.de (F.L.).
*E-mail: wolfgang.parak@uni-hamburg.de (W.J.P.).

ORCID

Marc Riedel: 0000-0001-6408-6067
Gregor Witte: 0000-0003-2237-0953
Wolfgang J. Parak: 0000-0003-1672-6650

Notes

The authors declare no competing financial interest.

■ ACKNOWLEDGMENTS

This work was supported by the Deutsche Forschungsgemeinschaft (DFG grants LI 706/8-1, PA 794/15-1, WI 1361/6-1 to F.L., W.J.P., and G.W.) and the National Natural Science Foundation of China (nos. 61871240 and 61471207 to Z.Y.). S.Z. acknowledges funding of a PhD fellowship by the Chinese Scholarship Council (CSC).

■ REFERENCES

(1) Yue, Z.; Lisdat, F.; Parak, W. J.; Hickey, S. G.; Tu, L.; Sabir, N.; Dorfs, D.; Bigall, N. C. Quantum-Dot-Based Photoelectrochemical Sensors for Chemical and Biological Detection. *ACS Appl. Mater. Interfaces* **2013**, *5*, 2800−2814.

(2) Lisdat, F.; Schäfer, D.; Kapp, A. Quantum Dots on Electrodes-New Tools for Bioelectroanalysis. *Anal. Bioanal. Chem.* **2013**, *405*, 3739−3752.

(3) Zhao, W.-W.; Xu, J.-J.; Chen, H.-Y. Photoelectrochemical Bioanalysis: the State of the Art. *Chem. Soc. Rev.* **2015**, *44*, 729−741.

(4) Lee, S. H.; Choi, D. S.; Kuk, S. K.; Park, C. B. Photobiocatalysis: Activating Redox Enzymes by Direct or Indirect Transfer of Photoinduced Electrons. *Angew. Chem.* **2018**, *57*, 7958−7985.

(5) Kornienko, N.; Zhang, J. Z.; Sakimoto, K. K.; Yang, P.; Reisner, E. Interfacing Nature's Catalytic Machinery with Synthetic Materials for Semi-artificial Photosynthesis. *Nat. Nanotechnol.* **2018**, *13*, 890−899.

(6) Garza, L. D. L.; Jeong, G.; Liddell, P. A.; Sotomura, T.; Moore, T. A.; Moore, A. L.; Gust, D. Enzyme-Based Photoelectrochemical Biofuel Cell. *J. Phys. Chem. B* **2003**, *107*, 10252−10260.

(7) Riedel, M.; Wersig, J.; Ruff, A.; Schuhmann, W.; Zouni, A.; Lisdat, F. A Z-Scheme-Inspired Photobioelectrochemical H_2O/O_2 Cell with a 1 V Open-Circuit Voltage Combining Photosystem II and PbS Quantum Dots. *Angew. Chem.* **2019**, *58*, 801−805.

(8) Yan, K.; Yang, Y.; Okoth, O. K.; Cheng, L.; Zhang, J. Visible-Light Induced Self-Powered Sensing Platform Based on a Photofuel Cell. *Anal. Chem.* **2016**, *88*, 6140−6144.

(9) Pardo-Yissar, V.; Katz, E.; Wasserman, J.; Willner, I. Acetylcholine Esterase-Labeled CdS Nanoparticles on Electrodes: Photoelectrochemical Sensing of the Enzyme Inhibitors. *J. Am. Chem. Soc.* **2003**, *125*, 622−623.

(10) Tanne, J.; Schäfer, D.; Khalid, W.; Parak, W. J.; Lisdat, F. Light-Controlled Bioelectrochemical Sensor Based on CdSe/ZnS Quantum Dots. *Anal. Chem.* **2011**, *83*, 7778−7785.

(11) Zhang, J.; Tu, L.; Zhao, S.; Liu, G.; Wang, Y.; Wang, Y.; Yue, Z. Fluorescent Gold Nanoclusters Based Photoelectrochemical Sensors for Detection of H_2O_2 and Glucose. *Biosens. Bioelectron.* **2015**, *67*, 296−302.

(12) Tang, J.; Wang, Y.; Li, J.; Da, P.; Geng, J.; Zheng, G. Sensitive Enzymatic Glucose Detection by TiO_2 Nanowire Photoelectrochemical Biosensors. *J. Mater. Chem. A* **2014**, *2*, 6153−6157.

(13) Riedel, M.; Hölzel, S.; Hille, P.; Schörmann, J.; Eickhoff, M.; Lisdat, F. InGaN/GaN Nanowires as a New Platform for Photoelectrochemical Sensors-Detection of NADH. *Biosens. Bioelectron.* **2017**, *94*, 298−304.

(14) Tel-Vered, R.; Yildiz, H. B.; Yan, Y.-M.; Willner, I. Plugging into Enzymes with Light: Photonic "Wiring" of Enzymes with Electrodes for Photobiofuel Cells. *Small* **2010**, *6*, 1593−1597.

(15) Metzger, T. S.; Chandaluri, C. G.; Tel-Vered, R.; Shenhar, R.; Willner, I. Donor/Acceptor-Modified Electrodes for Photoelectrochemical and Photobioelectrochemical Applications. *Adv. Funct. Mater.* **2016**, *26*, 7148−7155.

(16) Freeman, R.; Girsh, J.; Willner, I. Nucleic Acid/Quantum Dots (QDs) Hybrid Systems for Optical and Photoelectrochemical Sensing. *ACS Appl. Mater. Interfaces* **2013**, *5*, 2815−2834.

(17) Zhao, W.-W.; Xu, J.-J.; Chen, H.-Y. Photoelectrochemical Immunoassays. *Anal. Chem.* **2017**, *90*, 615−627.

(18) Shi, H.; Zhao, G.; Liu, M.; Zhu, Z. A Novel Photoelectrochemical Sensor Based on Molecularly Imprinted Polymer Modified TiO_2 Nanotubes and Its Highly Selective Detection of 2,4-Dichlorophenoxyacetic Acid. *Electrochem. Commun.* **2011**, *13*, 1404−1407.

(19) Zhao, W. W.; Xu, J. J.; Chen, Y. H. Photoelectrochemical Enzymatic Biosensors. *Biosens. Bioelectron.* **2017**, *92*, 294−304.

(20) Schubert, K.; Khalid, W.; Yue, Z.; Parak, W. J.; Lisdat, F. Quantum-Dot-Modified Electrode in Combination with NADH-Dependent Dehydrogenase Reactions for Substrate Analysis. *Langmuir* **2010**, *26*, 1395−1400.

(21) Sabir, N.; Khan, N.; Völkner, J.; Widdascheck, F.; del Pino, P.; Witte, G.; Riedel, M.; Lisdat, F.; Konrad, M.; Parak, W. J. Photoelectrochemical Bioanalysis of Guanosine Monophosphate Using Coupled Enzymatic Reactions at a CdS/ZnS Quantum Dot Electrode. *Small* **2015**, *11*, 5844−5850.

(22) Gooding, J. J.; Wibowo, R.; Liu, W.; Yang, W.; Losic, D.; Orbons, S.; Mearns, F. J.; Shapter, J. G.; Hibbert, D. B. Protein Electrochemistry Using Aligned Carbon Nanotube Arrays. *J. Am. Chem. Soc.* **2003**, *125*, 9006−9007.

(23) Wang, W.; Bao, L.; Lei, J.; Tu, W.; Ju, H. Visible Light Induced Photoelectrochemical Biosensing Based on Oxygen-Sensitive Quantum Dots. *Anal. Chim. Acta* **2012**, *744*, 33−38.

(24) Efrati, A.; Lu, C. H.; Michaeli, D.; Rachel, N.; Alsaoub, S.; Schuhmann, W.; Willner, I. Assembly of Photo-Bioelectrochemical Cells Using Photosystem I-Functionalized Electrodes. *Nat. Energy* **2016**, *1*, 15021.

DOI: 10.1021/acsami.9b03990
ACS Appl. Mater. Interfaces 2019, 11, 21830−21839

(25) Riedel, M.; Sabir, N.; Scheller, F. W.; Parak, W. J.; Lisdat, F. Connecting Quantum Dots with Enzymes: Mediator-Based Approaches for the Light-Directed Read-out of Glucose and Fructose Oxidation. *Nanoscale* **2017**, *9*, 2814−2823.
(26) Riedel, M.; Parak, W. J.; Ruff, A.; Schuhmann, W.; Lisdat, F. Light as Trigger for Biocatalysis: Photonic Wiring of Flavin Adenin Dinucleotide-Dependent Glucose Dehydrogenase to Quantum Dot-Sensitized Inverse Opal TiO_2 Architectures via Redox Polymers. *ACS Catal.* **2018**, *8*, 5212−5220.
(27) Stoll, C.; Kudera, S.; Parak, W. J.; Lisdat, F. Quantum Dots on Gold: Electrodes For Photoswitchable Cytochrome c Electrochemistry. *Small* **2006**, *2*, 741−743.
(28) Stoll, C.; Gehring, C.; Schubert, K.; Zanella, M.; Parak, W. J.; Lisdat, F. Photoelectrochemical Signal Chain Based on Quantum Dots on Gold-Sensitive to Superoxide Radicals in Solution. *Biosens. Bioelectron.* **2008**, *24*, 260−265.
(29) Zeng, T.; Leimkühler, S.; Koetz, J.; Wollenberger, U. Effective Electrochemistry of Human Sulfite Oxidase Immobilized on Quantum-Dots-Modified Indium Tin Oxide Electrode. *ACS Appl. Mater. Interfaces* **2015**, *7*, 21487−21494.
(30) Riedel, M.; Lisdat, F. Integration of Enzymes in Polyaniline-Sensitized 3D Inverse Opal TiO_2 Architectures for Light-Driven Biocatalysis and Light-to-Current Conversion. *ACS Appl. Mater. Interfaces* **2017**, *10*, 267−277.
(31) Riedel, M.; Göbel, G.; Abdelmonem, A. M.; Parak, W. J.; Lisdat, F. Photoelectrochemical Sensor Based on Quantum Dots and Sarcosine Oxidase. *Chemphyschem* **2013**, *14*, 2338−2342.
(32) George, M.; Parak, W. J.; Gaub, H. E. Highly Integrated Surface Potential Sensors. *Sens. Actuators, B* **2000**, *69*, 266−275.
(33) Engström, O.; Carlsson, A. Scanned Light Pulse Technique for the Investigation of Insulator-Semiconductor Interfaces. *J. Appl. Phys.* **1983**, *54*, 5245−5251.
(34) Hafeman, D.; Parce, J.; McConnell, H. Light-Addressable Potentiometric Sensor for Biochemical Systems. *Science* **1988**, *240*, 1182−1185.
(35) Sartore, M.; Adami, M.; Nicolini, C.; Bousse, L.; Mostarshed, S.; Hafeman, D. Minority Carrier Diffusion Length Effects on Light-Addressable Potentiometric Sensor (LAPS) Devices. *Sens. Actuators, A* **1992**, *32*, 431−436.
(36) Parak, W. J.; Hofmann, U. G.; Gaub, H. E.; Owicki, J. C. Lateral Resolution of Light-Addressable Potentiometric Sensors: an Experimental and Theoretical Investigation. *Sens. Actuators, A* **1997**, *63*, 47−57.
(37) Zhang, Y.; Ge, L.; Li, M.; Yan, M.; Ge, S.; Yu, J.; Song, X.; Cao, B. Flexible Paper-Based ZnO Nanorod Light-Emitting Diodes Induced Multiplexed Photoelectrochemical Immunoassay. *Chem. Commun.* **2014**, *50*, 1417−1419.
(38) Sun, G.; Zhang, Y.; Kong, Q.; Zheng, X.; Yu, J.; Song, X. CuO-Induced Signal Amplification Strategy for Multiplexed Photoelectrochemical Immunosensing Using CdS Sensitized ZnO Nanotubes Arrays as Photoactive Material and AuPd Alloy Nanoparticles as Electron Sink. *Biosens. Bioelectron.* **2015**, *66*, 565−571.
(39) Wang, J.; Liu, Z.; Hu, C.; Hu, S. Ultrasensitive Photoelectrochemical Biosensing of Multiple Biomarkers on a Single Electrode by a Light Addressing Strategy. *Anal. Chem.* **2015**, *87*, 9368−9375.
(40) Wang, J.; Long, J.; Liu, Z.; Wu, W.; Hu, C. Label-Free and High-Throughput Biosensing of Multiple Tumor Markers on a Single Light-Addressable Photoelectrochemical Sensor. *Biosens. Bioelectron.* **2017**, *91*, 53−59.
(41) Zheng, Y.; Liang, W.; Yuan, Y.; Xiong, C.; Xie, S.; Wang, H.; Chai, Y.; Yuan, R. Wavelength-Resolved Simultaneous Photoelectrochemical Bifunctional Sensor on Single Interface: A Newly in Vitro Approach for Multiplexed DNA Monitoring in Cancer Cells. *Biosens. Bioelectron.* **2016**, *81*, 423−430.
(42) Hühn, J.; Carrillo-Carrion, C.; Soliman, M. G.; Pfeiffer, C.; Valdeperez, D.; Masood, A.; Chakraborty, I.; Zhu, L.; Gallego, M.; Yue, Z.; Carril, M.; Feliu, N.; Escudero, A.; Alkilany, A. M.; Pelaz, B.; del Pino, P.; Parak, W. J. Selected Standard Protocols for the Synthesis, Phase Transfer, and Characterization of Inorganic Colloidal Nanoparticles. *Chem. Mater.* **2017**, *29*, 399−461.
(43) Soloviev, V. N.; Eichhöfer, A.; Fenske, D.; Banin, U. Molecular Limit of a Bulk Semiconductor: Size Dependence of the "Band Gap" in CdSe Cluster Molecules. *J. Am. Chem. Soc.* **2000**, *122*, 2673−2674.
(44) Sambur, J. B.; Parkinson, B. A. CdSe/ZnS Core/Shell Quantum Dot Sensitization of Low Index TiO_2 Single Crystal Surfaces. *J. Am. Chem. Soc.* **2010**, *132*, 2130−2131.
(45) Guijarro, N.; Campiña, J. M.; Shen, Q.; Toyoda, T.; Lana-Villarreal, T.; Gómez, R. Uncovering the Role of the ZnS Treatment in the Performance of Quantum Dot Sensitized Solar Cells. *Phys. Chem. Chem. Phys.* **2011**, *13*, 12024−12032.
(46) Hines, M. A.; Guyot-Sionnest, P. Synthesis and Characterization of Strongly Luminescing ZnS-Capped CdSe Nanocrystals. *J. Phys. Chem.* **1996**, *100*, 468−471.
(47) Jasieniak, J.; Califano, M.; Watkins, S. E. Size-Dependent Valence and Conduction Band-Edge Energies of Semiconductor Nanocrystals. *ACS Nano* **2011**, *5*, 5888−5902.
(48) Samia, A. C. S.; Chen, X.; Burda, C. Semiconductor Quantum Dots for Photodynamic Therapy. *J. Am. Chem. Soc.* **2003**, *125*, 15736−15737.
(49) Emin, S.; Alexandre, L.; Masanobu, W.; Seiichiro, N.; Yasuko, K. Photostability of Water-dispersible CdTe Quantum Dots: Capping Ligands and Oxygen. *Chem. Lett.* **2010**, *39*, 654−656.
(50) Nakamura, S.; Hayashi, S.; Koga, K. Effect of Periodate Oxidation on the Structure and Properties of Glucose Oxidase. *Biochim. Biophys. Acta* **1976**, *445*, 294−308.
(51) Matsuda, Y.; Hoshika, H.; Inouye, Y.; Ikuta, S.; Matsuura, K.; Nakamura, S. Purification and Characterization of Sarcosine Oxidase of Bacillus Origin. *Chem. Pharm. Bull.* **1987**, *35*, 711−717.
(52) Gregg, B. A.; Heller, A. Cross-Linked Redox Gels Containing Glucose Oxidase for Amperometric Biosensor Applications. *Anal. Chem.* **1990**, *62*, 258−263.
(53) Foulds, N. C.; Lowe, C. R. Enzyme Entrapment in Electrically Conducting Polymers. Immobilisation of Glucose Oxidase in Polypyrrole and Its Application in Amperometric Glucose Sensors. *J. Chem. Soc., Faraday Trans.* **1986**, *82*, 1259−1264.
(54) Malitesta, C.; Francesco, P.; Luisa, T.; Giorgio, Z. P. Glucose Fast-Response Amperometric Sensor Based on Glucose Oxidase Immobilized in an Electropolymerized Poly(o-phenylenediamine) Film. *Anal. Chem.* **1990**, *62*, 2735−2740.
(55) Yang, Y.; Mu, S. The Bioelectrochemical Response of the Polyaniline Sarcosine Oxidase Electrode. *J. Electroanal. Chem.* **1996**, *415*, 71−77.
(56) Lad, U.; Kale, G. M.; Bryaskova, R. Sarcosine Oxidase Encapsulated Polyvinyl Alcohol-Silica-AuNP Hybrid Films for Sarcosine Sensing Electrochemical Bioelectrode. *J. Electrochem. Soc.* **2014**, *161*, B98−B101.
(57) Khalid, W.; El Helou, M.; Murböck, T.; Yue, Z.; Montenegro, J.-M.; Schubert, K.; Göbel, G.; Lisdat, F.; Witte, G.; Parak, W. J. Immobilization of Quantum Dots via Conjugated Self-Assembled Monolayers and Their Application as a Light-Controlled Sensor for the Detection of Hydrogen Peroxide. *ACS Nano* **2011**, *5*, 9870−9876.
(58) Yue, Z.; Khalid, W.; Zanella, M.; Abbasi, A. Z.; Pfreundt, A.; Rivera Gil, P.; Schubert, K.; Lisdat, F.; Parak, W. J. Evaluation of Quantum Dots Applied as Switchable Layer in a Light-Controlled Electrochemical Sensor. *Anal. Bioanal. Chem.* **2010**, *396*, 1095−1103.

DOI: 10.1021/acsami.9b03990
ACS Appl. Mater. Interfaces 2019, 11, 21830−21839

ACS NANO

Cite This: ACS Nano 2019, 13, 6151−6169

www.acsnano.org

PERSPECTIVE

The Future of Layer-by-Layer Assembly: A Tribute to *ACS Nano* Associate Editor Helmuth Möhwald

Shuang Zhao,[†] Frank Caruso,[‡,⊗] Lars Dähne,[§] Gero Decher,[∥,⊥] Bruno G. De Geest,[#] Jinchen Fan,[¶] Neus Feliu,[†] Yury Gogotsi,[$] Paula T. Hammond,[□] Mark C. Hersam,[■] Ali Khademhosseini,[○] Nicholas Kotov,[¶,●] Stefano Leporatti,[△] Yan Li,[▲] Fred Lisdat,[▽] Luis M. Liz-Marzán,[▼,⬡] Sergio Moya,[▼] Paul Mulvaney,[⬢] Andrey L. Rogach,[††] Sathi Roy,[†] Dmitry G. Shchukin,[‡‡] Andre G. Skirtach,[§§] Molly M. Stevens,[%] Gleb B. Sukhorukov,[⊥⊥] Paul S. Weiss,[○,¶¶] Zhao Yue,[β] Dingcheng Zhu,[†] and Wolfgang J. Parak*[,†,▼]

[†]Fachbereich Physik, CHyN, Universität Hamburg, 22607 Hamburg, Germany

[‡]ARC Centre of Excellence in Convergent Bio-Nano Science and Technology, and the Department of Chemical Engineering, The University of Melbourne, Parkville, Victoria 3010, Australia

[§]Surflay Nanotec GmbH, 12489 Berlin, Germany

[∥]CNRS Institut Charles Sadron, Faculté de Chimie, Université de Strasbourg, Int. Center for Frontier Research in Chemistry, Strasbourg F-67034, France

[⊥]Int. Center for Materials Nanoarchitectonics, Ibaraki 305-0044, Japan

[#]Department of Pharmaceutics, Ghent University, 9000 Ghent, Belgium

[¶]Department of Chemical Engineering and Biointerfaces Institute, University of Michigan, Ann Arbor, Michigan 48105, United States

[$]Department of Materials Science and Engineering and A. J. Drexel Nanomaterials Institute, Drexel University, Philadelphia, Pennsylvania 19104, United States

[□]Department of Chemical Engineering, Massachusetts Institute of Technology, Cambridge, Massachusetts 02459, United States

[■]Department of Materials Science and Engineering, Northwestern University, Evanston, Illinois 60208-3108, United States

[○]Department of Bioengineering, Center for Minimally Invasive Therapeutics (C-MIT), California NanoSystems Institute (CNSI), University of California, Los Angeles, Los Angeles, California 90095, United States

[●]Michigan Institute for Translational Nanotechnology, Ypsilanti, Michigan 48198, United States

[△]CNR Nanotec-Istituto di Nanotecnologia, Italian National Research Council, Lecce 73100, Italy

[▲]College of Chemistry and Molecular Engineering, Peking University, Beijing 100871, China

[▽]Biosystems Technology, Institute for Applied Life Sciences, Technical University, D-15745 Wildau, Germany

[▼]CIC biomaGUNE, San Sebastian 20009, Spain

[⬡]Ikerbasque, Basque Foundation for Science, Bilbao 48013, Spain

[⬢]ARC Centre of Excellence in Exciton Science, School of Chemistry, University of Melbourne, Parkville, Victoria 3010, Australia

[††]Department of Materials Science and Engineering, and Centre for Functional Photonics (CFP), City University of Hong Kong, Kowloon Tong, Hong Kong SAR

[‡‡]Stephenson Institute for Renewable Energy, Department of Chemistry, University of Liverpool, Liverpool L69 7ZF, United Kingdom

[§§]Nano-BioTechnology group, Department of Biotechnology, Faculty of Bioscience Engineering, Ghent University, 9000 Ghent, Belgium

[%]Department of Materials, Department of Bioengineering and Institute for Biomedical Engineering, Imperial College London, London SW7 2AZ, United Kingdom

[⊥⊥]School of Engineering and Materials Science, Queen Mary University of London, London E1 4NS, United Kingdom

[¶¶]Department of Chemistry and Biochemistry and Department of Materials Science and Engineering, University of California, Los Angeles, Los Angeles, California 90095, United States

[β]Department of Microelectronics, Nankai University, Tianjin 300350, China

Published: May 24, 2019

DOI: 10.1021/acsnano.9b03326
ACS Nano 2019, 13, 6151−6169

ABSTRACT: **Layer-by-layer (LbL) assembly is a widely used tool for engineering materials and coatings. In this Perspective, dedicated to the memory of *ACS Nano* associate editor Prof. Dr. Helmuth Möhwald, we discuss the developments and applications that are to come in LbL assembly, focusing on coatings, bulk materials, membranes, nanocomposites, and delivery vehicles.**

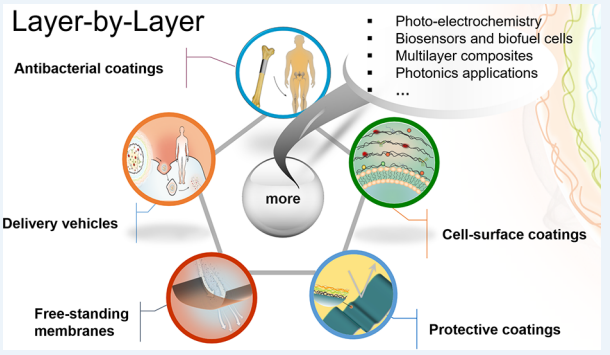

The classic realization of layer-by-layer (LbL) assembly was introduced three decades ago,[1−7] with significant contributions from our colleague, the late *ACS Nano* associate editor Helmuth Möhwald.[8−33] Research on Langmuir−Blodgett deposition and later LbL assembly carried out by Helmuth Möhwald[34] created a critically important foundation for development of multilayer composites based on hybrid organic−inorganic nanostructures and numerous related technologies. Early studies in this area involved self-assembly of multilayers from graphite oxide,[35] clay sheets,[36] nanoparticles,[8,37−42] and other materials, serving as conceptual growth points for the evolution of the fields of biomimetic composites, energy materials, and self-assembly. Numerous studies inspired and authored by Helmuth Möhwald not only paved the way for rapid expansion of nanoparticle-based design of nanocomposites, but also led to understanding biomineralization processes in Nature and their utilization in diverse areas of technology.[43] This field has since undergone massive expansion that continues to this day, and LbL is now an established and widely used technique for coating and encapsulation. With several publications per day, LbL assembly has matured from a scientific oddity to an accessible and useful tool for the preparation of nanoscale functional films. It continues to be used to create new commercial products, making it as interesting for various industries now as chemical vapor deposition (CVD) and physical vapor deposition (PVD) were in the 1960s. Whereas the past and the present of LbL have been extensively reviewed,[11,44−50] in this Perspective, we focus on future opportunities using this exciting technique.

The classic realization of layer-by-layer assembly as a dip-and-rinse process has several conceptual advantages over other methods of materials preparation that predicated its wide use in science and technology. First, compared to other techniques, for instance, sequential spin-coating, it enables preparation of nearly ideal conformal coatings on surfaces of any topography. Thus, it has been applied to planar surfaces, spherical particles, inside pores, and onto other more complex geometries.

Numerous studies authored and inspired by Helmuth Möhwald not only paved the way for rapid expansion of nanoparticle-based design of nanocomposites, but also led to understanding biomineralization processes in Nature and their utilization in diverse areas of technology.

Second, LbL is universal and flexible. It is compatible with other chemistries, meaning that a wide variety of different surfaces can be coated, not only charged substrates. The sequential assembly of the layers involves a washing step after the addition of each layer, which reduces the excess non-assembled materials or molecules. Because of the large variety of materials out of which layers can be formed, LbL enables convenient surface chemistry tailoring. Another important characteristic of LbL technology is the broad and independent variability of each double layer, which, in contrast to many other coating and encapsulation technologies, enables the modular construction of multifunctional devices like a box of bricks that have different properties and can be combined in different ways. These properties, combined with the availability of various stimuli[51−55] to control responsiveness of polyelectrolyte assemblies, make LbL an extremely versatile technology platform. Third, the LbL method replicates the essential aspects of physics and chemistry of materials engineering in living organisms, and therefore, it leads to the amazing spectrum of biomimetic materials. Importantly, they may or may not be based on biomacromolecules pertaining to a specific biological process. Replicating the molecular-scale adaptation of the different structural components at the interfaces taking place in, for instance, biomineralization, one can attain structures and properties equal to or better than those of materials found in biology.[56] Note, however, that as with biology, many LbL processes require time for atomistic relaxation at the interfaces. Although the formation of multilayers approaching thermodynamic equilibrium is a rather time-consuming process, many future technologies will require such highly complex structures. This complexity will be illustrated below for some especially promising developments in this field. Of note are several successful reports of accelerating LbL processes using automated procedures on both planar and colloidal templates.[57−61] In parallel, endeavors have also been undertaken to produce coatings with properties similar to those of LbL films but using single-step approaches.[62−64]

In this Perspective, we highlight future directions with a focus on three areas: (1) functional **coatings** on planar and highly curved surfaces, (2) free-standing **membranes** and **bulk materials**, and (3) delivery vehicles based on **encapsulation** for biomedical applications.

LAYER-BY-LAYER-BASED FUNCTIONAL SURFACE COATINGS

Versatility of Coatings. Layer-by-layer coatings are extremely versatile. They enable variability in (1) composition, *i.e.*, the integration of different materials; (2) vertical structuring normal to the surface, *i.e.*, the possibility to create defined

DOI: 10.1021/acsnano.9b03326
ACS Nano 2019, 13, 6151−6169

sequences of layers;[65] and (3) anisotropic alignment, *i.e.*, to orient anisotropic materials within layers.

(1) Toward Multinanocomposites. Among all methods for functionalizing surfaces, LbL assembly arguably has the largest choice of deployable components (inorganic salts, organic molecules, polymers, DNA,[66,67] graphene oxide, biomolecules, lipids, nanoparticles, or biological objects including cells[68]). In polyelectrolyte multilayers, one can bring tens (if not hundreds) of materials together in ordered ways, whereas the number of components in most current nanocomposites is less than ~20. The precision of LbL in controlling the structures of materials bridging the molecular, nano-, meso-, and microscales[69−72] makes it possible to create conformal coatings with exceptionally high curvatures, including functionalized particles,[73−76] and to design self-assembled nanocomposites with previously unexpected combinations of macroscale properties.[36,69,77] Along these lines, LbL makes it possible to demonstrate the transition between nano- and macroscale optical effects in gold films experimentally by precisely tuning interparticle distances in multilayers of silica-coated gold nanoparticles,[78,79] leading to extremely efficient substrates for surface-enhanced Raman scattering (SERS) detection.[80] The fundamental findings regarding rare combinations of properties made using LbL-based composites were confirmed using other techniques, such as vacuum-assisted filtration[81−83] and spin-coating.[84] Layer-by-layer assembly enables the design and preparation of materials with adjustable multifunctionality, which is difficult, if not impossible, using other formulation technologies. Thus, LbL offers the tools to fabricate advanced materials by combining heterogeneous components with potential applications in optoelectronic devices, smart surfaces, solar cells, *etc.*

(2) Toward Three-Dimensional (3D) Coatings. The LbL technique also offers multiple approaches for the fabrication of composite materials from heterogeneous components, where the compositions of the materials are varied in the direction normal to the substrate. In addition to gradients in chemical composition, one can also vary the mechanical, optical, and electronic properties of composites in the vertical direction. The LbL concept can also be integrated with other nano- and microfabrication techniques. In particular, the use of printing strategies and combinations with other 3D coatings with variable vertical composition are possible. Combining LbL assembly with other modern strategies (*e.g.*, roll-to-roll, lithography, and 3D printing, *etc.*) as well as high-throughput production methods[57,58,85−88] is beneficial for the preparation of novel functional LbL composites. Note that multilayer nanocomposites, made by LbL and Langmuir−Blodgett deposition, are extensively used in industry already, albeit produced using closely related, derivative methods. Some representative examples of these multilayer composites are those based on various forms of nanocarbons (graphene, graphene oxides, graphene, nanotubes, nanoribbons, graphene carbon quantum dots, *etc.*[81,82,89−91]) and those based on various forms of ceramic nanoplatelets (clay, metal oxides, MXenes, *etc.*[89,92−94]). The former are employed in energy technologies, whereas the latter are used in membrane and coating technologies. In each case, the composite multilayer production is reliable, scalable, and low cost due to self-assembly of anisotropic colloids. Future directions in multilayer biomimetic composites are likely to include computational design of the multilayers starting from molecular dynamics[95−97] and coarse-grained models of the multilayers.[92]

(3) Toward Materials with Complex Anisotropies. Most of the current materials are isotropic. Materials with anisotropic properties are, in general, more difficult to prepare and to characterize. For example, grazing incidence spraying[98] enables alignment of nanowires, nanorods, and nanofibers in plane[99,100] during the deposition of individual layers in LbL films. With unidirectionally oriented multilayers, one can fabricate films containing ultrathin polarizers.[100] This approach, however, is capable of producing more complex anisotropies, even over large surface areas, by changing the direction of alignment in each individual layer of a multilayer film. We are just starting to realize materials with crisscross and even helical superstructures. Materials with such anisotropies are likely to be interesting for various applications in mechanics, photonics, and other areas.

Protective Coatings. Layer-by-layer assembly provides a convenient coating strategy for the protection of consumer products, such as paints for corrosion protection or antigraffiti coatings.[101−104] Here, among the spectrum of technological advances based on LbL materials, one should mention anticorrosion coatings investigated by Möhwald and co-workers. Andreeva *et al.* deposited oppositely charged $(PEI/PSS)_n$ polyelectrolyte (PE) multilayers on aluminum surfaces.[102] The corrosion processes on the aluminum surfaces were blocked due to the pH-buffering ability of polyelectrolyte-based LbL coatings (Figure 1a). Another representative advance in this area is halloysite nanocontainers for anticorrosion coatings. Shchukin *et al.* first deposited LbL-assembled polyelectrolyte multilayers of $(PAH/PSS)_n$ on the surfaces of inhibitor-loaded halloysite nanotubes.[105] After the halloysite nanocontainers were embedded, the sol−gel SiO_x/ZrO_y active composite coatings with the nanocontainers showed long-term anticorrosion performance. The LbL composite multilayers provide effective storage and prolonged release of the inhibitor. Similarly, SiO_2 particles coated with LbL multilayers entrapping inhibitors were used as nanocontainers to achieve self-healing and anticorrosion composite coating simultaneously.[18,103] Li *et al.* also designed a silica/polymer double-walled hybrid nanotube loaded with active molecules for metal corrosion protection.[106] A new generation of anticorrosion coatings that possess passive matrix functionality and that actively respond to changes in the local environment has been introduced.[107] Active corrosion protection aims to *restore* the properties of the material when the passive coating matrix is broken and corrosion of the substrate has started. The main component of the self-healing anticorrosion coatings are capsules in flat layers, which provide controlled release of the corrosion inhibitor on demand and only inside the corroded area (see Figure 1a). This release acts as a local trigger for the mechanism that heals the defects. The LbL assembly approach is an effective tool for the fabrication of the capsule shells, controlling release of the corrosion inhibitor on demand. Layer-by-layer assembly enables the use of various materials as shell components, utilizing weak, mostly electrostatic forces for their assembly. Depending on the nature of the "smart" materials (*e.g.*, polymers, nanoparticles) introduced into the container shell, different stimuli can induce reversible and irreversible shell modifications: pH, ionic strength, temperature, ultrasonic treatment, and electromagnetic fields. The different responses that can be observed vary from fine effects, such as tunable permeability, to more profound ones, such as total rupture of the container shell. These different behaviors depend on the composition of the polyelectrolyte multilayers (*e.g.*, weak polyanion−weak polycation or strong polyanion−weak polycation-based interactions).

DOI: 10.1021/acsnano.9b03326
ACS Nano 2019, 13, 6151−6169

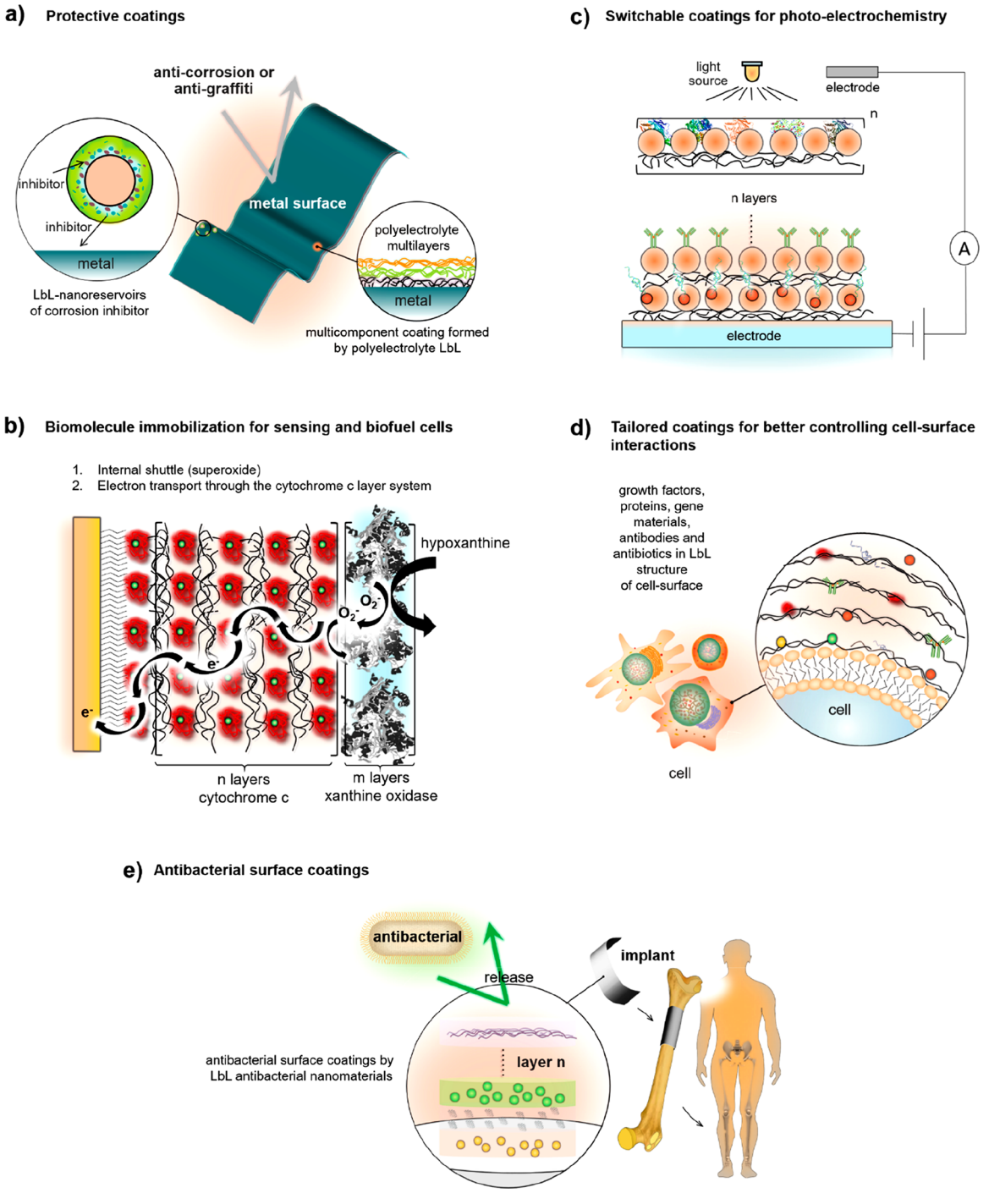

Figure 1. (a) Layer-by-layer assembly can be used in protective coatings in several ways, *e.g.*, as nanoreservoirs of corrosion inhibitors and in multicomponent coatings. (b) Layer-by-layer assembly can be used for biomolecule immobilization in sensing devices and biofuel cells. (c) Layer-by-layer assembly can be used in photoelectrochemical devices to create 3D structures; in medical devices, different biological materials can be assembled in each layer independently. (d) Tailored coatings for better control of cell−surface interactions. (e) Layer-by-layer assembly can be used in antibacterial coatings of implants.

Coatings for Photonics and Energy-Related Applications. There are numerous energy applications that can take advantage of the tunable mechanical, electrical, and chemical properties of LbL composites.[108] In fact, the first implementation of graphene composites on electrodes currently used in a variety of batteries, supercapacitors, conductive inks, and fuel cells was demonstrated in LbL composites referring to these materials as graphite oxide in 1996.[35] The excellent laminar organization of the films also afforded demonstration of the transition from the nonconductive state of graphite oxide to reduced graphene and their utilization in lithium batteries.[109] Composite materials with identical layered design were later produced by other techniques, such as vacuum-assisted filtration, are widely used in the technology.[81] There are also many other energy-conversion devices that employ LbL multilayers from electroconductive materials which include batteries, supercapacitors, catalysts, solar cells, and fuel cells, and these modern applications frequently place higher demands on the performance

DOI: 10.1021/acsnano.9b03326
ACS Nano 2019, 13, 6151−6169

of the composites.[110] Layer-by-layer multilayers can integrate the properties of different constituent materials, and judicious design enables them to take on multiple roles and functionalities, for instance, as battery anodes or ion-transporting membranes.[111−113] Layer-by-layer assembly also facilitates the creation of controlled assemblies to study photonic properties of materials. Layer-by-layer assembly enables composite functional materials that combine polymers with oppositely charged nanoparticles. Such structures can easily be created on planar substrates[114−117] and on colloidal microspheres.[23,118−120] The organized superstructures from semiconductor nanoparticles (NPs), also known as quantum dots (QDs), can also be made using LbL as was demonstrated for CdS, PbS, and TiO_2.[121] The advantage of QDs compared to graphite/graphene oxide is that they are capable of emitting in the visible[114,122] and near-infrared[122] parts of the spectrum; this property has been used to fabricate luminescent self-assembled films and to study energy transfer in such composites.[115] Directed energy transfer from specific layers of QDs toward an interface or electrode was made possible exactly due to the possibility of arranging the LbL layer in the order of decreasing or increasing band gaps in graded semiconductor nanostructures.[123] Excitation recycling in LbL-grown graded band gap QD structures has been demonstrated[116] and ascribed to superefficient exciton funneling to the layer containing the largest QDs.[117] Besides graphene, layer-by-layer assembly is also compatible with other emerging two-dimensional (2D) materials such as hexagonal boron nitride whose LbL coatings yield exceptional performance as gate dielectrics in graphene field-effect transistors.[124] Last but not least, LbL has been used to build coatings for electromagnetic shielding. Flexible and electrically conductive thin films are required for electromagnetic interference (EMI) shielding of portable and wearable electronic devices.[93] The LbL technique enables combinations of nanoparticles and polymers, providing a platform for developing hierarchical architectures with a combination of properties including mechanical strength, transparency, and conductivity.[89] Spin-spray LbL enables rapid assembly of 2D Ti_3C_2 MXene−carbon nanotube (CNT) composite films for EMI shielding. These semitransparent LbL MXene−CNT composite films showed high conductivities and high specific shielding effectiveness, which are among the highest reported values for flexible and semitransparent composite thin films.

Biomolecule Immobilization for Sensing and Biofuel Cells. The LbL technique has found widespread applications in the fixation of biomolecules to surfaces[49,125] because it enables (1) engineering of man-made materials with structural analogy to biomaterials; (2) the controlled deposition of biomolecules because deposition can be governed not only by the number of layers but also by adjusting pH, ion concentration, temperature, and polyelectrolyte and biomolecule concentrations in each layer; (3) the defined integration of different biomolecules in different layers and, thus, the creation of sequential signal chains; and (4) the incorporation of other functional components, such as mediators, which can facilitate electron transfer between immobilized molecules and electrodes or lipids, which, in turn, facilitates integration of more hydrophobic membrane proteins.[126] Furthermore, additional layers on top of the biomolecular assembly enhance the stability of the coatings and ensure efficient discrimination against unwanted species when the multilayer structure is used for sensing purposes. Interestingly, biomolecules cannot simply be passively incorporated into LbL architectures, but because they often carry charges, they can be used as separate building blocks in the assembly process. In this context, alternating polymer/biomolecule or NP/biomolecule structures can be formed,[127,128] as well as pure biomolecular LbL assemblies, such as DNA/protein or protein/protein multilayers.[129] The beauty of the technique can also be demonstrated by immobilizing different biomolecules in different layers on the sensing surface. This localization enables the construction of defined signal pathways by exploiting sequential reaction schemes. Here, reaction products formed in one layer can be further converted in a subsequent layer, as shown in Figure 1b.[13] These artificial architectures can mimic biological functions, such as sequential electron transfer reactions or switchable pathways.[130] This capability enabled, for instance, the first implementation of tissue-adapted neuroprosthetic implants from conductive composites[131] and light-induced excitation of neurons.[132] Further steps in this directions can be based on direct electron transfer between the immobilized protein molecules. The LbL technique enables the artificial arrangement of redox centers, while keeping them in or close to their natural states. Here, developments are still at early stages—more advanced structures appear to be feasible though, such as the arrangement of enzymes into complex cascades to create artificial metabolome structures with high efficiency.[133−135]

Switchable Coatings for Photoelectrochemistry. Electrochemical devices can be controlled by light based on photosensitive switches, such as QDs.[136−139] Light-generated charge carriers can create photo currents, which enables both control and monitoring of electrochemical reactions (see Figure 1c).[140] Inorganic, photoactive materials such as QDs are commonly used in such applications, but light-sensitive biomolecules have also gained considerable interest for the conversion of light into electrical or chemical energy.[141] An example is the protein supercomplex photosystem I, which can be assembled with the help of negatively charged DNA and the positively charged redox-protein cytochrome *c*. This system generates well-defined photocurrents, the magnitude of which depends on the number of deposited layers.[142] Charge transfer in LbL structures has been well-studied by numerous groups.[14,17,127,143−145] Layer-by-layer assembly can be used to increase the coverage of redox active molecules by assembling 3D structures, thereby dramatically increasing the analytical signal, but also improving the signal-to-noise ratio (SNR).[146,147] The response from multilayer structures is significantly enhanced compared to the response from single monolayer-based structures. In addition, different kinds of biological modifications can be introduced to the LbL structures of the photoelectrochemical devices. For example, LbL offers the convenient possibility to immobilize enzymes, thereby controlling redox reactions close to the light switches as fixed on the surface of the electrodes. The porous structures of LbL films enable sub-

The layer-by-layer technique enables combinations of nanoparticles and polymers, providing a platform for developing hierarchical architectures with a combination of properties including mechanical strength, transparency, and conductivity.

DOI: 10.1021/acsnano.9b03326
ACS Nano 2019, 13, 6151−6169

strates to reach the enzymes and cosubstrates or reaction products, such as O_2 or H_2O_2, to reach the light switches.[148−150] In the future, we expect antibodies and DNA to be incorporated as recognition elements into LbL-based structures. Creating defined sequences of antibodies or oligonucleotides within the 3D assemblies is also an important goal.[151,152] There is great potential for photoelectrochemical devices to be developed that can sense multiple analytes in parallel. Layer-by-layer structures can also introduce good biocompatibility by modifying working electrodes in such a way that applications in cell-based detection become possible. The detection of several metabolites will enable more specific studies of cellular activities.[152] Moreover, the biocompatibility and the ease of preparation of LbL-based systems will enable the fabrication of miniature sensors for human uses such as wearable health monitors and portable environmental monitoring devices. In addition, electrochromic coatings can be produced by self-assembly of 2D titanium carbide ($Ti_3C_2T_x$) MXene and gel electrolyte with a visible absorption peak shift from 770 to 670 nm and a 12% reversible change in transmittance with a switching rate of <1 s when cycled in an acidic electrolyte under applied potentials of less than 1 V.[153] The LbL film can act as both transparent conductive coating and active material in an electrochromic device, opening avenues for a number of optoelectronic, sensing, and photonic applications. Hybrid systems prepared by LbL assembly of polyoxometalate clusters and poly(4-vinylpyridine) also show reversible electro- and photochromic behavior.[154,155]

Tailored Coatings for Better Control of Cell−Surface Interactions. For many applications, detailed understanding of the interface between cells and underlying substrates is critical.[156,157] It is well established that LbL assembly offers a means to immobilize different biomolecules on surfaces using mild deposition conditions (see Figure 1d).[158] Layer-by-layer assemblies can integrate plasmids,[159] growth factors,[160] proteins, genetic material, antibodies, and antibiotics directly into the layers or the components can be precomplexed with polyelectrolytes and then assembled as complexes.[161] For such biological components, *e.g.*, for growth factors, their action can be extended in time[162] or triggered by external stimuli, whereas their controlled release can be regulated by barrier layers. Multilayers can be prepared from biocompatible polyelectrolytes and their mechanical properties; wettability, and interactions with proteins and cells, can be fine-tuned by chemical cross-linking, thermal annealing,[163] or the addition of nanoparticles into the assembly (see Figure 2).[164] This strategy enables the availability of biomolecules on surfaces to be controlled.[162,165,166] Imagine chemically identical surfaces (composition, roughness, *etc.*), below which nanoreinforced strata are hidden (*i.e.*, deposited) that enable control of the tensile strength of the interface. Other combinations of surface properties can be deposited on top of cell-culture gels. Such surface engineering would be extremely useful for implants and scaffolds as a means to enhance cell adhesion, mobility, and differentiation. In the long term, there are numerous different ways for the LbL technique to be implemented. For example, they can be used to modify scaffolds and implants to create customized environments and interfaces in tissue engineering. Layer-by-layer assembled surfaces can also be laterally patterned as substrates for the growth of cells. Micropatterned deposition of LbL films has been used to generate architecturally organized cellular structures that better mimic the complex microstructures of tissues in the body. For example, patterned cocultures were generated by sequentially

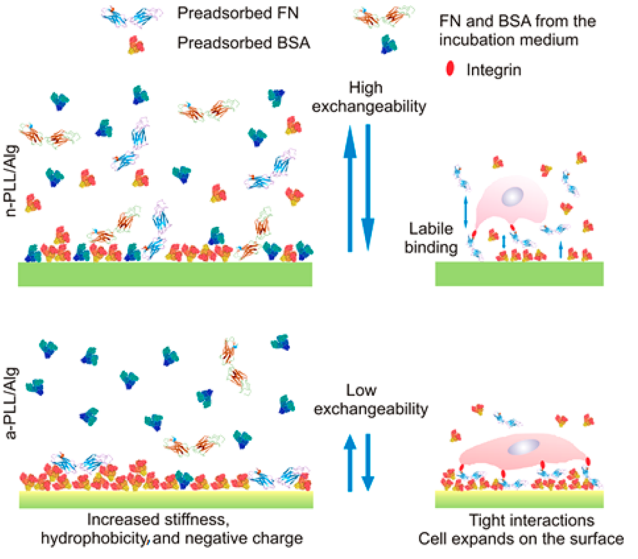

Figure 2. Scheme of the protein adhesion mechanism and the effects on cell adhesion for non-annealed poly(L-lysine/alginate) (PLL/Alg) and annealed-PLL/Alg.[157] Results from the exchangeability assays are schematically described. On annealed PLL/Alg layer-by-layer (LbL) surfaces, proteins exhibit augmented interactions with the substrate, the exchangeability is reduced, and fibronectin (FN), either alone or in cooperation with bovine serum albumin (BSA), has stronger interactions with the LbL surface coating. The effect on cell adhesion is also illustrated.[169] The objects depicted in the scheme are not to scale, and for FN, only the FN III fragment is represented. Adapted with permission from ref 150. Copyright 2019 John Wiley & Sons, Inc.

depositing micropatterned LbL films made of hyaluronic acid and polylysine or collagen that could be used to render regions of a surface adhesive to cells.[167,168] In such cultures, patterned cocultures of liver cells and fibroblasts showed increased functionality compared to various controls.

This strategy ultimately results in a multitude biomimetic composites including those made in bulk form. The diverse composite structures replicated using LbL assembly[170−173] made possible *ex vivo* replication of nacre,[36] enamel,[170] extracellular matrix,[174,175] and models of cellular organelles.[176−178] By combining LbL assembly with other fabrication techniques at the micrometer and millimeter scale, tissue replicas with

Micropatterned deposition of layer-by-layer films has been used to generate architecturally organized cellular structures that better mimic the complex microstructures of tissues in the body.

complex geometries have been obtained, such as for bone marrow.[179,180] The exceptional materials properties of the multilayer composites and the generality of the approach have also made possible the design, fabrication, and implementation of implantable devices,[132,181,182] sensors,[53,183,184] drug-delivery vehicles,[185,186] and optical devices,[187,188] exceeding the performance of existing technologies.

Antibacterial Surface Coatings. The advent of LbL films has led to several new strategies for the development of antibacterial coatings, from the fabrication of multilayers with

DOI: 10.1021/acsnano.9b03326
ACS Nano 2019, 13, 6151−6169

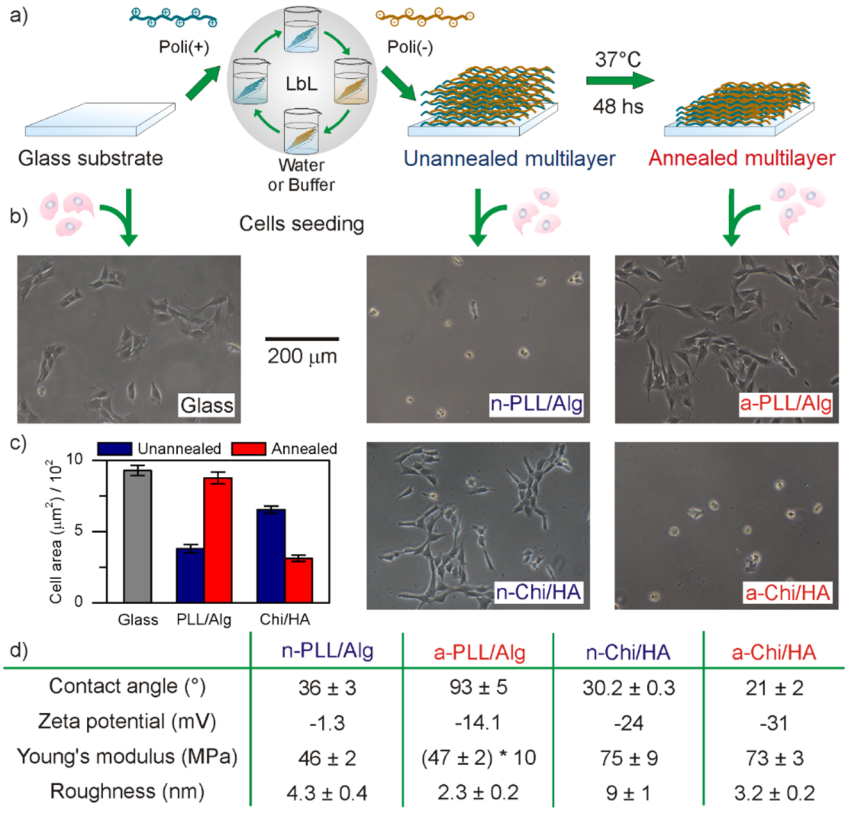

d)	n-PLL/Alg	a-PLL/Alg	n-Chi/HA	a-Chi/HA
Contact angle (°)	36 ± 3	93 ± 5	30.2 ± 0.3	21 ± 2
Zeta potential (mV)	-1.3	-14.1	-24	-31
Young's modulus (MPa)	46 ± 2	(47 ± 2) * 10	75 ± 9	73 ± 3
Roughness (nm)	4.3 ± 0.4	2.3 ± 0.2	9 ± 1	3.2 ± 0.2

Figure 3. Changes in cell adhesion and in the physicochemical properties of layer-by-layer (LbL) multilayer coatings induced by thermal annealing.[157] (a) Scheme of the assembly and annealing protocols. (b) Phase contrast images of C2C12 cells adhered on glass, poly-L-lysine/alginate (n-PLL/Alg, a-PLL/Alg), n-chitosan/hyaluronic acid (n-Chi/HA), or a-Chi/HA as indicated. (c) Average cell adhesion spreading area from cells seeded on glass, n-PLL/Alg, a-PLL/Alg, n-Chi/HA, or a-Chi/HA polyelectrolyte multilayers. (d) Changes in physicochemical properties of polyelectrolyte multilayers upon annealing. Adapted with permission from ref 150. Copyright 2019 John Wiley & Sons, Inc.

cationic polymers that disrupt bacterial membranes,[189] to the assembly of antibacterial nanomaterials such as silver nanoparticles or graphene oxide,[190] to the encapsulation of antibiotics in the multilayers, to combinations of all these elements.[191] The LbL assembly can include several layers of nanomaterials, combine layers of different nanomaterials in a film, or facilitate inclusion of antibiotics in the films by complexing with the polymers (see Figure 1e). Many antibiotics have charged groups that can be used to form complexes with polyelectrolytes in the LbL films or assembled in films replacing polyelectrolyte layers. The LbL technique has the advantage that it can be applied straightforwardly on almost any charged surface, and antibacterial coatings could be developed for medical devices as well as for implants. In particular, the LbL technique has significant potential in the design of antibacterial coatings that can inhibit nosocomial infections during implant surgery. An optimal antibacterial coating for bone implants based on release of an antibiotic should involve an initial burst release at the time of surgery, followed by prolonged release over the weeks following the surgical intervention to ensure bone tissue regeneration.[192] The LbL technique can be used to design films capable of fully or partially degrading and releasing antibiotics at different times and rates. Examples in the literature show that aminoglycans, such as gentamicin, can be released from LbL films, combining burst and steady releases that would be particularly suitable for implant surgery.[193] Moreover, the LbL technique enables the additional assembly of growth factors on the coating that can counteract negative effects on cell growth and differentiation caused by a high localized dose of antibiotics.[194] These combinations can result in films with enhanced antibacterial properties and in the design of coatings suitable for different environments in multiple medical settings or for antifouling applications.

LAYER-BY-LAYER-BASED MEMBRANES

Purification Technologies. Another future for LbL coatings lies in separation technologies, such as liquid or gas permeation membranes (see Figure 4).[69,195,196] Significant pioneering work has already been carried out,[197−201] starting with gas separation membranes,[69] but recently, LbL membrane modification for fresh water production has been explored further. Nanofiltration membranes for the removal of particles down to virus sizes of ∼35 nm are not able to retain dissolved materials, such as ions, leading to issues with water hardness, low molecular weight pharmaceutical agents, *etc.*, which become increasingly problematic in fresh water preparation. However, reverse osmosis (RO) membranes consume a great deal of energy and retain all salts, which is not useful for drinking water. In contrast, a few LbL-assembled layers of poly(diallyldimethylammonium chloride) (PDADMAC)/PSS on top of tubular filtration membranes of pore size 20 nm are able to increase the retention of magnesium sulfate from 5% to over 90% and for several endocrines above 50−90% depending on the endocrine type (see Figure 5).[202] In contrast to RO membranes, these LbL membranes allow permeation of sodium chloride, maintain high fluxes, and require much less pressure and energy. Up to now, the LbL coating of membranes has been evaluated only for films based on the

DOI: 10.1021/acsnano.9b03326
ACS Nano 2019, 13, 6151−6169

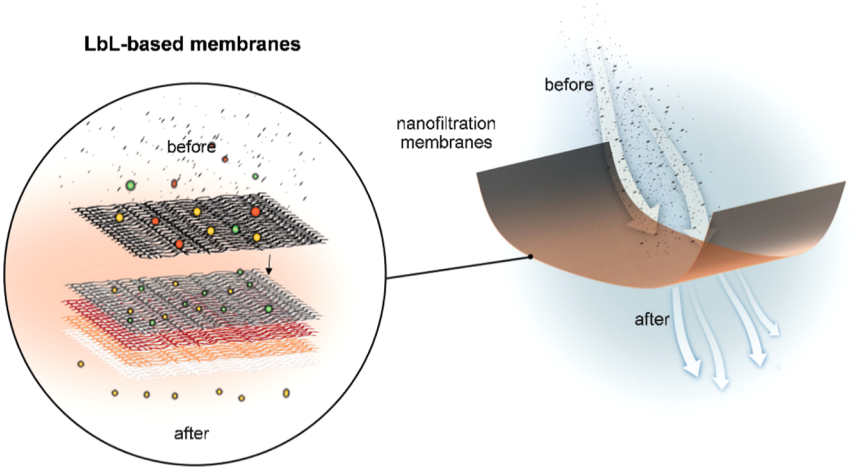

Figure 4. Layer-by-layer (LbL) assembly can be used for membranes for gases and liquids.

combination of one polycation with one polyanion. However, one can imagine that a multifunctional coating could improve the membranes further. The first layer on the membrane has to ensure a good connection of the LbL film to the membrane in order to resist sufficiently high-pressure backflushing cycles. Furthermore, the first polyelectrolyte has to be assembled exclusively on top of the pores and should not penetrate into the pores, as otherwise these would be blocked. The intermediate layers should utilize a design in which the mesh size controls the retention of the analyte and also ensures the removal of specific pollutants.[91] Finally, the outermost layer should reduce the fouling behavior of the membranes by controlling its hydrophilic properties and electrostatic repulsion.[203−205]

Introducing Channels in Biological Membranes. Biomimetic nature of LbL materials opens the possibility to replicate biological membranes. Cell membranes comprise not only lipids but also high protein content,[206] for example, transmembrane proteins that form channels for molecular transport into/out of cells. Lateral inhomogeneity is important. Here lies one big challenge for the future. To date, LbL structuring has predominantly only been possible perpendicular to the surface, *i.e.*, by variation of the compositions of the different layers. However, in order to create LbL-assembled membranes mimicking the function of biological membranes—for example, with integrated protein-based channels—lateral structuring would also be required. In the simplest case, "channels" in the form of holes could be introduced, for example, by nanoplasmonic heating.[207] Another option lies in tethered membranes. In recent work, dense membranes with limited defects and high resistivity were assembled on top of multilayers.[208−211] These membranes can contain channels with selective ion permeability.[212] For electronic sensing, the multilayers provide a means to control the distance of the lipid bilayer from the electrodes, which is particularly useful for membranes incorporating channels and transmembrane proteins, avoiding undesired effects from the electrode on channel and protein behavior.[212] Another method for lateral structuring might be based on the fusion of microcapsules.[213] Still, despite the numerous ideas outlined here, lateral structuring of LbL films remains a challenge.

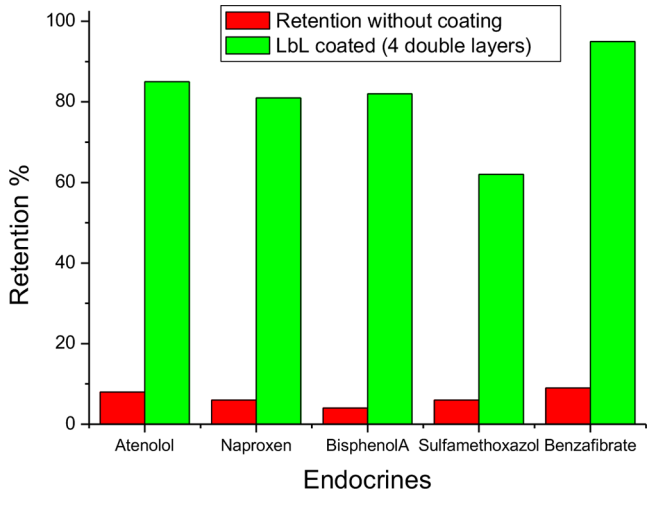

Figure 5. Retention of different endocrines by an uncoated poly(ether sulfone) membrane (red) and by a layer-by-layer (LbL)-coated $(PDADMAC/PSS)_4$ membrane (green). Unpublished data by the group of Lars Dähne.

LAYER-BY-LAYER-BASED ENCAPSULATION FOR DELIVERY VEHICLES

Layer-by-layer Assembly for Encapsulation. Layer-by-layer technology for micro- and nanoencapsulation was introduced ~20 years ago and initially looked extremely promising (see Figure 6).[10,11,214−219] The key advantage was considered to be the simplicity with which one could construct multifunctional delivery systems. In fact, LbL capsules can combine multiple functions and external responsiveness. However, LbL-based encapsulation suffers from high permeability of small, water-soluble molecules (*i.e.*, leaching) and rather time-consuming processes for fabrication. Some of these problems have been solved, such as expanding the class of molecules that can be encapsulated (*e.g.*, doxorubicin, paclitaxel, liquid crystals, siRNA) without severe leaching,[44,45,220−225] and inroads have been made into the problem of scale-up.[61,226,227] This approach has also been made possible by extending the initial capsule geometries to more sophisticated structures, such as capsosomes, *etc.*[228−235] The capsule shells can also be labeled with different types of nanoparticles, providing contrast for imaging[118−120] or enabling magnetic targeting.[236,237] Currently, the technology still has potential, particularly in areas where other technologies are not available. A number of studies on various cell types, including macrophages, dendritic cells, neurons, and stem cells, have

DOI: 10.1021/acsnano.9b03326
ACS Nano 2019, 13, 6151−6169

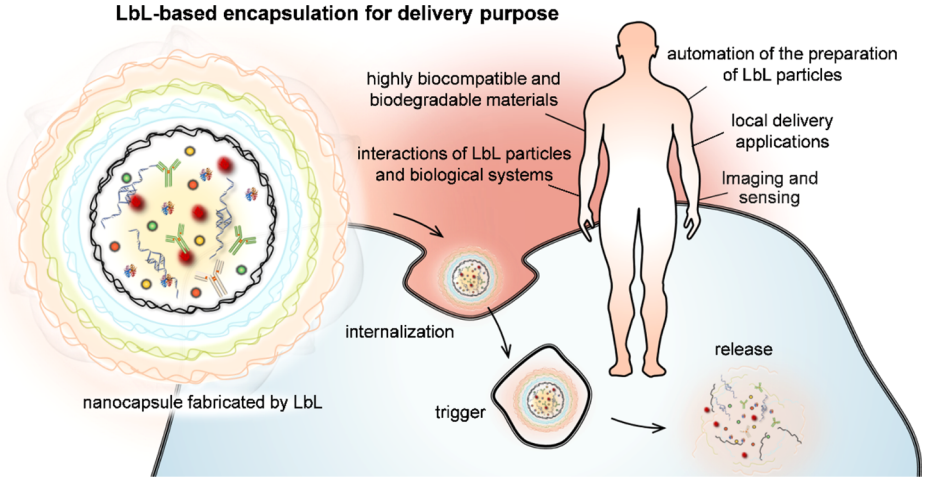

Figure 6. Layer-by-layer (LbL) assembly can be used to fabricate encapsulation platforms for nanodelivery.

demonstrated that incubation with cells results in internalization of capsules by cells without significant effects on cell viability.[238−240] The elastic properties facilitate their uptake as the capsules can easily be deformed during internalization.[241−244] In other words, cells were found to tolerate capsule internalization, which is not always the case for other delivery systems. Detailed studies on the tissue response after subcutaneous[245] and pulmonary[246] administration of degradable LbL capsules composed of polypeptide and polysaccharide building blocks have also demonstrated that LbL capsules exhibit a moderate foreign body response and are easily internalized by immune cells, such as macrophages and dendritic cells. This advance should pave the way for further development of such carriers in advanced vaccine technologies. In summary, LbL offers a good platform for delivery of encapsulated cargo inside cells, which is discussed below in terms of drug delivery and imaging/sensing. Because the capsules remain in endosomes/lysosomes after internalization, endosomal escape and translocation of encapsulated compounds to the cytosol remains a significant hurdle.

Delivery of Therapeutic Agents. The LbL technique opens the possibility of assembling therapeutics in between layers of polyelectrolytes, on top of nano/microparticles that protect a certain cargo, while, at the same time, making multiple functional groups available in the polyelectrolyte, which can be engineered to generate stealth coatings for targeting delivery. For the delivery of encapsulated therapeutics in polyelectrolyte multilayers, the assemblies must degrade, liberating the material entrapped between the layers. However, as we noted above, LbL assemblies have intrinsically semipermeable properties that can be tuned by means of layer numbers and thicknesses as well as by the type of the interacting polyelectrolyte pairs, resulting in leaching even before intended degradation and subsequent release. Thus, the initial euphoria in scientific articles to encapsulate low molecular weight drugs and to release them in a controlled manner on demand has not yet translated into real-world applications. As previously noted, the most critical reason for this difficulty in translation is the high permeability of the films for small molecules (see Figure 7). Even for the very dense polyelectrolyte system poly(allylamine hydrochloride)/polystyrenesulfonate (PAH/PSS), researchers recorded release rates ranging from minutes to a few hours for water-soluble molecules having molecular weights below 5 kDa.[247] In contrast, large molecules with molecular weights above 10 kDa can be permanently immobilized, either in the polyelectrolyte layers or in capsules comprising polyelectrolyte walls. This same conclusion has been shown over the past decade for a variety of biomolecules, including proteins, such as antibodies;[248] growth factors;[249] hormones;[250] enzymes;[251] nucleic acids, such as DNA plasmids;[237] different types of RNA molecules, such as silencing RNAs;[252] and polysaccharides such as alginate, carrageenan, chitosan, and hyaluronic acid.[253]

In parallel, new therapeutic avenues based on the delivery of high molecular weight drugs, for instance, at the site of the implantation of LbL material.[159] Plasmids, specific antibodies, RNA, or DNA can be delivered by incorporation in LbL films and can be utilized as personalized medicines. However, due to the sensitive and specialized recognition of such molecules by our immune system, it is hard to deliver them efficiently *in vivo* to the intended targets. For this purpose, LbL assemblies could have a bright future in the form of capsule formulations, because the necessary multifunctionality can be delivered by LbL technology. For example, an ideal capsule should have an inner surface that is not interacting with the biomolecule in order to retain its functionality. The intermediate layers determine the release behavior, which could be controlled slow release, immediate release caused by an internal trigger (*e.g.*, by

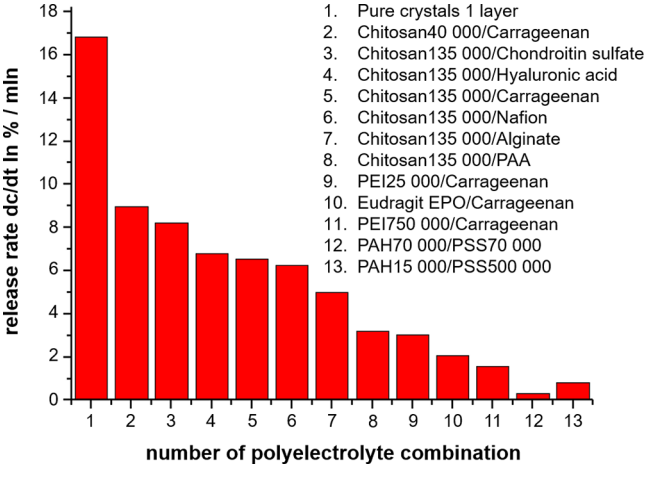

Figure 7. Permeability of layer-by-layer (LbL) membranes consisting of different polyelectrolyte combinations (8 layers) for small molecules (fluorescein). Unpublished data from the group of Lars Dähne.

DOI: 10.1021/acsnano.9b03326
ACS Nano 2019, 13, 6151−6169

the lower pH value in cancer cells or by specific enzymatic surroundings[254,255]) or release activated by an external trigger (*e.g.*, NIR light,[22,237,256−258] X-ray radiation, ultrasound (US),[259−261] or magnetic fields[262,263]). Internal triggers can readily be created by combining polycations and polyanions in such a way that their degradation will be fast or slow. The sequential assembly of polyelectrolytes in LbL enables control over the composition of the layers in the vertical direction and could be used to deliver different therapeutics progressively. For example, two siRNA molecules with complementary actions could be assembled in different positions within the LbL film, so that they are released sequentially. Degradation of the multilayers in biological fluids or intracellularly can be selected because matrices can be programmed by varying the assembly conditions, the number of assembled layers and the combination of polycations and polyanions. The surface layer is also important: It should not be recognizable by the immune system in order to realize high circulation times, but it should nonetheless bind specifically to a defined target. In the case of systemic delivery, there is the problem of targeting, *i.e.*, to produce locally enhanced concentrations of the pharmaceutic agent at the desired target site. One interesting approach, which has not yet been fully exploited, is cell-mediated delivery, where cells are used as natural transporters to carry the encapsulated materials to a targeted site.[264] Here, externally driven cell navigation could be used.[265] *In vitro* studies have demonstrated that cell motion is possible in magnetic field gradients if the cell has internalized magnetic capsules.[266] Magnetic capsules can bring genetic materials inside the cells and reprogram the cells in such a way that the follow-up sorting of altered and nonmodified cells can easily be done by magnetic sorting.[267] Such magnetic targeting is biocompatible. The ability of mesenchymal stem cells (MSCs) to differentiate was not affected by magnetic manipulation.[268] This is important, as MSCs impregnated with capsules could be used as natural cargo transporters. Also, whereas many applications focus on systemic delivery, local delivery may offer new approaches, which deliberately avoid the "targeting" issue. One interesting example is LbL particles that were designed for transdermal delivery of vaccine and adjuvant peptides *via* hair follicles. In contrast to dissolved molecules, particles in sizes ranging between 300 and 900 nm can be inserted in hair follicles by intense massage.[269] The diffusion of vaccines to the Langerhans cells in the skin is much easier through the follicle membrane than through the epidermis. In order to transport the vaccine peptides into the hair follicle, 600 nm silica particles were coated with polymethacrylate with LbL assembly, with an outermost layer having a pK_a value of 6.2. The pH difference between skin (pH 5−5.5) and follicle center (pH 7.4) was selected for the delivery of the peptides, which were tagged with four glutamic amino acids bearing negative total charge. The vaccines were efficiently adsorbed at pH 4.5 onto the partly positively charged particles and kept stably attached during the skin massage. After arriving at the follicle center where the pH was 7.4, the zeta-potential of the particles switched and became highly negative and the vaccines were released due to electrostatic repulsion. In general, LbL capsules have made the step from *in vitro* demonstration to *in vivo* experiments. For example, these particle systems can induce bone formation *in vivo* (when loaded with growth factors),[249] target atherosclerotic plaques *in vivo*,[270] and generate a significant immune response *in vivo* (when loaded with immunogenic peptides).[271] Both peptide- and protein-antigen-loaded LbL capsules generate a significant immune response *in vitro* and *in vivo*.[254] It was demonstrated that ovalbumin (OVA) (a model vaccine)-specific CD4 and CD8 T cells were activated to proliferate *in vivo* following intravenous[271] and subcutaneous[272] vaccination of mice with OVA protein- and OVA peptide-loaded LbL capsules. The OVA encapsulated within the capsules resulted in greatly enhanced antigen presentation and proliferation of antigen-specific CD4 and CD8 T cells that provided enhanced protection against viral infection and tumor growth. Furthermore, LbL capsules could be further engineered on their surface with immune-stimulatory molecules to boost the antigen-specific immune responses against encapsulated antigen.[273] The latter work was carried out with the idea of using LbL-coated microneedles for transdermal vaccination. Indeed, several groups have investigated codelivery of antigen and immune stimuli, both on colloidal and planar substrates.[273−275]

Imaging and Sensing. In diagnostic imaging, highly developed methods/modalities are applied, such as ultrasound imaging (US), X-ray computed tomography (CT), magnetic resonance imaging (MRI), near-infrared imaging (NIR), photoacoustic imaging (PAI) and nuclear imaging methods such positron emission tomography (PET) or single photon emission computed tomography (SPECT). Each of these imaging methods has advantages, but also drawbacks, such as limited spatial or time resolution, sensitivity, impairment of the patient, *etc.* Therefore, several methods must be combined in order to optimize the images and information obtained.[276] Instruments for this purpose are already under development, but suitable contrast agents providing contrast for different imaging modalities and methods are also necessary. These agents can be based on molecular materials or on particles. Solid particles should be in the nanometer range, whereas flexible particles could be used at the micron scale of erythrocytes. By means of LbL technology, such multifunctional contrast agents can be produced in a controlled way. One example was recently developed, which is simultaneously applicable for US, MRI, SPECT, and NIR imaging.[277] The core of the flexible 3 μm particles consisted of an air bubble, which is stably encapsulated by cross-linked poly(vinyl alcohol) (PVA) for US imaging. Positive charges were introduced in the PVA matrix in order to achieve controlled LbL coating. Two double layers of PSS/PAH-1,4,7-triazacyclononane-1,4,7-triacetic acid (NOTA) were assembled. The NOTA label complexes technetium for SPECT imaging. On top, double layers of citrate-stabilized iron oxide nanoparticles (SPION)/PAH were assembled for dark contrast in MRI imaging.[278] For NIR imaging, further fluorescent layers of PAH-Cy5/PSS were assembled. Finally, targeting was demonstrated by biotinylated antibodies coupled to an outermost PAH/streptavidin layer.[279,280] Thus, LbL enables convenient integration of different contrast modalities in one single particle. Apart from simple imaging, where contrast depends on the local concentration of contrast agent, functional imaging, *i.e.*, sensing, is possible. In this case, the signal of the contrast agent also depends on the local environment. There are several examples of encapsulated, analyte-sensitive fluorophores,[281−283] which enable the detection of local ion concentrations. The changes in environment must be taken into account when designing these multimodal particles. For example, many ion-sensitive fluorophores also respond to local pH, so one severe challenge concerning future *in vivo* applications is that particles will undergo massive local pH changes along their trajectories in the body, for example, upon endocytosis by macrophages. One solution might be to use more complex systems, such as sensors with distance-dependent

DOI: 10.1021/acsnano.9b03326
ACS Nano 2019, 13, 6151−6169

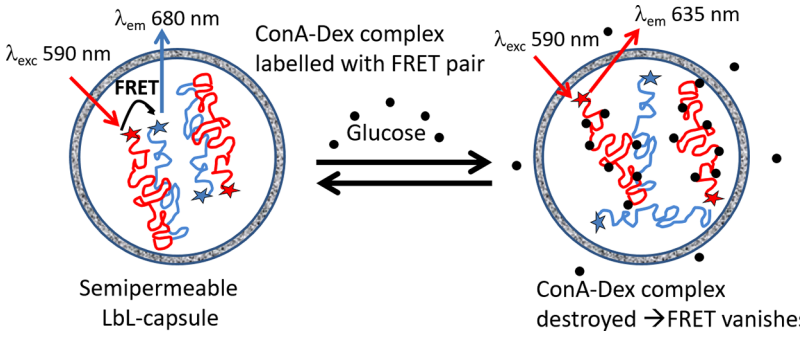

Figure 8. Glucose sensing in layer-by-layer (LbL) capsules, containing ConcanavalinA (ConA) and Dextran (Dex), labeled with fluorescence resonance energy transfer (FRET) pair. Unpublished data from the group of Lars Dähne.

quenching of optical or magnetic signals. In order to protect these systems from agglomeration, they could be encapsulated. The LbL shell around the sensors would then enable analytes to diffuse in and out, whereas it would retain and protect the actual sensor system. One developed glucose microsensor is depicted in Figure 8. Due to the possibility of multicompartment encapsulation of different molecules in different locations within one particle by LbL,[284] even feedback-controlled systems might be developed. A drug could be encapsulated for delivery in one compartment, whereas a sensor monitoring the action of the drug could be placed in an adjacent compartment.[285,286]

Challenges for Layer-by-Layer Coated Particles Intended for *in Vivo* Use. Following the above-outlined possibilities for applying LbL-based particles to *in vivo* delivery and imaging/sensing, one can summarize a number of key challenges for the future. (1) Highly biocompatible and biodegradable materials need to be developed and used. (2) Further fundamental studies need to be undertaken to understand the interactions of LbL particles and biological systems in order to probe parameters such as elasticity and shape and how these influence biological responses. (3) Automation of the preparation of LbL particles should be further developed, as this capability is critical to reproducibility and streamlining preparation. (4) More focus should be placed on such particles for local delivery applications (*e.g.*, their use as depots) and their interactions with the local cellular and protein environment, not only limiting their studies to systemic delivery applications. Thus, the development of LbL-based vehicles continues and important breakthroughs lie ahead.

> By means of layer-by-layer technology, multifunctional contrast agents for diagnostic imaging can be produced in a controlled way.

AUTHOR INFORMATION

Corresponding Author

*E-mail: wolfgang.parak@uni-hamburg.de.

ORCID

Frank Caruso: 0000-0002-0197-497X
Gero Decher: 0000-0002-7976-8818
Bruno G. De Geest: 0000-0001-9826-6170
Jinchen Fan: 0000-0002-8905-1693
Neus Feliu: 0000-0002-7886-1711
Yury Gogotsi: 0000-0001-9423-4032
Paula T. Hammond: 0000-0002-9835-192X
Mark C. Hersam: 0000-0003-4120-1426
Ali Khademhosseini: 0000-0002-2692-1524
Nicholas Kotov: 0000-0002-6864-5804
Stefano Leporatti: 0000-0001-5912-7565
Yan Li: 0000-0002-3828-8340
Luis M. Liz-Marzán: 0000-0002-6647-1353
Sergio Moya: 0000-0002-7174-1960
Paul Mulvaney: 0000-0002-8007-3247
Andrey L. Rogach: 0000-0002-8263-8141
Sathi Roy: 0000-0002-0645-5386
Dmitry G. Shchukin: 0000-0002-2936-804X
Andre G. Skirtach: 0000-0002-4468-7620
Molly M. Stevens: 0000-0002-7335-266X
Gleb B. Sukhorukov: 0000-0001-6213-0562
Paul S. Weiss: 0000-0001-5527-6248
Wolfgang J. Parak: 0000-0003-1672-6650

Author Contributions

⊗Authors are listed in alphabetic order.

Notes

The authors declare no competing financial interest.

ACKNOWLEDGMENTS

S.Z. was supported by the Chinese Scholarship Council (CSC). F.C. acknowledges the award of a National Health and Medical Research Council (NHMRC) Senior Principal Research Fellowship (APP1135806) and support from the Australian Research Council Centre of Excellence in Convergent Bio-Nano Science and Technology (Project No. CE140100036). L.D. thanks the BMBF (topical vaccination) and the EU FP6 and FP7 (LbL Brane, 3M and Sight) for supporting the research. S.E.M. thanks the MAT2017-88752-R Retos project from the Ministerio de Economia, Industria y Competitividad, gobierno de España. M.C.H. acknowledges support from the Materials Research Science and Engineering Center (MRSEC) of Northwestern University (NSF DMR-1720139). N.A.K. acknowledges the Alexander von Humboldt Foundation for a visiting professorship to Hamburg University. S.L. is supported by Progetto FISR-CNR "Tecnopolo di Nanotecnologia e Fotonica per la Medicina di Precisione"-CUP B83B17000010001. P.M. acknowledges support through ARC Grant CE170100026. A.L.R. was supported by a grant from the Germany/Hong Kong Joint Research Scheme sponsored by the Research Grants Council of Hong Kong and the Germany Academic Exchange Service of Germany (Reference No. G-CityU106/18). S.R. was supported by Fazit Stiftung. D.S. acknowledges an ERC Consolidator Grant No.

DOI: 10.1021/acsnano.9b03326
ACS Nano 2019, 13, 6151−6169

647969. A.G.S. acknowledges support of BOF-UGent (01IO3618, BAS094-18, BOF14/IOP/003) and FWO-Vlaanderen (G043219). W.J.P. received funding from the Deutsche Forschungsgemeinschaft (DFG PA 794/21-1). Z.Y. was supported by the National Natural Science Foundation of China (61871240).

DEDICATION

This article is dedicated to the memory of our beloved colleague and friend Prof. Dr. Helmuth Möhwald (19 January 1946−27 March 2018).

REFERENCES

(1) Decher, G.; Hong, J. D.; Schmitt, J. Buildup of Ultrathin Multilayer Films by a Self-Assembly Process: III. Consecutively Alternating Adsorption of Anionic and Cationic Polyelectrolytes on Charged Surfaces. *Thin Solid Films* **1992**, *210*, 831−835.

(2) Lvov, Y.; Decher, G.; Möhwald, H. Assembly, Structural Characterization, and Thermal-Behavior of Layer-by-Layer Deposited Ultrathin Films of Poly(vinyl sulfate) and Poly(allylamine). *Langmuir* **1993**, *9*, 481−486.

(3) Schmitt, J.; Gruenewald, T.; Decher, G.; Pershan, P. S.; Kjaer, K.; Lösche, M. Internal Structure of Layer-by-Layer Adsorbed Polyelectrolyte Films: A Neutron and X-Ray Reflectivity Study. *Macromolecules* **1993**, *26*, 7058−7063.

(4) Decher, G.; Lehr, B.; Lowack, K.; Lvov, Y.; Schmitt, J. New Nanocomposite Films for Biosensors: Layer-by-Layer Adsorbed Films of Polyelectrolytes, Proteins or DNA. *Biosens. Bioelectron.* **1994**, *9*, 677−684.

(5) Lvov, Y.; Haas, H.; Decher, G.; Möhwald, H.; Mikhailov, A.; Mtchedlishvily, B.; Morgunova, E.; Vainshtein, B. Successive Deposition of Alternate Layers of Polyelectrolytes and a Charged Virus. *Langmuir* **1994**, *10*, 4232−4236.

(6) Sukhorukov, G. B.; Lvov, Y. M.; Möhwald, H.; Decher, G. Assembly of Polyelectrolyte Multilayer Films by Consecutively Alternating Adsorption of Polynucleotides and Polycations. *Thin Solid Films* **1996**, *284*−*285*, 220−223.

(7) Decher, G. Fuzzy Nanoassemblies: Toward Layered Polymeric Multicomposites. *Science* **1997**, *277*, 1232−1237.

(8) Caruso, F.; Caruso, R. A.; Möhwald, H. Nanoengineering of Inorganic and Hybrid Hollow Spheres by Colloidal Templating. *Science.* **1998**, *282*, 1111−1114.

(9) Caruso, F.; Lichtenfeld, H.; Giersig, M.; Möhwald, H. Electrostatic Self-Assembly of Silica Nanoparticle-Polyelectrolyte Multilayers on Polystyrene Latex Particles. *J. Am. Chem. Soc.* **1998**, *120*, 8523−8524.

(10) Zhang, R.; Shang, J.; Xin, J.; Xie, B.; Li, Y.; Möhwald, H. Self-Assemblies of Luminescent Rare Earth Compounds in Capsules and Multilayers. *Adv. Colloid Interface Sci.* **2014**, *207*, 361−375.

(11) Kolesnikova, T. A.; Skirtach, A. G.; Möhwald, H. Red Blood Cells and Polyelectrolyte Multilayer Capsules: Natural Carriers *versus* Polymer-Based Drug Delivery Vehicles. *Expert Opin. Drug Delivery* **2013**, *10*, 47−58.

(12) Shchukin, D. G.; Möhwald, H. Multilayer Polyelectrolyte Assembly in Feedback Active Coatings and Films. In *Multilayer Thin Films: Sequential Assembly of Nanocomposite Materials*, 2nd ed.; Decher, G., Schlenoff, J. B., Eds.; Wiley-VCH: Weinheim, Germany, 2012; Vol. 2, pp 1039−1050.

(13) Dronov, R.; Kurth, D. G.; Möhwald, H.; Scheller, F. W.; Lisdat, F. A Self-Assembled Cytochrome *c*/Xanthine Oxidase Multilayer Arrangement on Gold. *Electrochim. Acta* **2007**, *53*, 1107−1113.

(14) Tang, F.; Cui, Q.; Wu, F.; Li, L.; Möhwald, H. Photoinduced Long-Range Charge Transfer in Polyelectrolyte Multilayers. *J. Photopolym. Sci. Technol.* **2008**, *21*, 729−731.

(15) Li, Z.; Xu, F.; Li, Q.; Liu, S.; Wang, H.; Möhwald, H.; Cui, X. Synthesis of Multifunctional Bovine Serum Albumin Microcapsules by the Sonochemical Method for Targeted Drug Delivery and Controlled Drug Release. *Colloids Surf., B* **2015**, *136*, 470−478.

(16) Malcher, M.; Volodkin, D.; Heurtault, B.; André, P.; Schaaf, P.; Möhwald, H.; Voegel, J. C.; Sokolowski, A.; Ball, V.; Boulmedais, F.; Frisch, B. Embedded Silver Ions-Containing Liposomes in Polyelectrolyte Multilayers: Cargos Films for Antibacterial Agents. *Langmuir* **2008**, *24*, 10209−10215.

(17) Sezer, M.; Feng, J. J.; Khoa Ly, H.; Shen, Y.; akanishi, T.; Kuhlmann, U.; Hildebrandt, P.; Möhwald, H.; Weidinger, I. M. Multi-Layer Electron Transfer Across Nanostructured Ag-SAM-Au-SAM Junctions Probed by Surface Enhanced Raman Spectroscopy. *Phys. Chem. Chem. Phys.* **2010**, *12*, 9822−9829.

(18) Shchukin, D. G.; Zheludkevich, M.; Yasakau, K.; Lamaka, S.; Ferreira, M. G. S.; Möhwald, H. Layer-by-Layer Assembled Nanocontainers for Self-Healing Corrosion Protection. *Adv. Mater.* **2006**, *18*, 1672−1678.

(19) Tong, W. J.; Gao, C. Y.; Möhwald, H. Single Polyelectrolyte Microcapsules Fabricated by Glutaraldehyde-Mediated Covalent Layer-by-Layer Assembly. *Macromol. Rapid Commun.* **2006**, *27*, 2078−2083.

(20) Volodkin, D.; Skirtach, A.; Möhwald, H. Bioapplications of Light-Sensitive Polymer Films and Capsules Assembled Using the Layer-by-Layer Technique. *Polym. Int.* **2012**, *61*, 673−679.

(21) Ibarz, G.; Dähne, L.; Donath, E.; Möhwald, H. Smart Micro- and Nanocontainers for Storage, Transport, and Release. *Adv. Mater.* **2001**, *13*, 1324−1327.

(22) Skirtach, A. G.; Munoz Javier, A.; Kreft, O.; Köhler, K.; Piera Alberola, A.; Möhwald, H.; Parak, W. J.; Sukhorukov, G. B. Laser-Induced Release of Encapsulated Materials Inside Living Cells. *Angew. Chem., Int. Ed.* **2006**, *45*, 4612−4617.

(23) Skirtach, A. G.; Dejugnat, C.; Braun, D.; Susha, A. S.; Rogach, A. L.; Parak, W. J.; Möhwald, H.; Sukhorukov, G. B. The Role of Metal Nanoparticles in Remote Release of Encapsulated Materials. *Nano Lett.* **2005**, *5*, 1371−1377.

(24) Beissenhirtz, M. K.; Scheller, F. W.; Stocklein, W. F. M.; Kurth, D. G.; Möhwald, H.; Lisdat, F. Electroactive Cytochrome c Multilayers within a Polyelectrolyte Assembly. *Angew. Chem., Int. Ed.* **2004**, *43*, 4357−4360.

(25) Sukhorukov, G.; Dähne, L.; Hartmann, J.; Donath, E.; Möhwald, H. Controlled Precipitation of Dyes into Hollow Polyelectrolyte Capsules Based on Colloids and Biocolloids. *Adv. Mater.* **2000**, *12*, 112−115.

(26) Ibarz, G.; Dahne, L.; Donath, E.; Möhwald, H. Controlled Permeability of Polyelectrolyte Capsules *via* Defined Annealing. *Chem. Mater.* **2002**, *14*, 4059−4062.

(27) Dähne, L.; Leporatti, S.; Donath, E.; Möhwald, H. Fabrication of Micro Reaction Cages with Tailored Properties. *J. Am. Chem. Soc.* **2001**, *123*, 5431−5436.

(28) Dai, Z.; Voigt, A.; Leporatti, S.; Donath, E.; Dähne, L.; Möhwald, H. Layer-by-Layer Self-Assembly of Polyelectrolyte and Low Molecular Weight Species into Capsules. *Adv. Mater.* **2001**, *13*, 1339−1342.

(29) Dai, Z. F.; Dähne, L.; Donath, E.; Möhwald, H. Mimicking Photosynthetic Two-Step Energy Transfer in Cyanine Triads Assembled into Capsules. *Langmuir* **2002**, *18*, 4553−4555.

(30) Dai, Z.; Dähne, L.; Donath, E.; Möhwald, H. Downhill Energy Transfer *via* Ordered Multichromophores in Light-Harvesting Capsules. *J. Phys. Chem. B* **2002**, *106*, 11501−11508.

(31) Dai, Z. F.; Möhwald, H.; Tiersch, B.; Dähne, L. Nano-engineering of Polymeric Capsules with a Shell-in-Shell Structure. *Langmuir* **2002**, *18*, 9533−9538.

(32) Dai, Z.; Dähne, L.; Möhwald, H.; Tiersch, B. Novel Capsules with High Stability and Controlled Permeability by Hierarchic Templating. *Angew. Chem., Int. Ed.* **2002**, *41*, 4019−4022.

(33) Donath, E.; Sukhorukov, G. B.; Caruso, F.; Davis, S. A.; Möhwald, H. Novel Hollow Polymer Shells by Colloid-Templated Assembly of Polyelectrolytes. *Angew. Chem., Int. Ed.* **1998**, *37*, 2201−2205.

DOI: 10.1021/acsnano.9b03326
ACS Nano 2019, 13, 6151−6169

(34) Möbius, D.; Möhwald, H. Structural Characterization of Monolayers at the Air-Water Interface. *Adv. Mater.* **1991**, *3*, 19−24.
(35) Kotov, N. A.; Dekany, I.; Fendler, J. H. Ultrathin Graphite Oxide-Polyelectrolyte Composites Prepared by Self-Assembly: Transition Between Conductive and Non-Conductive States. *Adv. Mater.* **1996**, *8*, 637−641.
(36) Tang, Z.; Kotov, N. A.; Magonov, S.; Ozturk, B. Nanostructured Artificial Nacre. *Nat. Mater.* **2003**, *2*, 413−418.
(37) Kotov, N. A.; Putyera, K.; Fendler, J. H.; Tombácz, E.; Dékány, I. Cadmium Sulfide Particles in Organomontmorillonite Complexes. *Colloids Surf., A* **1993**, *71*, 317−326.
(38) Kotov, N. A.; Meldrum, F. C.; Fendler, J. H. Monoparticulate Layers of Titanium Dioxide Nanocrystallites with Controllable Interparticle Distances. *J. Phys. Chem.* **1994**, *98*, 8827−8830.
(39) Kotov, N. A.; Meldrum, F. C.; Wu, C.; Fendler, J. H. Monoparticulate Layer and Langmuir-Blodgett-Type Multiparticulate Layers of Size-Quantized Cadmium Sulfide Clusters: A Colloid-Chemical Approach to Superlattice Construction. *J. Phys. Chem.* **1994**, *98*, 2735−2738.
(40) Motte, L.; Billoudet, F.; Lacaze, E.; Pileni, M. P. Self-Organization of Size-Selected, Nanoparticles into Three-Dimensional Superlattices. *Adv. Mater.* **1996**, *8*, 1018−1020.
(41) Yonezawa, T.; Matsune, H.; Kunitake, T. Layered Nanocomposite of Close-Packed Gold Nanoparticles and TiO_2 Gel Layers. *Chem. Mater.* **1999**, *11*, 33−35.
(42) Berndt, P.; Kurihara, K.; Kunitake, T. Adsorption of Poly(styrenesulfonate) onto an Ammonium Monolayer on Mica: A Surface Forces Study. *Langmuir* **1992**, *8*, 2486−2490.
(43) Kilper, S.; Facey, S. J.; Burghard, Z.; Hauer, B.; Rothenstein, D.; Bill, J. Macroscopic Properties of Biomimetic Ceramics Are Governed by the Molecular Recognition at the Bioorganic-Inorganic Interface. *Adv. Funct. Mater.* **2018**, *28*, 1705842.
(44) Cui, J.; Richardson, J. J.; Bjornmalm, M.; Faria, M.; Caruso, F. Nanoengineered Templated Polymer Particles: Navigating the Biological Realm. *Acc. Chem. Res.* **2016**, *49*, 1139−1148.
(45) Richardson, J. J.; Björnmalm, M.; Caruso, F. Technology-Driven Layer-by-Layer Assembly of Nanofilms. *Science* **2015**, *348*, No. aaa2491.
(46) Peyratout, C. S.; Dähne, L. Tailor-Made Polyelectrolyte Microcapsules: From Multilayers to Smart Containers. *Angew. Chem., Int. Ed.* **2004**, *43*, 3762−3783.
(47) Dähne, L.; Peyratout, C. Nanoengineered Capsules with Specific Layer Structures. *Dekker Encyclopedia of Nanoscience and Nanotechnology*, 2nd ed. six volume set (print version); CRC Press: Boca Raton, FL, 2004; pp 2355−2367.
(48) Möhwald, H.; Lichtenfeld, H.; Moya, S.; Voigt, A.; Sukhorukov, G.; Leporatti, S.; Dähne, L.; Antipov, A.; Gao, C. Y.; Donath, E. From Polymeric Films to Nanocapsules. In *Adsorption and Aggregation of Surfactants in Solution*; Mittal, K. L., Shah, D. O., Eds.; Marcel Dekker: New York, 2002; Vol. *132*, pp 485−490.
(49) Lisdat, F. Trends in the Layer-by-Layer Assembly of Redox Proteins and Enzymes in Bioelectrochemistry. *Curr. Opin. Electrochem.* **2017**, *5*, 165−172.
(50) De Geest, B. G.; Sukhorukov, G. B.; Möhwald, H. The Pros and Cons of Polyelectrolyte Capsules in Drug Delivery. *Expert Opin. Drug Delivery* **2009**, *6*, 613−624.
(51) Delcea, M.; Möhwald, H.; Skirtach, A. G. Stimuli-Responsive LbL Capsules and Nanoshells for Drug Delivery. *Adv. Drug Delivery Rev.* **2011**, *63*, 730−747.
(52) Zhuk, A.; Sukhishvili, S. A. Stimuli-Responsive Layer-by-Layer Nanocomposites. *Soft Matter* **2013**, *9*, 5149−5154.
(53) Hua, F.; Cui, T.; Lvov, Y. M. Ultrathin Cantilevers Based on Polymer-Ceramic Nanocomposite Assembled through Layer-by-Layer Adsorption. *Nano Lett.* **2004**, *4*, 823−825.
(54) Kang, S.; Wang, L.; Zhang, J.; Du, J.; Li, M.; Chen, Q. Electroreductive Coupling Layer-by-Layer Assembly. *ACS Appl. Mater. Interfaces* **2017**, *9*, 32179−32183.
(55) Ma, Y.; Zhang, Y.; Wu, B.; Sun, W.; Li, Z.; Sun, J. Polyelectrolyte Multilayer Films for Building Energetic Walking Devices. *Angew. Chem.* **2011**, *123*, 6378−6381.
(56) Podsiadlo, P.; Kaushik, A. K.; Shim, B. S.; Agarwal, A.; Tang, Z.; Waas, A. M.; Arruda, E. M.; Kotov, N. A. Can Nature's Design be Improved Upon? High Strength, Transparent Nacre-Like Nanocomposites with Double Network of Sacrificial Cross Links. *J. Phys. Chem. B* **2008**, *112*, 14359−14363.
(57) Schlenoff, J. B.; Dubas, S. T.; Farhat, T. Sprayed Polyelectrolyte Multilayers. *Langmuir* **2000**, *16*, 9968−9969.
(58) Krogman, K. C.; Zacharia, N. S.; Schroeder, S.; Hammond, P. T. Automated Process for Improved Uniformity and Versatility of Layer-by-Layer Deposition. *Langmuir* **2007**, *23*, 3137−3141.
(59) Krogman, K. C.; Lowery, J. L.; Zacharia, N. S.; Rutledge, G. C.; Hammond, P. T. Spraying Asymmetry into Functional Membranes Layer-by-Layer. *Nat. Mater.* **2009**, *8*, 512−518.
(60) Lefort, M.; Popa, G.; Seyrek, E.; Szamocki, R.; Felix, O.; Hemmerlé, J.; Vidal, L.; Voegel, J. C.; Boulmedais, F.; Decher, G.; Schaaf, P. Spray-on Organic/Inorganic Films: a General Method for the Formation of Functional Nano- to Microscale Coatings. *Angew. Chem., Int. Ed.* **2010**, *49*, 10110−10113.
(61) Richardson, J. J.; Ejima, H.; Lorcher, S. L.; Liang, K.; Senn, P.; Cui, J.; Caruso, F. Preparation of Nano- and Microcapsules by Electrophoretic Polymer Assembly. *Angew. Chem., Int. Ed.* **2013**, *52*, 6455−6458.
(62) Ejima, H.; Richardson, J. J.; Liang, K.; Best, J. P.; Van Koeverden, M. P.; Such, G. K.; Cui, J.; Caruso, F. One-Step Assembly of Coordination Complexes for Versatile Film and Particle Engineering. *Science* **2013**, *341*, 154−157.
(63) Dierendonck, M.; De Koker, S.; Cuvelier, C.; Grooten, J.; Vervaet, C.; Remon, J. P.; De Geest, B. G. Facile Two-Step Synthesis of Porous Antigen-Loaded Degradable Polyelectrolyte Microspheres. *Angew. Chem., Int. Ed.* **2010**, *49*, 8620−8624.
(64) Porcel, C. H.; Izquierdo, A.; Ball, V.; Decher, G.; Voegel, J. C.; Schaaf, P. Ultrathin Coatings and (Poly(glutamic acid)/Polyallylamine) Films Deposited by Continuous and Simultaneous Spraying. *Langmuir* **2005**, *21*, 800−802.
(65) Muzzio, N. E.; Pasquale, M. A.; Gregurec, D.; Diamanti, E.; Kosutic, M.; Azzaroni, O.; Moya, S. E. Polyelectrolytes Multilayers To Modulate Cell Adhesion: A Study of the Influence of Film Composition and Polyelectrolyte Interdigitation on the Adhesion of the A549 Cell Line. *Macromol. Biosci.* **2016**, *16*, 482−495.
(66) Liao, W. C.; Sohn, Y. S.; Riutin, M.; Cecconello, A.; Parak, W. J.; Nechushtai, R.; Willner, I. The Application of Stimuli-Responsive VEGF- and ATP-Aptamer-Based Microcapsules for the Controlled Release of an Anticancer Drug, and the Selective Targeted Cytotoxicity toward Cancer Cells. *Adv. Funct. Mater.* **2016**, *26*, 4262−4273.
(67) Liao, W.; Lu, C.; Hartmann, R.; Wang, F.; Sohn, Y. S.; Parak, W. J.; Willner, I. Adenosine Triphosphate-Triggered Release of Macromolecular and Nanoparticle Loads from Aptamer/DNA-Cross-Linked Microcapsules. *ACS Nano* **2015**, *9*, 9078−9086.
(68) Seyrek, E.; Decher, G. Layer-by-Layer Assembly of Multifunctional Hybrid Materials and Nanoscale Devices. In *Polymer Science: A Comprehensive Reference*; Matyjaszewski, K., Müller, M., Eds.; Elsevier: Amsterdam, 2012; Vol. *7*, pp 159−185.
(69) Kotov, N. A.; Magonov, S.; Tropsha, E. Layer-by-Layer Self-Assembly of Alumosilicate-Polyelectrolyte Composites: Mechanism of Deposition, Crack Resistance, and Perspectives for Novel Membrane Materials. *Chem. Mater.* **1998**, *10*, 886−895.
(70) Kotov, N. A. Ordered Layered Assemblies of Nanoparticles. *MRS Bull.* **2001**, *26*, 992−997.
(71) Yashchenok, A. M.; Gorin, D. A.; Badylevich, M.; Serdobintsev, A. A.; Bedard, M.; Fedorenko, Y. G.; Khomutov, G. B.; Grigoriev, D. O.; Möhwald, H. Impact of Magnetite Nanoparticle Incorporation on Optical and Electrical Properties of Nanocomposite LbL Assemblies. *Phys. Chem. Chem. Phys.* **2010**, *12*, 10469−10475.
(72) Malikova, N.; Pastoriza-Santos, I.; Schierhorn, M.; Kotov, N. A.; Liz-Marzán, L. M. Layer-by-Layer Assembled Mixed Spherical and

DOI: 10.1021/acsnano.9b03326
ACS Nano 2019, 13, 6151−6169

Planar Gold Nanoparticles: Control of Interparticle Interactions. *Langmuir* **2002**, *18*, 3694−3697.
(73) Salgueirino-Maceira, V.; Caruso, F.; Liz-Marzan, L. M. Coated Colloids with Tailored Optical Properties. *J. Phys. Chem. B* **2003**, *107*, 10990−10994.
(74) Schneider, G.; Decher, G.; Nerambourg, N.; Praho, R.; Werts, M. H.; Blanchard-Desce, M. Distance-Dependent Fluorescence Quenching on Gold Nanoparticles Ensheathed with Layer-by-Layer Assembled Polyelectrolytes. *Nano Lett.* **2006**, *6*, 530−536.
(75) Dykman, L.; Khlebtsov, N. Gold Nanoparticles in Biomedical Applications: Recent Advances and Perspectives. *Chem. Soc. Rev.* **2012**, *41*, 2256−2282.
(76) Del Pino, P.; Pelaz, B.; Zhang, Q.; Maffre, P.; Nienhaus, G. U.; Parak, W. J. Protein Corona Formation around Nanoparticles—From the Past to the Future. *Mater. Horiz.* **2014**, *1*, 301−313.
(77) Ariga, K.; Hill, J. P.; Ji, Q. Layer-by-Layer Assembly as a Versatile Bottom-Up Nanofabrication Technique for Exploratory Research and Realistic Application. *Phys. Chem. Chem. Phys.* **2007**, *9*, 2319−2340.
(78) Ung, T.; Liz-Marzán, L. M.; Mulvaney, P. Optical Properties of Thin Films of Au@SiO_2 Particles. *J. Phys. Chem. B* **2001**, *105*, 3441−3452.
(79) Vial, S.; Pastoriza-Santos, I.; Perez-Juste, J.; Liz-Marzan, L. M. Plasmon Coupling in Layer-by-Layer Assembled Gold Nanorod Films. *Langmuir* **2007**, *23*, 4606−4611.
(80) Abalde-Cela, S.; Ho, S.; Rodriguez-Gonzalez, B.; Correa-Duarte, M. A.; Alvarez-Puebla, R. A.; Liz-Marzan, L. M.; Kotov, N. A. Loading of Exponentially Grown LbL Films with Silver Nanoparticles and Their Application to Generalized SERS Detection. *Angew. Chem., Int. Ed.* **2009**, *48*, 5326−5329.
(81) Stankovich, S.; Dikin, D. A.; Dommett, G. H. B.; Kohlhaas, K. M.; Zimney, E. J.; Stach, E. A.; Piner, R. D.; Nguyen, S. T.; Ruoff, R. S. Graphene-Based Composite Materials. *Nature* **2006**, *442*, 282−286.
(82) Wan, S.; Li, Y.; Mu, J.; Aliev, A. E.; Fang, S.; Kotov, N. A.; Jiang, L.; Cheng, Q.; Baughman, R. H. Sequentially Bridged Graphene Sheets with High Strength, Toughness, and Electrical Conductivity. *Proc. Natl. Acad. Sci. U. S. A.* **2018**, *115*, 5359−5364.
(83) Mao, L. B.; Gao, H. L.; Yao, H. B.; Liu, L.; Cölfen, H.; Liu, G.; Chen, S. M.; Li, S. K.; Yan, Y. X.; Liu, Y. Y.; Yu, S. H. Synthetic Nacre by Predesigned Matrix-Directed Mineralization. *Science* **2016**, *354*, 107−110.
(84) Jiang, C.; Markutsya, S.; Pikus, Y.; Tsukruk, V. V. Freely Suspended Nanocomposite Membranes as Highly Sensitive Sensors. *Nat. Mater.* **2004**, *3*, 721−728.
(85) Li, Y.; Wang, X.; Sun, J. Layer-by-Layer Assembly for Rapid Fabrication of Thick Polymeric Films. *Chem. Soc. Rev.* **2012**, *41*, 5998−6009.
(86) Mannarino, M. M.; Liu, D. S.; Hammond, P. T.; Rutledge, G. C. Mechanical and Transport Properties of Layer-by-Layer Electrospun Composite Proton Exchange Membranes for Fuel Cell Applications. *ACS Appl. Mater. Interfaces* **2013**, *5*, 8155−8164.
(87) Jiang, C.; Tsukruk, V. V. Freestanding Nanostructures via Layer-by-Layer Assembly. *Adv. Mater.* **2006**, *18*, 829−840.
(88) Zhang, X.; Chen, H.; Zhang, H. Layer-by-Layer Assembly: From Conventional to Unconventional Methods. *Chem. Commun.* **2007**, *0*, 1395−1405.
(89) Weng, G. M.; Li, J.; Alhabeb, M.; Karpovich, C.; Wang, H.; Lipton, J.; Maleski, K.; Kong, J.; Shaulsky, E.; Elimelech, M.; Gogotsi, Y.; Taylor, A. D. Layer-by-Layer Assembly of Cross-Functional Semi-Transparent MXene-Carbon Nanotubes Composite Films for Next-Generation Electromagnetic Interference Shielding. *Adv. Funct. Mater.* **2018**, *28*, 1803360.
(90) Feifel, S. C.; Lisdat, F. Silica Nanoparticles for the Layer-by-Layer Assembly of Fully Electro-Active Cytochrome c Multilayers. *J. Nanobiotechnol.* **2011**, *9*, 59.
(91) Irigoyen, J.; Laakso, T.; Politakos, N.; Dahne, L.; Pihlajamäki, A.; Mänttäri, M.; Moya, S. E. Design and Performance Evaluation of Hybrid Nanofiltration Membranes Based on Multiwalled Carbon Nanotubes and Polyelectrolyte Multilayers for Larger Ion Rejection and Separation. *Macromol. Chem. Phys.* **2016**, *217*, 804−811.
(92) Kaushik, A. K.; Podsiadlo, P.; Qin, M.; Shaw, C. M.; Waas, A. M.; Kotov, N. A.; Arruda, E. M. The Role of Nanoparticle Layer Separation in the Finite Deformation Response of Layered Polyurethane-Clay Nanocomposites. *Macromolecules* **2009**, *42*, 6588−6595.
(93) Shahzad, F.; Alhabeb, M.; Hatter, C. B.; Anasori, B.; Hong, S. M.; Koo, C. M.; Gogotsi, Y. Electromagnetic Interference Shielding with 2D Transition Metal Carbides (MXenes). *Science* **2016**, *353*, 1137−1140.
(94) Zhou, Z.; Panatdasirisuk, W.; Mathis, T. S.; Anasori, B.; Lu, C.; Zhang, X.; Liao, Z.; Gogotsi, Y.; Yang, S. Layer-by-Layer Assembly of MXene and Carbon Nanotubes on Electrospun Polymer Films for Flexible Energy Storage. *Nanoscale* **2018**, *10*, 6005−6013.
(95) Hoda, N.; Larson, R. G. Explicit- and Implicit-Solvent Molecular Dynamics Simulations of Complex Formation between Polycations and Polyanions. *Macromolecules* **2009**, *42*, 8851−8863.
(96) Patel, P. A.; Jeon, J.; Mather, P. T.; Dobrynin, A. V. Molecular Dynamics Simulations of Layer-by-Layer Assembly of Polyelectrolytes at Charged Surfaces: Effects of Chain Degree of Polymerization and Fraction of Charged Monomers. *Langmuir* **2005**, *21*, 6113−6122.
(97) Lacevic, N. M.; Joshi, S. P. Energy Dissipation Mechanism in Nanocomposites Studied *via* Molecular Dynamics Simulation. In Challenges in Mechanics of Time-Dependent Materials and Processes in Conventional and Multifunctional Materials. In *Conference Proceedings of the Society for Experimental Mechanics Series*; Antoun, B., Qi, H., Hall, R., Randon, G., Lu, H., Lu, C., Eds.; Springer: New York, 2013; Vol. *2*, pp 23−27.
(98) Blell, R.; Lin, X.; Lindström, T.; Ankerfors, M.; Pauly, M.; Felix, O.; Decher, G. Generating In-Plane Orientational Order in Multilayer Films Prepared by Spray-Assisted Layer-by-Layer Assembly. *ACS Nano* **2017**, *11*, 84−94.
(99) Sekar, S.; Lemaire, V.; Hu, H.; Decher, G.; Pauly, M. Anisotropic Optical and Conductive Properties of Oriented 1D-Nanoparticle Thin Films Made by Spray-Assisted Self-Assembly. *Faraday Discuss.* **2016**, *191*, 373−389.
(100) Hu, H.; Pauly, M.; Felix, O.; Decher, G. Spray-Assisted Alignment of Layer-by-Layer Assembled Silver Nanowires: A General Approach for the Preparation of Highly Anisotropic Nano-Composite Films. *Nanoscale* **2017**, *9*, 1307−1314.
(101) Shchukin, D.; Möhwald, H. A Coat of Many Functions. *Science* **2013**, *341*, 1458−1459.
(102) Andreeva, D. V.; Fix, D.; Möhwald, H.; Shchukin, D. G. Buffering Polyelectrolyte Multilayers for Active Corrosion Protection. *J. Mater. Chem.* **2008**, *18*, 1738−1740.
(103) Zheludkevich, M. L.; Shchukin, D. G.; Yasakau, K. A.; Möhwald, H.; Ferreira, M. G. S. Anticorrosion Coatings with Self-Healing Effect Based on Nanocontainers Impregnated with Corrosion Inhibitor. *Chem. Mater.* **2007**, *19*, 402−411.
(104) Andreeva, D. V.; Skorb, E. V.; Shchukin, D. G. Layer-by-Layer Polyelectrolyte/Inhibitor Nanostructures for Metal Corrosion Protection. *ACS Appl. Mater. Interfaces* **2010**, *2*, 1954−1962.
(105) Shchukin, D. G.; Lamaka, S. V.; Yasakau, K. A.; Zheludkevich, M. L.; Ferreira, M. G. S.; Möhwald, H. Active Anticorrosion Coatings with Halloysite Nanocontainers. *J. Phys. Chem. C* **2008**, *112*, 958−964.
(106) Li, G. L.; Zheng, Z.; Möhwald, H.; Shchukin, D. G. Silica/Polymer Double-Walled Hybrid Nanotubes: Synthesis and Application as Stimuli-Responsive Nanocontainers in Self-Healing Coatings. *ACS Nano* **2013**, *7*, 2470−2478.
(107) Shchukin, D. G.; Shchukina, E. Capsules with External Navigation and Triggered Release. *Curr. Opin. Pharmacol.* **2014**, *18*, 42−46.
(108) Pomerantseva, E.; Gogotsi, Y. Two-Dimensional Heterostructures for Energy Storage. *Nat. Energy.* **2017**, *2*, 17089.
(109) Fendler, J. H. Colloid Chemical Approach to the Construction of High Energy Density Rechargeable, Lithium-Ion Batteries. *J. Dispersion Sci. Technol.* **1999**, *20*, 13−25.

DOI: 10.1021/acsnano.9b03326
ACS Nano 2019, 13, 6151−6169

(110) Xiao, F. X.; Pagliaro, M.; Xu, Y. J.; Liu, B. Layer-by-Layer Assembly of Versatile Nanoarchitectures with Diverse Dimensionality: A New Perspective for Rational Construction of Multilayer Assemblies. *Chem. Soc. Rev.* **2016**, *45*, 3088−3121.
(111) Liu, L.; Choi, B. G.; Tung, S. O.; Lyu, J.; Li, T.; Zhao, T.; Kotov, N. A. Materials Engineering of High-Performance Anodes as Layered Composites with Self-Assembled Conductive Networks. *J. Phys. Chem. C* **2018**, *122*, 14014−14028.
(112) Tung, S. O.; Ho, S.; Yang, M.; Zhang, R.; Kotov, N. A. A Dendrite-Suppressing Composite Ion Conductor from Aramid Nanofibres. *Nat. Commun.* **2015**, *6*, 6152.
(113) Wang, M.; Emre, A.; Tung, S.; Gerber, A.; Wang, D.; Huang, Y.; Cecen, V.; Kotov, N. A. Biomimetic Solid-State Zn^{2+} Electrolyte for Corrugated Structural Batteries. *ACS Nano* **2019**, *13*, 1107−1115.
(114) Gao, M.; Lesser, C.; Kirstein, S.; Möhwald, H.; Rogach, A. L.; Weller, H. Electroluminescence of Different Colors from Polycation/CdTe Nanocrystal Self-Assembled Films. *J. Appl. Phys.* **2000**, *87*, 2297−2302.
(115) Franzl, T.; Koktysh, D. S.; Klar, T. A.; Rogach, A. L.; Feldmann, J.; Gaponik, N. Fast Energy Transfer in Layer-by-Layer Assembled CdTe Nanocrystal Bilayers. *Appl. Phys. Lett.* **2004**, *84*, 2904−2906.
(116) Franzl, T.; Klar, T. A.; Schietinger, S.; Rogach, A. L.; Feldmann, J. Exciton Recycling in Graded Gap Nanocrystal Structures. *Nano Lett.* **2004**, *4*, 1599−1603.
(117) Klar, T. A.; Franzl, T.; Rogach, A. L.; Feldmann, J. Super-Efficient Exciton Funneling in Layer-by-Layer Semiconductor Nanocrystal Structures. *Adv. Mater.* **2005**, *17*, 769−773.
(118) Susha, A. S.; Caruso, F.; Rogach, A. L.; Sukhorukov, G. B.; Kornowski, A.; Möhwald, H.; Giersig, M.; Eychmüller, A.; Weller, H. Formation of Luminescent Spherical Core-Shell Particles by the Consecutive Adsorption of Polyelectrolyte and CdTe(S) Nanocrystals on Latex Colloids. *Colloids Surf., A* **2000**, *163*, 39−44.
(119) Gaponik, N.; Radtchenko, I. L.; Gerstenberger, M. R.; Fedutik, Y. A.; Sukhorukov, G. B.; Rogach, A. L. Labeling of Biocompatible Polymer Microcapsules with Near-Infrared Emitting Nanocrystals. *Nano Lett.* **2003**, *3*, 369−372.
(120) Gaponik, N.; Radtchenko, I. L.; Sukhorukov, G. B.; Rogach, A. L. Luminescent Polymer Microcapsules Addressable by a Magnetic Field. *Langmuir* **2004**, *20*, 1449−1452.
(121) Kotov, N. A.; Dekany, I.; Fendler, J. H. Layer-by-Layer Self-Assembly of Polyelectrolyte-Semiconductor Nanoparticle Composite Films. *J. Phys. Chem.* **1995**, *99*, 13065−13069.
(122) Rogach, A. L.; Koktysh, D. S.; Harrison, M.; Kotov, N. A. Layer-by-Layer Assembled Films of HgTe Nanocrystals with Strong Infrared Emission. *Chem. Mater.* **2000**, *12*, 1526−1528.
(123) Mamedov, A. A.; Belov, A.; Giersig, M.; Mamedova, N. N.; Kotov, N. A. Nanorainbows: Graded Semiconductor Films from Quantum Dots. *J. Am. Chem. Soc.* **2001**, *123*, 7738−7739.
(124) Zhu, J.; Kang, J.; Kang, J.; Jariwala, D.; Wood, J. D.; Seo, J. W. T.; Chen, K. S.; Marks, T. J.; Hersam, M. C. Solution-Processed Dielectrics Based on Thickness-Sorted Two-Dimensional Hexagonal Boron Nitride Nanosheets. *Nano Lett.* **2015**, *15*, 7029−7036.
(125) Feifel, S. C.; Kapp, A.; Lisdat, F. Protein Multilayer Architectures on Electrodes for Analyte Detection. In *Biosensors Based on Aptamers and Enzymes*; Gu, M. B., Kim, H. S., Eds.; Springer: Berlin, 2013; Vol. *140*, pp 253−298.
(126) Heath, G. R.; Li, M.; Rong, H.; Radu, V.; Frielingsdorf, S.; Lenz, O.; Butt, J. N.; Jeuken, L. J. C. Multilayered Lipid Membrane Stacks for Biocatalysis Using Membrane Enzymes. *Adv. Funct. Mater.* **2017**, *27*, 1606265.
(127) Dronov, R.; Kurth, D. G.; Möhwald, H.; Scheller, F. W.; Lisdat, F. Communication in a Protein Stack: Electron Transfer between Cytochrome c and Bilirubin Oxidase within a Polyelectrolyte Multilayer. *Angew. Chem., Int. Ed.* **2008**, *47*, 3000−3003.
(128) Grant, G. G. S.; Koktysh, D. S.; Yun, B.; Matts, R. L.; Kotov, N. A. Layer-by-Layer Assembly of Collagen Thin Films: Controlled Thickness and Biocompatibility. *Biomed. Microdevices* **2001**, *3*, 301−306.
(129) Dronov, R.; Kurth, D. G.; Möhwald, H.; Spricigo, R.; Leimkuehler, S.; Wollenberger, U.; Rajagopalan, K. V.; Scheller, F. W.; Lisdat, F. Layer-by-Layer Arrangement by Protein-Protein Interaction of Sulfite Oxidase and Cytochrome c Catalyzing Oxidation of Sulfite. *J. Am. Chem. Soc.* **2008**, *130*, 1122−1123.
(130) Feifel, S. C.; Kapp, A.; Ludwig, R.; Lisdat, F. Nano-biomolecular Multiprotein Clusters on Electrodes for the Formation of a Switchable Cascadic Reaction Scheme. *Angew. Chem., Int. Ed.* **2014**, *53*, 5676−5679.
(131) Gheith, M. K.; Sinani, V. A.; Wicksted, J. P.; Matts, R. L.; Kotov, N. A. Single-Walled Carbon Nanotube Polyelectrolyte Multilayers and Freestanding Films as a Biocompatible Platform for Neuroprosthetic Implants. *Adv. Mater.* **2005**, *17*, 2663−2670.
(132) Pappas, T. C.; Wickramanyake, W. M. S.; Jan, E.; Motamedi, M.; Brodwick, M.; Kotov, N. A. Nanoscale Engineering of a Cellular Interface with Semiconductor Nanoparticle Films for Photoelectric Stimulation of Neurons. *Nano Lett.* **2007**, *7*, 513−519.
(133) Rabe, K. S.; Müller, J.; Skoupi, M.; Niemeyer, C. M. Cascades in Compartments: En Route to Machine-Assisted Biotechnology. *Angew. Chem., Int. Ed.* **2017**, *56*, 13574−13589.
(134) Kreft, O.; Skirtach, A. G.; Sukhorukov, G. B.; Möhwald, H. Remote Control of Bioreactions in Multicompartment Capsules. *Adv. Mater.* **2007**, *19*, 3142−3145.
(135) Bäumler, H.; Georgieva, R. Coupled Enzyme Reactions in Multicompartment Microparticles. *Biomacromolecules* **2010**, *11*, 1480−1487.
(136) Stoll, C.; Kudera, S.; Parak, W. J.; Lisdat, F. Quantum Dots on Gold: Electrodes For Photoswitchable Cytochrome c Electrochemistry. *Small* **2006**, *2*, 741−743.
(137) Katz, E.; Zayats, M.; Willner, I.; Lisdat, F. Controlling the Direction of Photocurrents by Means of CdS Nanoparticles and Cytochrome c-Mediated Biocatalytic Cascades. *Chem. Commun.* **2006**, *0*, 1395−1397.
(138) Rajendran, V.; Lehnig, M.; Niemeyer, C. M. Photocatalytic Activity of Colloidal CdS Nanoparticles with Different Capping Ligands. *J. Mater. Chem.* **2009**, *19*, 6348−6353.
(139) Ipe, B. I.; Niemeyer, C. M. Nanohybrids Composed of Quantum Dots and Cytochrome P450 as Photocatalysts. *Angew. Chem., Int. Ed.* **2006**, *45*, 504−507.
(140) Yue, Z.; Lisdat, F.; Parak, W. J.; Hickey, S. G.; Tu, L. P.; Sabir, N.; Dorfs, D.; Bigall, N. C. Quantum-Dot-Based Photoelectrochemical Sensors for Chemical and Biological Detection. *ACS Appl. Mater. Interfaces* **2013**, *5*, 2800−2814.
(141) Friebe, V. M.; Frese, R. N. Photosynthetic Reaction Center-Based Biophotovoltaics. *Curr. Opin. Electrochem.* **2017**, *5*, 126−134.
(142) Stieger, K. R.; Ciornii, D.; Kölsch, A.; Hejazi, M.; Lokstein, H.; Feifel, S. C.; Zouni, A.; Lisdat, F. Engineering of Supramolecular Photoactive Protein Architectures: the Defined Co-Assembly of Photosystem I and Cytochrome c Using a Nanoscaled DNA-Matrix. *Nanoscale* **2016**, *8*, 10695−10705.
(143) Carregal-Romero, S.; Rinklin, P.; Schulze, S.; Schäfer, M.; Ott, A.; Hühn, D.; Yu, X.; Wolfrum, B.; Weitzel, K. M.; Parak, W. J. Ion Transport through Polyelectrolyte Multilayers. *Macromol. Rapid Commun.* **2013**, *34*, 1820−1826.
(144) Wesp, V.; Hermann, M.; Schäfer, M.; Hühn, J.; Parak, W. J.; Weitzel, K. M. Bombardment Induced Ion Transport-Part IV: Ionic Conductivity of Ultra-Thin Polyelectrolyte Multilayer Films. *Phys. Chem. Chem. Phys.* **2016**, *18*, 4345−4351.
(145) v. Klitzing, R. Internal Structure of Polyelectrolyte Multilayer Assemblies. *Phys. Chem. Chem. Phys.* **2006**, *8*, 5012−5033.
(146) Zhao, S.; Zhang, J.; Li, Z.; Zhang, P.; Li, Y.; Liu, G.; Wang, Y.; Yue, Z. Photoelectrochemical Determination of Hydrogen Peroxide Using a Gold Electrode Modified with Fluorescent Gold Nanoclusters and Graphene Oxide. *Microchim. Acta* **2017**, *184*, 677−686.
(147) Zhao, S.; Li, Z.; Li, Y.; Yu, J.; Liu, G.; Liu, R.; Yue, Z. BSA-AuNCs Based Enhanced Photoelectrochemical Biosensors and Its Potential Use in Multichannel Detections. *J. Photochem. Photobiol., A* **2017**, *342*, 15−24.

DOI: 10.1021/acsnano.9b03326
ACS Nano 2019, 13, 6151−6169

(148) Khalid, W.; El Helou, M.; Murböck, T.; Yue, Z.; Montenegro, J. M.; Schubert, K.; Göbel, G.; Lisdat, F.; Witte, G.; Parak, W. J. Immobilization of Quantum Dots *via* Conjugated Self-Assembled Monolayers and Their Application as a Light-Controlled Sensor for the Detection of Hydrogen Peroxide. *ACS Nano* **2011**, *5*, 9870−9876.
(149) Sabir, N.; Khan, N.; Völkner, J.; Widdascheck, F.; del Pino, P.; Witte, G.; Riedel, M.; Lisdat, F.; Konrad, M.; Parak, W. J. Photo-Electrochemical Bioanalysis of Guanosine Monophosphate Using Coupled Enzymatic Reactions at a CdS/ZnS Quantum Dot Electrode. *Small* **2015**, *11*, 5844−5850.
(150) Tanne, J.; Schafer, D.; Khalid, W.; Parak, W. J.; Lisdat, F. Light-Controlled Bioelectrochemical Sensor Based on CdSe/ZnS Quantum Dots. *Anal. Chem.* **2011**, *83*, 7778−7785.
(151) Meyer, R.; Sacca, B.; Niemeyer, C. M. Site-Directed, On-Surface Assembly of DNA Nanostructures. *Angew. Chem.* **2015**, *127*, 12207−12211.
(152) Chen, X.; Venkatachalapathy, M.; Kamps, D.; Weigel, S.; Kumar, R.; Orlich, M.; Garrecht, R.; Hirtz, M.; Niemeyer, C. M.; Wu, Y. W.; Dehmelt, L. Molecular Activity Painting": Switch-Like, Light-Controlled Perturbations inside Living Cells. *Angew. Chem., Int. Ed.* **2017**, *56*, 5916−5920.
(153) Salles, P.; Pinto, D.; Hantanasirisakul, K.; Maleski, K.; Shuck, C. E.; Gogotsi, Y. Electrochromic Effect in Titanium Carbide MXene Thin Films Produced by Dip-Coating. *Adv. Funct. Mater.* **2019**, *29*, 1809223.
(154) Liu, S.; Kurth, D. G.; Möhwald, H.; Volkmer, D. A Thin-Film Electrochromic Device Based on a Polyoxometalate Cluster. *Adv. Mater.* **2002**, *14*, 225−228.
(155) Liu, S.; Möhwald, H.; Volkmer, D.; Kurth, D. G. Polyoxometalate-Based Electro- and Photochromic Dual-Mode Devices. *Langmuir* **2006**, *22*, 1949−1951.
(156) Sergeeva, Y. N.; Huang, T.; Felix, O.; Jung, L.; Tropel, P.; Viville, S.; Decher, G. What is Really Driving Cell-Surface Interactions? Layer-by-Layer Assembled Films May Help To Answer Questions Concerning Cell Attachment and Response to Biomaterials. *Biointerphases* **2016**, *11*, 019009.
(157) Muzzio, N. E.; Pasquale, M. A.; Rios, X.; Azzaroni, O.; Llop, J.; Moya, S. E. Adsorption and Exchangeability of Fibronectin and Serum Albumin Protein Corona on Annealed Polyelectrolyte Multilayers and Their Consequences on Cell Adhesion. *Adv. Mater. Interfaces* **2019**, *6*, 1900008.
(158) El-Khouri, R. J.; Szamocki, R.; Sergeeva, Y.; Felix, O.; Decher, G. Multifunctional Layer-by-Layer Architectures for Biological Applications. In *Functional Polymer Films*; Knoll, W., Advincula, R. C., Eds.; Wiley-VCH: Weinheim, Germany, 2011; Vol. *2*, pp 11−58.
(159) Jan, E.; Pereira, F. N.; Turner, D. L.; Kotov, N. A. In Situ Gene Transfection and Neuronal Programming on Electroconductive Nanocomposite to Reduce Inflammatory Response. *J. Mater. Chem.* **2011**, *21*, 1109−1114.
(160) Crouzier, T.; Boudou, T.; Picart, C. Polysaccharide-Based Polyelectrolyte Multilayers. *Curr. Opin. Colloid Interface Sci.* **2010**, *15*, 417−426.
(161) Romero, G.; Ochoteco, O.; Sanz, D. J.; Estrela-Lopis, I.; Donath, E.; Moya, S. E. Poly(lactide-co-glycolide) Nanoparticles, Layer-by-Layer Engineered for the Sustainable Delivery of AntiTNF-α. *Macromol. Biosci.* **2013**, *13*, 903−912.
(162) Naves, A. F.; Motay, M.; Mérindol, R.; Davi, C. P.; Felix, O.; Catalani, L. H.; Decher, G. Layer-by-Layer Assembled Growth Factor Reservoirs for Steering the Response of 3T3-cells. *Colloids Surf., B* **2016**, *139*, 79−86.
(163) Muzzio, N. E.; Gregurec, D.; Diamanti, E.; Irigoyen, J.; Pasquale, M. A.; Azzaroni, O.; Moya, S. E. Thermal Annealing of Polyelectrolyte Multilayers: An Effective Approach for the Enhancement of Cell Adhesion. *Adv. Mater. Interfaces* **2017**, *4*, 1600126.
(164) Skirtach, A. G.; Volodkin, D. V.; Möhwald, H. Bio-Interfaces-Interaction of PLL/HA Thick Films with Nanoparticles and Microcapsules. *ChemPhysChem* **2010**, *11*, 822−829.
(165) Kohler, D.; Madaboosi, N.; Delcea, M.; Schmidt, S.; De Geest, B. G.; Volodkin, D. V.; Möhwald, H.; Skirtach, A. G. Patchiness of Embedded Particles and Film Stiffness Control through Concentration of Gold Nanoparticles. *Adv. Mater.* **2012**, *24*, 1095−1100.
(166) Merindol, R.; Diabang, S.; Felix, O.; Roland, T.; Gauthier, C.; Decher, G. Bio-Inspired Multiproperty Materials: Strong, Self-Healing, and Transparent Artificial Wood Nanostructures. *ACS Nano* **2015**, *9*, 1127−1136.
(167) Khademhosseini, A.; Suh, Y. K.; Yang, M. J.; Eng, G.; Yeh, J.; Levenberg, S.; Langer, R. Layer-by-Layer Deposition of Hyaluronic Acid and Poly-L-lysine for Patterned Cell Co-Cultures. *Biomaterials* **2004**, *25*, 3583−3592.
(168) Fukuda, J.; Khademhosseini, A.; Yeh, J.; Eng, G.; Cheng, J.; Farokhzad, O. C.; Langer, R. Micropatterned Cell Co-Cultures Using Layer-by-Layer Deposition of Extracellular Matrix Components. *Biomaterials* **2006**, *27*, 1479−1486.
(169) Tamada, Y.; Ikada, Y. Effect of Preadsorbed Proteins on Cell Adhesion to Polymer Surfaces. *J. Colloid Interface Sci.* **1993**, *155*, 334−339.
(170) Yeom, B.; Sain, T.; Lacevic, N.; Bukharina, D.; Cha, S. H.; Waas, A. M.; Arruda, E. M.; Kotov, N. A. Abiotic Tooth Enamel. *Nature* **2017**, *543*, 95−98.
(171) Vendamme, R.; Onoue, S. Y.; Nakao, A.; Kunitake, T. Robust Free-Standing Nanomembranes of Organic/Inorganic Interpenetrating Networks. *Nat. Mater.* **2006**, *5*, 494−501.
(172) Ariga, K.; Yamauchi, Y.; Rydzek, G.; Ji, Q.; Yonamine, Y.; Wu, K. C. W.; Hill, J. P. Layer-by-Layer Nanoarchitectonics: Invention, Innovation, and Evolution. *Chem. Lett.* **2014**, *43*, 36−68.
(173) Tang, Z.; Wang, Y.; Podsiadlo, P.; Kotov, N. A. Biomedical Applications of Layer-by-Layer Assembly: From Biomimetics to Tissue Engineering. *Adv. Mater.* **2006**, *18*, 3203−3224.
(174) Sinani, V. A.; Koktysh, D. S.; Yun, B. G.; Matts, R. L.; Pappas, T. C.; Motamedi, M.; Thomas, S. N.; Kotov, N. A. Collagen Coating Promotes Biocompatibility of Semiconductor Nanoparticles in Stratified LbL Films. *Nano Lett.* **2003**, *3*, 1177−1182.
(175) Zhang, Y.; Sun, J. Multilevel and Multicomponent Layer-by-Layer Assembly for the Fabrication of Nanofibrillar Films. *ACS Nano* **2015**, *9*, 7124−7132.
(176) Volodkin, D.; von Klitzing, R.; Möhwald, H. Polyelectrolyte Multilayers: Towards Single Cell Studies. *Polymers* **2014**, *6*, 1502−1527.
(177) Johnston, A. P. R.; Cortez, C.; Angelatos, A. S.; Caruso, F. Layer-by-Layer Engineered Capsules and Their Applications. *Curr. Opin. Colloid Interface Sci.* **2006**, *11*, 203−209.
(178) Sukhorukov, G. B.; Donath, E.; Lichtenfeld, H.; Knippel, E.; Knippel, M.; Budde, A.; Möhwald, H. Layer-by-Layer Self Assembly of Polyelectrolytes on Colloidal Particles. *Colloids Surf., A* **1998**, *137*, 253−266.
(179) Kotov, N. A.; Liu, Y. F.; Wang, S. P.; Cumming, C.; Eghtedari, M.; Vargas, G.; Motamedi, M.; Nichols, J.; Cortiella, J. Inverted Colloidal Crystals as Three-Dimensional Cell Scaffolds. *Langmuir* **2004**, *20*, 7887−7892.
(180) Nichols, J. E.; Cortiella, J. Q.; Lee, J.; Niles, J. A.; Cuddihy, M.; Wang, S. P.; Bielitzki, J.; Cantu, A.; Mlcak, R.; Valdivia, E.; Yancy, R.; McClure, M. L.; Kotov, N. A. *In Vitro* Analog of Human Bone Marrow from 3D Scaffolds with Biomimetic Inverted Colloidal Crystal Geometry. *Biomaterials* **2009**, *30*, 1071−1079.
(181) Kozai, T. D. Y.; Langhals, N. B.; Patel, P. R.; Deng, X.; Zhang, H.; Smith, K. L.; Lahann, J.; Kotov, N. A.; Kipke, D. R. Ultrasmall Implantable Composite Microelectrodes with Bioactive Surfaces for Chronic Neural Interfaces. *Nat. Mater.* **2012**, *11*, 1065−1073.
(182) Kotov, N. A.; Winter, J. O.; Clements, I. P.; Jan, E.; Timko, B. P.; Campidelli, S.; Pathak, S.; Mazzatenta, A.; Lieber, C. M.; Prato, M.; Bellamkonda, R. V.; Silva, G. A.; Kam, N. W. S.; Patolsky, F.; Ballerini, L. Nanomaterials for Neural Interfaces. *Adv. Mater.* **2009**, *21*, 3970−4004.
(183) Montjoy, D. G.; Bahng, J. H.; Eskafi, A.; Hou, H.; Kotov, N. A. Omnidispersible Hedgehog Particles with Multilayer Coatings for Multiplexed Biosensing. *J. Am. Chem. Soc.* **2018**, *140*, 7835−7845.
(184) Lvov, Y. M.; Lu, Z.; Schenkman, J. B.; Zu, X.; Rusling, J. F. Direct Electrochemistry of Myoglobin and Cytochrome $P450_{cam}$ in

DOI: 10.1021/acsnano.9b03326
ACS Nano 2019, 13, 6151−6169

Alternate Layer-by-Layer Films with DNA and Other Polyions. *J. Am. Chem. Soc.* **1998**, *120*, 4073−4080.
(185) Tong, W.; Song, X.; Gao, C. Layer-by-Layer Assembly of Microcapsules and Their Biomedical Applications. *Chem. Soc. Rev.* **2012**, *41*, 6103−6124.
(186) Yashchenok, A. M.; Bratashov, D. N.; Gorin, D. A.; Lomova, M. V.; Pavlov, A. M.; Sapelkin, A. V.; Shim, B. S.; Khomutov, G. B.; Kotov, N. A.; Sukhorukov, G. B.; Möhwald, H.; Skirtach, A. G. Carbon Nanotubes on Polymeric Microcapsules: Free-Standing Structures and Point-Wise Laser Openings. *Adv. Funct. Mater.* **2010**, *20*, 3136−3142.
(187) Shyu, T. C.; Damasceno, P. F.; Dodd, P. M.; Lamoureux, A.; Xu, L.; Shlian, M.; Shtein, M.; Glotzer, S. C.; Kotov, N. A. A Kirigami Approach to Engineering Elasticity in Nanocomposites Through Patterned Defects. *Nat. Mater.* **2015**, *14*, 785−789.
(188) Kim, Y.; Yeom, B.; Arteaga, O.; Yoo, S. J.; Lee, S. G.; Kim, J. G.; Kotov, N. A. Reconfigurable Chiroptical Nanocomposites with Chirality Transfer From the Macro- to the Nanoscale. *Nat. Mater.* **2016**, *15*, 461−468.
(189) Muzzio, N. E.; Pasquale, M. A.; Diamanti, E.; Gregurec, D.; Moro, M. M.; Azzaroni, O.; Moya, S. E. Enhanced Antiadhesive Properties of Chitosan/Hyaluronic Acid Polyelectrolyte Multilayers Driven by Thermal Annealing: Low Adherence for Mammalian Cells and Selective Decrease in Adhesion for Gram-Positive Bacteria. *Mater. Sci. Eng., C* **2017**, *80*, 677−687.
(190) Dubas, S. T.; Kumlangdudsana, P.; Potiyaraj, P. Layer-by-Layer Deposition of Antimicrobial Silver Nanoparticles on Textile Fibers. *Colloids Surf., A* **2006**, *289*, 105−109.
(191) Moskowitz, J. S.; Blaisse, M. R.; Samuel, R. E.; Hsu, H. P.; Harris, M. B.; Martin, S. D.; Lee, J. C.; Spector, M.; Hammond, P. T. The Effectiveness of the Controlled Release of Gentamicin from Polyelectrolyte Multilayers in the Treatment of *Staphylococcus aureus* Infection in a Rabbit Bone Model. *Biomaterials* **2010**, *31*, 6019−6030.
(192) Shah, N. J.; Macdonald, M. L.; Beben, M. Y.; Padera, R. F.; Samuel, R. E.; Hammond, P. T. Tunable Dual Growth Factor Delivery from Polyelectrolyte Multilayer Films. *Biomaterials* **2011**, *32*, 6183−6193.
(193) Hammond, P. T. Building Biomedical Materials Layer-by-Layer. *Mater. Today* **2012**, *15*, 196−206.
(194) Macdonald, M. L.; Samuel, R. E.; Shah, N. J.; Padera, R. F.; Beben, Y. M.; Hammond, P. T. Tissue Integration of Growth Factor-Eluting Layer-by-Layer Polyelectrolyte Multilayer Coated Implants. *Biomaterials* **2011**, *32*, 1446−1453.
(195) Joseph, N.; Ahmadiannamini, P.; Hoogenboom, R.; Vankelecom, I. F. J. Layer-by-Layer Preparation of Polyelectrolyte Multilayer Membranes for Separation. *Polym. Chem.* **2014**, *5*, 1817−1831.
(196) Miller, M. D.; Bruening, M. L. Controlling the Nanofiltration Properties of Multilayer Polyelectrolyte Membranes through Variation of Film Composition. *Langmuir* **2004**, *20*, 11545−11551.
(197) Krasemann, L.; Tieke, B. Composite Membranes with Ultrathin Separation Layer Prepared by Self-Assembly of Polyelectrolytes. *Mater. Sci. Eng., C* **1999**, *8*−*9*, 513−518.
(198) van Ackern, F.; Krasemann, L.; Tieke, B. Ultrathin Membranes for Gas Separation and Pervaporation Prepared upon Electrostatic Self-Assembly of Polyelectrolytes. *Thin Solid Films* **1998**, *327*−*329*, 762−766.
(199) White, N.; Misovich, M.; Alemayehu, E.; Yaroshchuk, A.; Bruening, M. L. Highly Selective Separations of Multivalent and Monovalent Cations in Electrodialysis through Nafion Membranes Coated with Polyelectrolyte Multilayers. *Polymer* **2016**, *103*, 478−485.
(200) Krasemann, L.; Tieke, B. Selective Ion Transport Across Self-Assembled Alternating Multilayers of Cationic and Anionic Polyelectrolytes. *Langmuir* **2000**, *16*, 287−290.
(201) Liu, G.; Dotzauer, M. D.; Bruening, M. L. Ion-Exchange Membranes Prepared Using Layer-by-Layer Polyelectrolyte Deposition. *J. Membr. Sci.* **2010**, *354*, 198−205.
(202) de Grooth, J.; Oborný, R.; Potreck, J.; Nijmeijer, K.; de Vos, W. M. The Role of Ionic Strength and Odd-Even Effects on the Properties of Polyelectrolyte Multilayer Nanofiltration Membranes. *J. Membr. Sci.* **2015**, *475*, 311−319.
(203) Menne, D.; Üzüm, C.; Koppelmann, A.; Wong, J. E.; Foeken, C. V.; Borre, F.; Dähne, L.; Laakso, T.; Pihlajamäki, A.; Wessling, M. Regenerable Polymer/Ceramic Hybrid Nanofiltration Membrane Based on Polyelectrolyte Assembly by Layer-by-Layer Technique. *J. Membr. Sci.* **2016**, *520*, 924−932.
(204) Cho, K. L.; Hill, A. J.; Caruso, F.; Kentish, S. E. Chlorine Resistant Glutaraldehyde Crosslinked Polyelectrolyte Multilayer Membranes for Desalination. *Adv. Mater.* **2015**, *27*, 2791−2796.
(205) Irigoyen, J.; Politakos, N.; Murray, R.; Moya, S. E. Design and Fabrication of Regenerable Polyelectrolyte Multilayers for Applications in Foulant Removal. *Macromol. Chem. Phys.* **2014**, *215*, 1543−1550.
(206) Singer, S. J.; Nicolson, G. L. The Fluid Mosaic of the Structure of Cell Membranes. *Science* **1972**, *175*, 720−731.
(207) Palankar, R.; Pinchasik, B. E.; Khlebtsov, B. N.; Kolesnikova, T. A.; Möhwald, H.; Winterhalter, M.; Skirtach, A. G. Nanoplasmonically-Induced Defects in Lipid Membrane Monitored by Ion Current: Transient Nanopores *versus* Membrane Rupture. *Nano Lett.* **2014**, *14*, 4273−4279.
(208) Diamanti, E.; Andreozzi, P.; Anguiano, R.; Yate, L.; Gregurec, D.; Politakos, N.; Ziolo, R. F.; Donath, E.; Moya, S. E. The Effect of Top-Layer Chemistry on the Formation of Supported Lipid Bilayers on Polyelectrolyte Multilayers: Primary *versus* Quaternary Amines. *Phys. Chem. Chem. Phys.* **2016**, *18*, 32396−32405.
(209) Diamanti, E.; Gregurec, D.; Rodríguez-Presa, M. J.; Gervasi, C. A.; Azzaroni, O.; Moya, S. E. High Resistivity Lipid Bilayers Assembled on Polyelectrolyte Multilayer Cushions: An Impedance Study. *Langmuir* **2016**, *32*, 6263−6271.
(210) Diamanti, E.; Cuellar, L.; Gregurec, D.; Moya, S. E.; Donath, E. Role of Hydrogen Bonding and Polyanion Composition in the Formation of Lipid Bilayers on Top of Polyelectrolyte Multilayers. *Langmuir* **2015**, *31*, 8623−8632.
(211) Diamanti, E.; Andreozzi, P.; Kirby, C.; Anguiano, R.; Yate, L.; Heinz, H.; Ziolo, R. F.; Donath, E.; Moya, S. E. Study of the Impact of Polyanions on the Formation of Lipid Bilayers on Top of Polyelectrolyte Multilayers with Poly(allylamine hydrochloride) as the Top Layer. *J. Phys. Chem. B* **2017**, *121*, 1158−1167.
(212) Diamanti, E.; Gutiérrez-Pineda, E.; Politakos, N.; Andreozzi, P.; Rodriguez-Presa, M. J.; Knoll, W.; Azzaroni, O.; Gervasi, C. A.; Moya, S. E. Gramicidin Ion Channels in a Lipid Bilayer Supported on Polyelectrolyte Multilayer Films: An Electrochemical Impedance Study. *Soft Matter* **2017**, *13*, 8922−8929.
(213) Zhang, R. J.; Kohler, K.; Kreft, O.; Skirtach, A.; Möhwald, H.; Sukhorukov, G. Salt-Induced Fusion of Microcapsules of Polyelectrolytes. *Soft Matter* **2010**, *6*, 4742−4747.
(214) Skorb, E. V.; Möhwald, H. Smart" Surface Capsules for Delivery Devices. *Adv. Mater. Interfaces* **2014**, *1*, 1400237.
(215) Skirtach, A.; Yashchenok, A.; Möhwald, H. Encapsulation, Release and Applications of LbL Polyelectrolyte Multilayer Capsules. *Chem. Commun.* **2011**, *47*, 12736−12746.
(216) Liu, X. Y.; Gao, C. Y.; Shen, J. C.; Möhwald, H. Multilayer Microcapsules as Anti-Cancer Drug Delivery Vehicle: Deposition, Sustained Release, and *in Vitro* Bioactivity. *Macromol. Biosci.* **2005**, *5*, 1209−1219.
(217) De Geest, B. G.; Sanders, N. N.; Sukhorukov, G. B.; Demeester, J.; De Smedt, S. C. Release Mechanisms for Polyelectrolyte Capsules. *Chem. Soc. Rev.* **2007**, *36*, 636−649.
(218) Donath, E.; Moya, S.; Neu, B.; Sukhorukov, G. B.; Georgieva, R.; Voigt, A.; Baumler, H.; Kiesewetter, H.; Möhwald, H. Hollow Polymer Shells from Biological Templates: Fabrication and Potential Applications. *Chem. - Eur. J.* **2002**, *8*, 5481−5485.
(219) Sukhorukov, G. B.; Donath, E.; Moya, S.; Susha, A. S.; Voigt, A.; Hartmann, J.; Möhwald, H. Microencapsulation by Means of Step-Wise Adsorption of Polyelectrolytes. *J. Microencapsulation* **2000**, *17*, 177−185.

DOI: 10.1021/acsnano.9b03326
ACS Nano 2019, 13, 6151−6169

(220) Dai, Q.; Bertleff-Zieschang, N.; Braunger, J. A.; Björnmalm, M.; Cortez-Jugo, C.; Caruso, F. Particle Targeting in Complex Biological Media. *Adv. Healthcare Mater.* **2018**, *7*, 1700575.
(221) Richardson, J. J.; Cui, J.; Björnmalm, M.; Braunger, J. A.; Ejima, H.; Caruso, F. Innovation in Layer-by-Layer Assembly. *Chem. Rev.* **2016**, *116*, 14828−14867.
(222) Such, G. K.; Yan, Y.; Johnston, A. P. R.; Gunawan, S. T.; Caruso, F. Interfacing Materials Science and Biology for Drug Carrier Design. *Adv. Mater.* **2015**, *27*, 2278−2297.
(223) Sivakumar, S.; Gupta, J. K.; Abbott, N. L.; Caruso, F. Monodisperse Emulsions through Templating Polyelectrolyte Multilayer Capsules. *Chem. Mater.* **2008**, *20*, 2063−2065.
(224) Becker, A. L.; Orlotti, N. I.; Folini, M.; Cavalieri, F.; Zelikin, A. N.; Johnston, A. P. R.; Zaffaroni, N.; Caruso, F. Redox-Active Polymer Microcapsules for the Delivery of a Survivin-Specific siRNA in Prostate Cancer Cells. *ACS Nano* **2011**, *5*, 1335−1344.
(225) Björnmalm, M.; Cui, J.; Bertleff-Zieschang, N.; Song, D.; Caruso, F. Nanoengineering Particles through Template Assembly. *Chem. Mater.* **2017**, *29*, 289−306.
(226) Noi, K. F.; Roozmand, A.; Björnmalm, M.; Richardson, J. J.; Franks, G. V.; Caruso, F. Assembly-Controlled Permeability of Layer-by-Layer Polymeric Microcapsules Using a Tapered Fluidized Bed. *ACS Appl. Mater. Interfaces* **2015**, *7*, 27940−27947.
(227) Richardson, J. J.; Teng, D.; Björnmalm, M.; Gunawan, S. T.; Guo, J.; Cui, J.; Franks, G. V.; Caruso, F. Fluidized Bed Layer-by-Layer Microcapsule Formation. *Langmuir* **2014**, *30*, 10028−10034.
(228) Chandrawati, R.; Hosta-Rigau, L.; Vanderstraaten, D.; Lokuliyana, S. A.; Stadler, B.; Albericio, F.; Caruso, F. Engineering Advanced Capsosomes: Maximizing the Number of Subcompartments, Cargo Retention, and Temperature-Triggered Reaction. *ACS Nano* **2010**, *4*, 1351−1361.
(229) Hosta-Rigau, L.; Stadler, B.; Yan, Y.; Nice, E. C.; Heath, J. K.; Albericio, F.; Caruso, F. Capsosomes with Multilayered Subcompartments: Assembly and Loading with Hydrophobic Cargo. *Adv. Funct. Mater.* **2010**, *20*, 59−66.
(230) Stadler, B.; Chandrawati, R.; Goldie, K.; Caruso, F. Capsosomes: Subcompartmentalizing Polyelectrolyte Capsules Using Liposomes. *Langmuir* **2009**, *25*, 6725−6732.
(231) Hosta-Rigau, L.; Chung, S. F.; Postma, A.; Chandrawati, R.; Staedler, B.; Caruso, F. Capsosomes with "Free-Floating" Liposomal Subcompartments. *Adv. Mater.* **2011**, *23*, 4082−4087.
(232) Maina, J. W.; Richardson, J. J.; Chandrawati, R.; Kempe, K.; van Koeverden, M. P.; Caruso, F. Capsosomes as Long-Term Delivery Vehicles for Protein Therapeutics. *Langmuir* **2015**, *31*, 7776−7781.
(233) Chandrawati, R.; Odermatt, P. D.; Chong, S. F.; Price, A. D.; Städler, B.; Caruso, F. Triggered Cargo Release by Encapsulated Enzymatic Catalysis in Capsosomes. *Nano Lett.* **2011**, *11*, 4958−4963.
(234) Chandrawati, R.; Chong, S. F.; Zelikin, A. N.; Hosta-Rigau, L.; Städler, B.; Caruso, F. Degradation of Liposomal Subcompartments in PEGylated Capsosomes. *Soft Matter* **2011**, *7*, 9638−9646.
(235) Hosta-Rigau, L.; Chandrawati, R.; Saveriades, E.; Odermatt, P. D.; Postma, A.; Ercole, F.; Breheney, K.; Wark, K. L.; Städler, B.; Caruso, F. Noncovalent Liposome Linkage and Miniaturization of Capsosomes for Drug Delivery. *Biomacromolecules* **2010**, *11*, 3548−3555.
(236) Zebli, B.; Susha, A. S.; Sukhorukov, G. B.; Rogach, A. L.; Parak, W. J. Magnetic Targeting and Cellular Uptake of Polymer Microcapsules Simultaneously Functionalized with Magnetic and Luminescent Nanocrystals. *Langmuir* **2005**, *21*, 4262−4265.
(237) Ochs, M.; Carregal Romero, S.; Rejman, J.; Braeckmans, K.; De Smedt, S. C.; Parak, W. J. Light-Addressable Capsules as Caged Compound Matrix for Controlled *in Vitro* Release. *Angew. Chem., Int. Ed.* **2013**, *52*, 695−699.
(238) Kirchner, C.; Javier, A. M.; Susha, A. S.; Rogach, A. L.; Kreft, O.; Sukhorukov, G. B.; Parak, W. J. Cytotoxicity of Nanoparticle-Loaded Polymer Capsules. *Talanta* **2005**, *67*, 486−491.
(239) Kastl, L.; Sasse, D.; Wulf, V.; Hartmann, R.; Mircheski, J.; Ranke, C.; Carregal-Romero, S.; Martínez-López, J. A.; Fernández-Chacón, R.; Parak, W. J.; Elsaesser, H. P.; Rivera Gil, P. Multiple Internalization Pathways of Polyelectrolyte Multilayer Capsules into Mammalian Cells. *ACS Nano* **2013**, *7*, 6605−6618.
(240) Zyuzin, M. V.; Díez, P.; Goldsmith, M.; Carregal-Romero, S.; Teodosio, C.; Rejman, J.; Feliu, N.; Escudero, A.; Almendral, M. J. S.; Linne, U.; Peer, D.; Fuentes, M.; Parak, W. J. Comprehensive and Systematic Analysis of the Immunocompatibility of Polyelectrolyte Capsules. *Bioconjugate Chem.* **2017**, *28*, 556−564.
(241) Delcea, M.; Schmidt, S.; Palankar, R.; Fernandes, P. A. L.; Fery, A.; Möhwald, H.; Skirtach, A. G. P. Mechanobiology: Correlation between Mechanical Stability of Microcapsules Studies by AFM and Impact of Cell-Induced Stresses. *Small* **2010**, *6*, 2858−2862.
(242) Hartmann, R.; Weidenbach, M.; Neubauer, M.; Fery, A.; Parak, W. J. Stiffness-Dependent *in Vitro* Uptake and Lysosomal Acidification of Colloidal Particles. *Angew. Chem., Int. Ed.* **2015**, *54*, 1365−1368.
(243) Sun, H. L.; Wong, E. H. H.; Yan, Y.; Cui, J. W.; Dai, Q.; Guo, J. L.; Qiao, G. G.; Caruso, F. The Role of Capsule Stiffness on Cellular Processing. *Chem. Sci.* **2015**, *6*, 3505−3514.
(244) Shimoni, O.; Yan, Y.; Wang, Y.; Caruso, F. Shape-Dependent Cellular Processing of Polyelectrolyte Capsules. *ACS Nano* **2013**, *7*, 522−530.
(245) De Koker, S.; De Geest, B. G.; Cuvelier, C.; Ferdinande, L.; Deckers, W.; Hennink, W. E.; De Smedt, S.; Mertens, N. *In Vivo* Cellular Uptake, Degradation, and Biocompatibility of Polyelectrolyte Microcapsules. *Adv. Funct. Mater.* **2007**, *17*, 3754−3763.
(246) De Koker, S.; Naessens, T.; De Geest, B. G.; Bogaert, P.; Demeester, J.; De Smedt, S.; Grooten, J. Biodegradable Polyelectrolyte Microcapsules: Antigen Delivery Tools with Th17 Skewing Activity after Pulmonary Delivery. *J. Immunol.* **2010**, *184*, 203−211.
(247) Antipov, A. A.; Sukhorukov, G. B.; Leporatti, S.; Radtchenko, I. L.; Donath, E.; Möhwald, H. Polyelectrolyte Multilayer Capsule Permeability Control. *Colloids Surf., A* **2002**, *198*, 535−541.
(248) Kamphuis, M. M. J.; Johnston, A. P. R.; Such, G. K.; Dam, H. H.; Evans, R. A.; Scott, A. M.; Nice, E. C.; Heath, J. K.; Caruso, F. Targeting of Cancer Cells Using Click-Functionalized Polymer Capsules. *J. Am. Chem. Soc.* **2010**, *132*, 15881−15883.
(249) Facca, S.; Cortez, C.; Mendoza-Palomares, C.; Messadeq, N.; Dierich, A.; Johnston, A. P.; Mainard, D.; Voegel, J. C.; Caruso, F.; Benkirane-Jessel, N. Active Multilayered Capsules for *in Vivo* Bone Formation. *Proc. Natl. Acad. Sci. U. S. A.* **2010**, *107*, 3406−3411.
(250) Chluba, J.; Voegel, J. C.; Decher, G.; Erbacher, P.; Schaaf, P.; Ogier, J. Peptide Hormone Covalently Bound to Polyelectrolytes and Embedded into Multilayer Architectures Conserving Full Biological Activity. *Biomacromolecules* **2001**, *2*, 800−805.
(251) Yu, A. M.; Wang, Y. J.; Barlow, E.; Caruso, F. Mesoporous Silica Particles as Templates for Preparing Enzyme-Loaded Biocompatible Microcapsules. *Adv. Mater.* **2005**, *17*, 1737−1741.
(252) Ganas, C.; Weiß, A.; Nazarenus, M.; Rösler, S.; Kissel, T.; Rivera Gil, P.; Parak, W. J. Biodegradable Capsules as Non-Viral Vectors for *in Vitro* Delivery of PEI/siRNA Polyplexes for Efficient Gene Silencing. *J. Controlled Release* **2014**, *196*, 132−138.
(253) Wood, K. C.; Boedicker, J. Q.; Lynn, D. M.; Hammond, P. T. Tunable Drug Release from Hydrolytically Degradable Layer-by-Layer Thin Films. *Langmuir* **2005**, *21*, 1603−1609.
(254) De Koker, S.; De Geest, B. G.; Singh, S. K.; De Rycke, R.; Naessens, T.; Van Kooyk, Y.; Demeester, J.; De Smedt, S. C.; Grooten, J. Polyelectrolyte Microcapsules as Antigen Delivery Vehicles to Dendritic Cells: Uptake, Processing, and Cross-Presentation of Encapsulated Antigens. *Angew. Chem., Int. Ed.* **2009**, *48*, 8485−8489.
(255) Rivera Gil, P.; De Koker, S.; De Geest, B. G.; Parak, W. J. Intracellular Processing of Proteins Mediated by Biodegradable Polyelectrolyte Capsules. *Nano Lett.* **2009**, *9*, 4398−4402.
(256) Radt, B.; Smith, T. A.; Caruso, F. Optically Addressable Nanostructured Capsules. *Adv. Mater.* **2004**, *16*, 2184−2189.
(257) Ambrosone, A.; Marchesano, V.; Carregal-Romero, S.; Intartaglia, D.; Parak, W. J.; Tortiglione, C. Control of Wnt/β-

DOI: 10.1021/acsnano.9b03326
ACS Nano 2019, 13, 6151−6169

Catenin Signaling Pathway *in Vivo via* Light Responsive Capsules. *ACS Nano* **2016**, *10*, 4828−4834.
(258) Lengert, E.; Parakhonskiy, B.; Khalenkow, D.; Zečić, A.; Vangheel, M.; Monje Moreno, J. M.; Braeckman, B. P.; Skirtach, A. G. Laser-Induced Remote Release *in Vivo* in *C. elegans* from Novel Silver Nanoparticles-Alginate Hydrogel Shells. *Nanoscale* **2018**, *10*, 17249−17256.
(259) Kolesnikova, T. A.; Gorin, D. A.; Fernandes, P.; Kessel, S.; Khomutov, G. B.; Fery, A.; Shchukin, D. G.; Möhwald, H. Nanocomposite Microcontainers with High Ultrasound Sensitivity. *Adv. Funct. Mater.* **2010**, *20*, 1189−1195.
(260) De Geest, B. G.; Skirtach, A. G.; Mamedov, A. A.; Antipov, A. A.; Kotov, N. A.; De Smedt, S. C.; Sukhorukov, G. B. Ultrasound-Triggered Release from Multilayered Capsules. *Small* **2007**, *3*, 804−808.
(261) Shchukin, D. G.; Gorin, D. A.; Möhwald, H. Ultrasonically Induced Opening of Polyelectrolyte Microcontainers. *Langmuir* **2006**, *22*, 7400−7404.
(262) Cui, X.; Li, Z.; Zhong, S.; Wang, B.; Han, Y.; Wang, H.; Möhwald, H. A Facile Sonochemical Route for the Fabrication of Magnetic Protein Microcapsules for Targeted Delivery. *Chem. - Eur. J.* **2013**, *19*, 9485−9488.
(263) Lu, Z.; Prouty, M. D.; Guo, Z.; Golub, V. O.; Kumar, C. S.; Lvov, Y. M. Magnetic Switch of Permeability for Polyelectrolyte Microcapsules Embedded with Co@Au Nanoparticles. *Langmuir* **2005**, *21*, 2042−2050.
(264) Timin, A. S.; Litvak, M. M.; Gorin, D. A.; Atochina-Vasserman, E. N.; Atochin, D. N.; Sukhorukov, G. B. Drug Delivery: Cell-Based Drug Delivery and Use of Nano- and Microcarriers for Cell Functionalization. *Adv. Healthcare Mater.* **2018**, *7*, 1700818.
(265) Vidiasheva, I. V.; Abalymov, A. A.; Kurochkin, M. A.; Mayorova, O. A.; Lomova, M. V.; German, S. V.; Khalenkow, D. N.; Zharkov, M. N.; Gorin, D. A.; Skirtach, A. G.; Tuchin, V. V.; Sukhorukov, G. B. Transfer of Cells with Uptaken Nanocomposite, Magnetite-Nanoparticle Functionalized Capsules with Electromagnetic Tweezers. *Biomater. Sci.* **2018**, *6*, 2219−2229.
(266) Pavlov, A. M.; DeGeest, B. G.; Louage, B.; Lybaert, L.; DeKoker, S.; Koudelka, Z.; Sapelkin, A. V.; Sukhorukov, G. B. Magnetically Engineered Microcapsules as Intracellular Anchors for Remote Control over Cellular Mobility. *Adv. Mater.* **2013**, *25*, 6945−6950.
(267) Muslimov, A.; Timin, A. S.; Petrova, A.; Epifanovskaya, O.; Shakirova, A. I.; Lepik, K. V.; Gorshkov, A.; Il'inskaja, E. V.; Vasin, A. V.; Afanasyev, B. V.; Fehse, B.; Sukhorukov, G. B. Mesenchymal Stem Cells Engineering: Microcapsules-Assisted Gene Transfection and Magnetic Cell Separation. *ACS Biomater. Sci. Eng.* **2017**, *3*, 2314−2324.
(268) Lepik, K. V.; Muslimov, A. R.; Timin, A. S.; Sergeev, V. S.; Romanyuk, D. S.; Moiseev, I. S.; Popova, E. V.; Radchenko, I. L.; Vilesov, A. D.; Galibin, O. V.; Sukhorukov, G. B.; Afanasyev, B. V. Mesenchymal Stem Cell Magnetization: Magnetic Multilayer Microcapsule Uptake, Toxicity, Impact on Functional Properties, and Perspectives for Magnetic Delivery. *Adv. Healthcare Mater.* **2016**, *5*, 3182−3190.
(269) Baleeiro, R. B.; Wiesmüller, K. H.; Reiter, Y.; Baude, B.; Dähne, L.; Patzelt, A.; Lademann, J.; Barbuto, J. A.; Walden, P. Topical Vaccination with Functionalized Particles Targeting Dendritic Cells. *J. Invest. Dermatol.* **2013**, *133*, 1933−1941.
(270) Richardson, J. J.; Choy, M. Y.; Guo, J.; Liang, K.; Alt, K.; Ping, Y.; Cui, J.; Law, L. S.; Hagemeyer, C. E.; Caruso, F. Polymer Capsules for Plaque-Targeted *in Vivo* Delivery. *Adv. Mater.* **2016**, *28*, 7703−7707.
(271) Sexton, A.; Whitney, P. G.; Chong, S. F.; Zelikin, A. N.; Johnston, A. P. R.; De Rose, R.; Brooks, A. G.; Caruso, F.; Kent, S. J. A Protective Vaccine Delivery System for *in Vivo* T Cell Stimulation Using Nanoengineered Polymer Hydrogel Capsules. *ACS Nano* **2009**, *3*, 3391−3400.
(272) De Geest, B. G.; Willart, M. A.; Hammad, H.; Lambrecht, B. N.; Pollard, C.; Bogaert, P.; De Filette, M.; Saelens, X.; Vervaet, C.; Remon, J. P.; Grooten, J.; De Koker, S. Polymeric Multilayer Capsule-Mediated Vaccination Induces Protective Immunity against Cancer and Viral Infection. *ACS Nano* **2012**, *6*, 2136−2149.
(273) De Geest, B. G.; Willart, M. A.; Lambrecht, B. N.; Pollard, C.; Vervaet, C.; Remon, J. P.; Grooten, J.; De Koker, S. Surface-Engineered Polyelectrolyte Multilayer Capsules-Synthetic Vaccines Mimicking Microbial Structure and Function. *Angew. Chem., Int. Ed.* **2012**, *51*, 3862−3866.
(274) DeMuth, P. C.; Min, Y.; Huang, B.; Kramer, J. A.; Miller, A. D.; Barouch, D. H.; Hammond, P. T.; Irvine, D. J. Polymer Multilayer Tattooing for Enhanced DNA Vaccination. *Nat. Mater.* **2013**, *12*, 367−376.
(275) Tostanoski, L. H.; Chiu, Y. C.; Andorko, J. I.; Guo, M.; Zeng, X.; Zhang, P.; Royal, W.; Jewell, C. M. Design of Polyelectrolyte Multilayers to Promote Immunological Tolerance. *ACS Nano* **2016**, *10*, 9334−9345.
(276) Khalenkow, D.; Donche, S.; Braeckman, K.; Vanhove, C.; Skirtach, A. G. Added Value of Microscale Raman Chemical Analysis in Mild Traumatic Brain Injury (TBI): A Comparison with Macroscale MRI. *ACS Omega.* **2018**, *3*, 16806−16811.
(277) Barrefelt, Å. A.; Brismar, T. B.; Egri, G.; Aspelin, P.; Olsson, A.; Oddo, L.; Margheritelli, S.; Caidahl, K.; Paradossi, G.; Dähne, L.; Axelsson, R.; Hassan, M. Multimodality Imaging Using SPECT/CT and MRI and Ligand Functionalized ^{99m}Tc-Labeled Magnetic Microbubbles. *EJNMMI Res.* **2013**, *3*, 12.
(278) Barrefelt, Å.; Saghafian, M.; Kuiper, R.; Ye, F.; Egri, G.; Klickermann, M.; Brismar, T. B.; Aspelin, P.; Muhammed, M.; Dähne, L.; Hassan, M. Biodistribution, Kinetics, and Biological Fate of SPION Microbubbles in the Rat. *Int. J. Nanomed.* **2013**, *8*, 3241−3254.
(279) Ahmed, M.; Gustafsson, B.; Aldi, S.; Dusart, P.; Egri, G.; Butler, L. M.; Bone, D.; Dähne, L.; Hedin, U.; Caidahl, K. Molecular Imaging of a New Multimodal Microbubble for Adhesion Molecule Targeting. *Cell. Mol. Bioeng.* **2019**, *12*, 15−32.
(280) Barrefelt, A.; Zhao, Y.; Larsson, M. K.; Egri, G.; Kuiper, R. V.; Hamm, J.; Saghafian, M.; Caidahl, K.; Brismar, T. B.; Aspelin, P.; Heuchel, R.; Muhammed, M.; Dähne, L.; Hassan, M. Fluorescence Labeled Microbubbles for Multimodal Imaging. *Biochem. Biophys. Res. Commun.* **2015**, *464*, 737−742.
(281) Del Mercato, L. L.; Abbasi, A. Z.; Parak, W. J. Synthesis and Characterization of Ratiometric Ion-Sensitive Polyelectrolyte Capsules. *Small* **2011**, *7*, 351−363.
(282) Del Mercato, L. L.; Abbasi, A. Z.; Ochs, M.; Parak, W. J. Multiplexed Sensing of Ions with Barcoded Polyelectrolyte Capsules. *ACS Nano* **2011**, *5*, 9668−9674.
(283) Rivera Gil, P.; Nazarenus, M.; Ashraf, S.; Parak, W. J. pH Sensitive Capsules as Intracellular Optical Reporters for Monitoring Lysosomal pH Changes upon Stimulation. *Small* **2012**, *8*, 943−948.
(284) Delcea, M.; Yashchenok, A.; Videnova, K.; Kreft, O.; Möhwald, H.; Skirtach, A. G. Multicompartmental Micro- and Nanocapsules: Hierarchy and Applications in Biosciences. *Macromol. Biosci.* **2010**, *10*, 465−474.
(285) Harimech, P. K.; Hartmann, R.; Rejman, J.; Del Pino, P.; Rivera Gil, P.; Parak, W. J. Encapsulated Enzymes with Integrated Fluorescence-Control of Enzymatic Activity. *J. Mater. Chem. B* **2015**, *3*, 2801−2807.
(286) Xiong, R.; Soenen, S. J.; Braeckmans, K.; Skirtach, A. G. Towards Theranostic Multicompartment Microcapsules: *In-Situ* Diagnostics and Laser-Induced Treatment. *Theranostics* **2013**, *3*, 141−151.

DOI: 10.1021/acsnano.9b03326
ACS Nano 2019, 13, 6151−6169

Declaration on oath

“I hereby declare on oath, that I have written the present dissertation by my own and have not used other than the acknowledged resources and aids. The submitted written version corresponds to the version on the electronic storage medium. I hereby declare that I have not previously applied or pursued for a doctorate (Ph.D. studies).”

Date: Signature: